Land Surface Modeling with Enhanced Considerations of Soil Hydraulic Properties and Terrestrial Ecosystems

A Dissertation
Presented to
The Academic Faculty

By

Qing Liu

In Partial Fulfillment
Of the Requirement for the Degree
Doctor of Philosophy in the
School of Earth and Atmospheric Sciences

Georgia Institute of Technology

May 2004

Land Surface Modeling with Enhanced Considerations of Soil Hydraulic Properties and Terrestrial Ecosystems

Approved by:

Dr. Robert E. Dickinson, Advisor

Dr. Robert B. Jackson

Dr. Judith A. Curry

Dr. Rong Fu

Dr. William Chameides

April 07. 2004

ACKNOWLEDGMENTS

It is very difficult to say enough to express how thankful I am to Dr. Robert Dickinson, my thesis advisor, who has supervised me since January, 2000. He inspired and influenced me in many ways. His sound advice, encouragement and patience helped me build up my research skills and overcome many challenges and frustrations. The way he does science with pure passion and enthusiasm touched everyone around and taught me to enjoy what I am doing more than ever. He treated me not only as a student but also as a friend and a collaborator and was always supportive in a respectful way whenever help was needed. I believe that the things that I learned from him will benefit me over the course of my lifetime.

I wish also to thank Dr. Rong Fu, Dr. Judith Curry, Dr. William Chameides and Dr. Robert Jackson for their valuable suggestions and comments on this thesis.

I have been fortunate to interact with many people who helped greatly. I am grateful to Yongjiu Dai, who helped me to learn the CLM bit by bit starting from scratch. Special thanks go to Yuhong Tian, who not only provided me information of satellite data and taught me fundamental knowledge of remote sensing but also shared with me all the experiences she got during her PhD and early post doctoral periods. I am also indebted to Liming Zhou, Wanru Wu and Hongbin Yu. They gave me numerous suggestions on my thesis from methods selection to final writing and always encouraged me. It is a great pain leaving this group after working with them for several years. I appreciate Janet Mcgraw and Muhanmmad Shaikh for their help as well.

I would also like to thank Keith Oleson and Peter Thornton at NCAR. Keith

provided me his diagnostic code and answered my many stupid questions about the NCAR model source code and scripts patiently. I gained ideas and learned a lot from Peter during our several discussions on land ecosystems and biogeochemical models.

I will never forget the company I had from my fellow students and friends of EAS. In particular, I'm thankful to Ping Jing, Mi Zhou, Yan Zhang, Arsineh Hecobian, Lei Zhu, Tao Zeng for many helps and exchanges of happiness and experiences as PhD students. I also wish to thank my best friends from many years ago in China, Xiaoling Zhang and Linli Liu. Their friendship made me never feel alone.

Last, but not the least, I thank my parents for their understanding and help in cheering me up whenever I was down. My husband, Dong Song, has been my best friend, my personal consultant and stress-release therapist. I appreciate him for his love and patience during all these years.

TABLE OF CONTENTS

LIST OF TABLES

LIST OF FIGURES

SUMMARY

This thesis research consists of two separate studies. The first study presents the assessment and representation of the effects of soil macropores on the soil hydraulic properties in land surface models for more accurate simulations of soil moisture and surface hydrology. Hydraulic properties determine the soil water content and its transport in the soil. They are provided in most current climate models as empirical formulas by functions of the soil texture. Such is not realistic if the soil contains a substantial amount of macropores. A two-mode soil pore size distribution is incorporated into a land surface model and tested using an observational dataset at a tropical forest site with aggregated soils. The result showed that the existence of macropores greatly affects the estimation of hydraulic properties. Their influence can be included in land models by adding a second function to the pore-size distribution. A practical hydraulic scheme with macropore considerations was proposed given that the existing schemes are not applicable for large-scale simulations. The developed scheme was based on the physical attributes of the water in soil capillary pores and the statistics of several global soil databases. The preliminary test showed that it captures part of soil macropore hydraulic features without sacrificing the estimation accuracy of hydraulic properties of water in soil matrix.

The second study presents the development of an integrated land/ecosystem model by combining the advanced features of a biophysically based land model, the Community Land Model, and an ecosystem biochemical model. The results from tests of the integrated model at four forest sites showed that the model reasonably captures the

seasonal and interannual dynamics of leaf area index and leaf nitrogen control on carbon assimilation across different environments. With being coupled to an atmospheric general circulation model (AGCM), the integrated model showed a strong ability to simulate terrestrial ecosystem carbon fluxes together with heat and water fluxes. Its simulated land surface physical variables are reasonable in both geographic distribution and temporal variation with considering the interactive vegetation parameters.

CHAPTER 1

Introduction

Land surface and its ecosystems play an important role in the climate system and global carbon cycle through their exchanges of energy, momentum, water, heat and carbon with the atmosphere [IPCC, 2001]. These exchanges are largely determined by the surface soil and vegetation properties, which can vary either naturally through the land ecosystems responses to environment such as the seasonal cycle of plant canopy thickness or the soil moisture or unnaturally through man-made modifications such as the change of land vegetation cover by human deforestation. The changes of surface properties also involve exchange of greenhouse gases with the atmosphere. The dynamic role of the land ecosystem in the climate system is further enhanced through its effect on the atmosphere carbon dioxide concentrations. Thus, it is essential to understand not only how the atmosphere is affected by the land surface but also how the land ecosystems respond to the changing environment in order to understand both greenhouse warming and natural climate variability.

Numerical models have now become indispensable tools to study the complicated interactions between components of the climate system. The land-atmosphere interactions are primarily modeled using the land component of the climate model, which is often referred as Land Surface Models (LSMs). The LSMs have experienced significant improvement in the last two decades from the original simple,

unrealistic schemes into explicit representations of the global soil-vegetation-atmosphere transfer system (SVAT) due to advances in plant physiological and hydrological research and progresses in satellite data interpretation [Sellers et al., 1997]. However, simulations of the soil moisture-climate interactions still remain a difficult task and the new generation land models that can simulate changes in vegetation parameters and carbon cycle variables in response to climate change are just beginning to be designed and implemented within climate models [IPCC, 2001].

In this thesis work, modeling studies and developments were conducted to explore two specific aspects of the land surface properties and the dynamics of the terrestrial ecosystems: 1) the effect of soil properties on surface hydrology, and 2) the feedbacks of the land ecosystems and the atmosphere through the dynamic control of the vegetation on surface physical processes. The overall objectives of this thesis study are to enhance understanding of the land-atmosphere interactions and to improve simulation performance of current LSMs.

1.1 Development of the LSMs

The LSMs were originally developed to provide the lower boundary conditions for modeling the atmospheric circulations. The inclusion of land processes in climate models has been found to have major effects on the model climate, especially near the land surface [e.g., Charney et al., 1975; Koster and Suarez, 1994]. The simplest LSMs developed were based on simple aerodynamic bulk transfer formulas. Their surface parameters such as albedo, aerodynamic roughness and soil moisture were often prescribed to be uniform. Such prescriptions did not take into account the effect of

vegetation and ignored potential land-atmosphere feedbacks, some of which are key factors to determine climate sensitivities [Dickinson, 1983; Carson and Sangster, 1981].

In mid-1980s, soil-vegetation-atmosphere transfer schemes (SVAT) of LSMs [e.g., Sellers et al., 1986; Dickinson et al., 1986] were developed to explicitly model the biophysical effect of the vegetation-soil system in the calculation of the surface energy and water balances through consideration of the dynamic biophysical properties of plants, in particular, canopy leaf area in terms of leaf area index (LAI) and leaf stomatal conductance. The radiative, momentum, and hydrological processes at the land surface were linked to these two biophysical properties. For instance, the process of evapotranspiration (ET) was represented with a resistance diagram where the stomatal resistance is its basis; and the LAI determines precipitation interception and vegetation absorption of radiation as well as surface roughness.

In such biophysically based SVATs, the stomatal resistance was empirically related to the environmental conditions that control photosynthesis, and the seasonal evolution of LAI was prescribed as a monthly constant and repeated for each modeling year. Global parameter datasets such as the classification of the vegetation types based on ecological surveys provided spatial distribution of the surface biophysical attributes [Sellers et al., 1996; Buermann et al., 2001; Dickinson, 1995]. Such treatments account for part of the vegetation dynamics but the enforced vegetation cover does not consider any ecosystem feedback.

The biophysically based models coupled with the atmospheric general circulation models (AGCM) led to improved simulation of surface energy and water distributions [Sato et al., 1989]. Nevertheless, significant inter-model differences in the simulated

surface energy and water fluxes were found with the same atmospheric forcing [Chen et al., 1997; Pitman et al., 1993]. The inter-model variations of annual water balances were primarily attributed to their different functional relationships to both ET and runoff [Koster and Milly, 1997]; The ET and runoff simulations in LSMs remained a difficult task, indicating that the presence of significant uncertainties in the modeled soil moisture and its transport within soil column.

The recognized importance of the ET and runoff parameterizations has stimulated sustained efforts to develop new schemes to represent the vegetation and soil more realistically. New strategies have begun to be incorporated into LSMs to improve the runoff prediction. The one-dimensional framework of the LSMs has been found inadequate to model the runoff generation. Thus, catchment-based "statistical-dynamical" approach runoff models, e.g. the TOPMODEL [Beven and kirkby, 1979], have begun to be adopted by many LSMs so that the lateral runoff caused by surface topography can be modeled [Koster et al., 2000; Stieglitz et al., 1997; Liang et al., 1994; Dai et el., 2003].

To improve the ET simulation, biochemical-based photosynthesis models were incorporated in the SVATs to model the physiological control of vegetation on the ET processes explicitly [e.g. Dickinson et al., 1998; Sellers et al., 1996; Cox et al., 1998; Foley et al., 1996; Wang and Leuning, 1998; Knorr, 2000]. Such implementation is based on the concept that the significant loss of water through leaves during CO_2 uptake was controlled by the stomatal pores which is managed by the plants to achieve maximum photosynthesis. The stomatal resistance that controls the transpiration rate of plant canopy was determined directly from the rate of carbon assimilation. This physiological transpiration scheme made LSMs biologically more realistic, in that the water, energy

and carbon were calculated collectively resulting in a reduction of model parameters [Sellers et al., 1997].

1.2 Description of research topics and objectives

1.2.1 The role of soil macropores in climate prediction

Given the strong dependence of the runoff generation and the ET on the soil moisture, proper prediction of soil moisture and its transport is a prerequisite for validation and accurate prediction of ET and runoff. The soil water storage and transport largely depend on soil hydraulic properties. The description of soil hydraulic properties for each grid cell is also critical for applying a hydrological model to the LSM of climate models. Soil hydraulic properties, i.e. the soil water retention characteristics and hydraulic conductivities, are physical properties that determine the ability of soil to transport and to retain water. They are fundamental in partitioning water inputs at ground surface as well as in determining the availability of soil water for extraction by plants. The quantification of soil hydraulic properties serves as the basis for the calculation of surface hydrological processes.

It has been illustrated in several studies that the estimation of soil moisture and surface water flux are sensitively related to the prescribed soil hydraulic properties in different LSMs [Shao and Henderson-Sellers, 1996; Xue et al., 1996; Ek and Cuenca, 1994]. Because their measurements are expensive and time-consuming, hydraulic properties are generally estimated from more basic soil properties such as soil texture using empirical equations. However, the widely used empirical equations, e.g., the hydraulic model developed by Campbell [1974], have been found to be seriously limited

especially for soils that contain substantial amount of macropores [Saxton et al., 1986; Ross and Semttem, 1992; Chen et al., 1993].

The limitation of the current-used hydraulic equations may be caused by their lack of consideration of soil structure because they were originated based on data for compacted soils [Campbell, 1974; van Genuthten, 1978] and included only soil texture information. The primary mineral particles in soil can be grouped together by environmental factors under suitable conditions to form aggregates [Hillel, 1998]. The inter-aggregate porous space, also referred to as macropores, is largely defined by the soil structure and hence can not be described by the current hydraulic equations and by the soil texture alone. Because the existence of soil macropores is an ubiquitous phenomenon in the natural undisturbed soils [Young et al., 1998] and they can change the hydraulic properties in the moisture range of near saturation substantially [Beven and Germann, 1982], the estimated hydraulic properties in current LSMs may cause serious errors when used to predict the soil moisture and the surface hydrology. Although the soil-structure effects on hydraulic properties have been extensively studied in the soil hydrology community, they have not been investigated and considered in the LSMs. The first part of this thesis work was attempted to amend the situation and aimed to answer the questions of 1) can the lack of consideration of the soil structure in a land model affect the soil moisture prediction significantly? And 2) can the structural effect be represented in land models for large scale application in a practical manner?

1.2.2 Numerical representation of land physical-biochemical interactions

The land surface biophysical processes are tied to the dynamics of vegetation and ecosystems as the exchanges between the land and the atmosphere affect not only

climatic parameters but also the presence and productivity of land ecosystems. The vegetation-climate feedbacks have been discussed in terms of albedo induced land-cover change [e.g., Charney et al., 1977; Dickinson and Henderson-Sellers, 1988; Xue and Shukla; 1993; Zhang and Henderson-Sellers 1996], the biosphere effect on the climate variability [e.g., Dickinson, 2000; Wang and Eltahir, 2000 a,b] and change of vegetation dynamics [e.g., Foley et al.,1994]. Such long term changes in vegetation dynamics and climate variations are strongly linked to short term natural climate variability on timescales from several hours to several years [Dickinson, 2001].

The carbon assimilation is also a chief consideration in determining the major contributions to the land-atmosphere exchange of CO_2. The implementation of the biochemical based photosynthesis scheme in many LSMs made it possible to couple it with the terrestrial biochemical carbon cycles. Such inclusion allows the atmosphere to interact with terrestrial ecosystems. It also provides important vegetation properties such as vegetation canopy in terms of LAI dynamically, thus reduces the number of prescribed biophysical parameters of the LSMs. In addition, the development of the integrated land biophysical/biochemical models is consistent with the development of climate system models which have started to model the coupled physical climate system and biogeochemical carbon cycles. In developing such integrated biophysical/biochemical models, the complicated ecosystem processes such as plant and soil respiration, assimilated carbon allocation, plant phenology, etc., that are all strongly dependent on environmental conditions, need to be reasonably represented. The simulated fluxes of carbon and water and energy that are in part controlled by the modeled biophysical and physiological properties should together agree with the measured values [Shaver et al.,

2000].

Accurate prediction of the photosynthesis becomes important in the coupled biophysical/biochemical models as it determines both the carbon uptake and leaf transpiration. The current widely-used photosynthesis models simulate the rate of carbon assimilation as it is limited by the slower of the light-limited and the Rubisco (ribulose, 1,5-bisphosphate carboxylase/oxygenase) limited processes. The Rubisco is the enzyme that incorporates CO_2 into plants during photosynthesis and is strongly related to the leaf nitrogen content [Evans and Caemmerer, 1996]. The carbon assimilation rate has been found to be nitrogen limited in many terrestrial ecosystems [Field and Mooney, 1986] so that it depends largely on the ecosystem available nitrogen and the ecosystem nitrogen cycling. Thus, coupling an ecosystem nitrogen cycle to the ecosystem carbon cycle is more realistic in simulating the carbon assimilation, and hence the stomatal resistance and leaf ET [Dickinson et al., 2002].

As yet, although many LSMs have treated the biophysical-vegetation controls on the surface energy and water balances to varying degrees of realism, only a few have modeled the biochemical processes that determine the land-atmosphere exchange of CO_2, and dynamic changes in vegetation canopy [Dickinson, et al., 1998; Sellers et al., 1996], and even fewer have taken into account the dynamic control on the carbon cycle of the ecosystem biochemical cycles of other element such as nitrogen and associated physical processes [Dickinson et al., 2002]. Existing ecosystem models that derive carbon from foliage photosynthesis are normally developed based on a monthly or longer timestep [e.g., Aber and Federer, 1992; Parton et al. 1993; Field et al., 1995] and thus are not adequate to capture the vegetation dynamics for shorter timescales. The existing models

that include the dynamic role of both vegetation canopy and nitrogen cycle have not been extensively tested. Fast improvement of the ecological formulations in existing SVAT models is limited primarily due to the lack of ground data for validation purposes [Canadell et al., 1999].

The objectives of the second part of this thesis study were to extend the current state-of-the-art SVAT with coupled ecosystem carbon and nitrogen biochemical cycling processes and validate it with field observations, and to use it to simulate the biophysical and biochemical controls of the land vegetation on the atmosphere and the environmental constraints on the terrestrial ecosystems, as well as the carbon exchanges between the land and the atmosphere together over timescales from several hours to several years.

1.3 Approaches

A recently developed SVAT, the Community Land Model (CLM) [Dai et al., 2003] was utilized as the base model to conduct this research. The CLM is the standard land component of the new Community Climate System Model [CCSM] and has the state-of-the-art model structure and parameterizations of many surface processes. It was developed by combining good features of several successful land models and has been tested extensively in both offline mode [Dai et al., 2003] and global coupled-mode with the AGCM [Zeng et al., 2002; Bonan et al., 2002].

To accomplish the first objective of this thesis, the soil hydraulic scheme used in the CLM is first compared with a more explicit hydraulic scheme that has successfully accounted for the soil macropore effect, and a new scheme is proposed to estimate the hydraulic properties with consideration of the global distribution of soil macropore

features. Several global soil databases, the Data and Information System of the International Geosphere Biosphere Programme (IGBP-DIS) [Tempel et al., 1996], the Unsaturated Soil Database (UNSODA) [Leij et al., 1996] and the World Inventory of Soil Emission Potential (WISE), version 1.1 at International Soil and Reference Information Centre (ISRIC) [Batjes, 2002], were used to extract useful information for the global soil parameters.

To accomplish the second objective, the explicit ecosystem carbon and nitrogen biochemical descriptions proposed in Dickinson et al. [1998, 2002] were modified and integrated into the CLM. The model establishes an explicit linkage between the biochemical and biophysical processes of land ecosystems and captures the dynamic control of vegetation canopy and the ecosystem nitrogen cycle on the surface water and energy fluxes. The state-of-the-art model-features of the CLM provided a sound biophysical basis for the ecosystem to be better simulated. The short-term based, i.e. minutes to hours, description of the biochemical carbon cycle and the explicit modeling of the nitrogen cycle in Dickinson et al. [1998, 2002] make it possible to investigate the ecosystem variation with much higher temporal resolution than general ecosystem models use. Recently collected flux tower data are used to validate the accuracy of the integrated model for its simulation of the energy, water and carbon cycle. How the ecosystem responds to the natural variation of the climate is demonstrated in a coupled simulation with the atmospheric component of the CCSM.

1.4 Thesis organization

The abovementioned two research topics are presented in chapter 2 and chapter 3

respectively.

In chapter 2, section 2.1 introduces the background of the soil hydraulic properties and how they are estimated in the LSMs in general as well as the possible limitations of such estimations; section 2.2 presents the performance of the CLM with an improved hydraulic scheme to estimate the soil hydraulic properties with consideration of the macropores by comparing its modeled soil moisture and surface ET with the field observation and the standard run results of the CLM at a forest site; section 2.3 describes the development of a practical hydraulic scheme that accounts for the soil macropores and is applicable to the climate models for global simulations. It also shows the primary results of the global simulation of the surface hydrology forced by atmospheric data with the new scheme implemented in the CLM.

Chapter 3 presents the development of the coupled land/ecosystem model. Section 3.1 describes the model structure and the detail parameterizations of the ecological portion of the model. Section 3.2 tests the model against field observed surface fluxes at 4 different sites. The parameterizations of the model that contribute mainly to simulation-observation difference are investigated and adjusted. Then, the model is coupled to the atmospheric component of the CCSM and the results are presented and discussed in section 3.3.

Chapter 4 summarizes the findings of this thesis and discusses future investigation plan.

CHAPTER 2

Soil structural effects on the hydraulic properties and their potential influence on simulated soil moisture

2.1 Background and introduction

Soil is a three-phase system. The solid phase forms the soil matrix. The liquid phase is soil water and gaseous the soil air that can be stored or flow through the porous area within the soil matrix. Increasing soil water content is associated with increasing the number of water-filled pores.

Soil texture is a measure of the various particle-sizes found in the soil. Soil particle sizes are defined in terms of their diameters, for instance, International Soil Science Society (ISSS) defined soil mineral particle diameter ranges from 2 mm to 0.05 mm as sand; 0.05- 0.002 mm as silt; less than 0.002 as clay and above 2 mm as Gravel. Texture class is determined on the basis of the mass ratios of the three fractions of the sand, silt and clay, as shown in figure 2.1.

The geometric characteristics of the pore spaces in which water and air are transmitted and retained define the soil structure. The matrix also contains amorphous substances, particularly organic materials, which are attached to the mineral grains and may bind them in aggregates. The structure of soils can be changed through formation of the aggregates from the primary mineral particles.

The energy status of soil water can be represented by potentials. Differences in

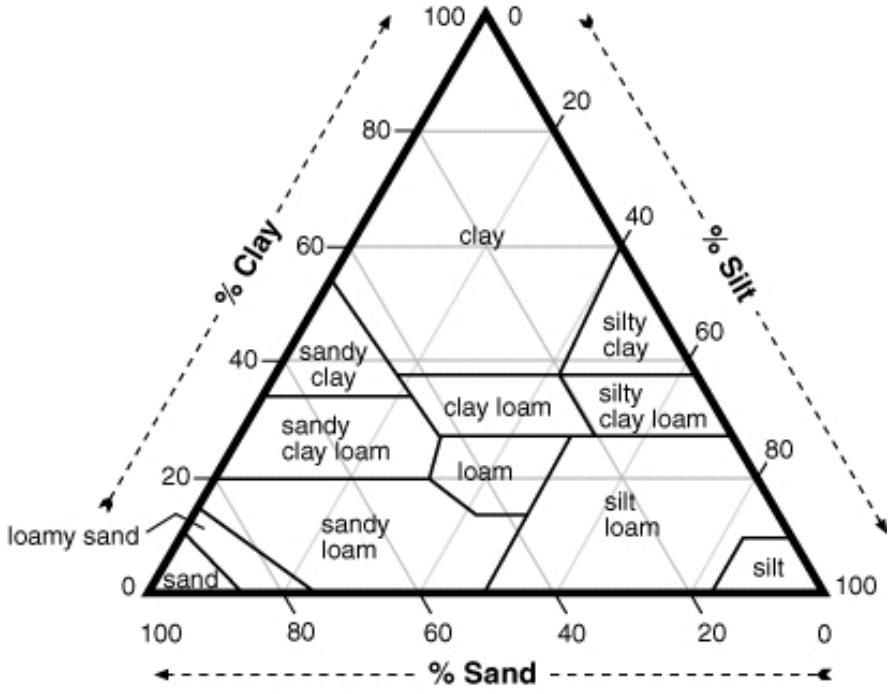

Figure 2.1. Textural triangle, showing the percentages of clay (below 0.002 mm), silt (0.002-0.05 mm), and (0.05-2.0 mm) in the conventional soil textural classes.

potential energy of water between one point and another give rise to the tendency of water to flow from where potential energy is higher to where it is lower. The major forces on the soil water are the gravitational force and the capillary force. Thus, the total soil-water potential can be represented as the sum of gravitational potential and the matric potential. The latter is due to the capillary forces between the liquid water and the solid matrix, which in effect bind water in the soil and lower its potential energy below that of bulk water. The free water in a saturated soil is defined at reference matric potential of zero. The matric potential is hence always negative. Sometimes, the term of "suction" is used interchangeably with the "matric potential" to refer to the absolute value of the matric potential, so that large soil suctions indicate low matric potentials.

The largest soil pores begin to empty with the increase of soil suction. The critical potential of the threshold of de-saturation is called the "air-entry potential". As suction is applied incrementally, more pores are gradually emptied of water from the largest to the smallest. The net effect is that small pores are able to hold water under a larger suction than larger pores do. Thus, the change of matric potential of the water in a soil is associated with the change of the soil's wetness. The value of water content remaining in a unit volume of soil after downward gravity drainage has already ceased is termed as "field capacity". It is often refers to the moisture content at -33 kPa matric potential. In nature, water can be removed from a soil that has reached field capacity, only by direct evaporation or by plant uptake through transpiration. Plants usually can not extract soil water below matric potential of -1500 kPa, at which plant wilting occurs, so the water content at -1500 kPa is termed the "permanent wilting point". The difference between the field capacity and permanent wilting point defines the amount of water available for plant extraction.

The macroscopic feature of water in a soil column can be represented by the one-dimensional vertical water conservation equation in climate models because the horizontal water transport within soil is negligible at the interested horizontal resolutions for climate studies. The vertical water equation can be written as

$$\frac{\partial W}{\partial t} = -\frac{\partial q}{\partial z} + S\,, \tag{2.1}$$

where W is liquid mass, q is the water flux in the soil with downward as the positive direction, and S is a source term, corresponding to root extraction and the phase changes between ice and liquid. The t denotes time and z is the vertical length. The soil water flux in both saturated and unsaturated zones follows Darcy's Law. It says that the flux density

is proportional to the potential gradient along the flow direction, and is expressed as,

$$q = k(\frac{\partial \psi}{\partial z} + 1), \tag{2.2}$$

where, the proportionality k is the hydraulic conductivity. It represents the ability of soil medium to transmit water. The first term in the right hand side is the gradient of the matric potential, ψ. The second term, i.e., the value of 1, is the gradient of the gravitational potential.

The parameters k and ψ are not constant soil attributes. Instead they both vary with the soil water content θ. The functional relationships of the $k(\theta)$ and the $\psi(\theta)$ are indispensable to prediction of the soil water content and its transport. They are normally referred to as soil hydraulic properties. The dependences of potential on soil water, i.e. $\psi(\theta)$, are commonly called soil-water retention characteristics or simply retention functions. The $k(\theta)$, sometimes $k(\psi)$ relationship defines the soil-water conductivity. These soil hydraulic properties depend strongly on the soil texture and structure [Hillel, 1998]. Their schematic shapes for different textural soils are illustrated in figure 2.2.

Although ψ and k can measured at discrete water contents in field or in laboratory, their measurements are very expensive, complicated and time-consuming [Klute, 1986; Klute and Dirksen, 1986]. It is not practical to obtain $\psi(\theta)$ and $k(\theta)$ through measurements for large area applications. Rather, they are often estimated from more readily available soil properties such as soil texture, bulk density, soil organic matter content using indirect method when to simulate field conditions. The method that relates the soil hydraulic properties to basic soil properties are known as pedotransfer functions (PTF) [Bouma, 1989].

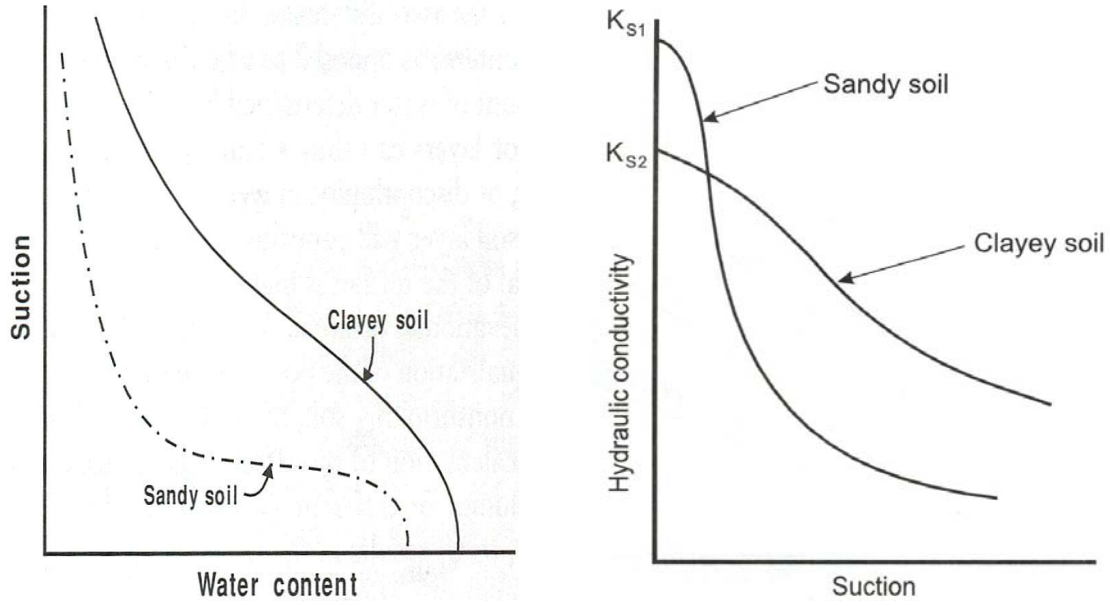

Figure 2.2. Soil-water retention (left), and dependence of conductivity on suction (right) in different soils (Schematic) (from Hillel [1998]).

Generally used PTFs can be grouped into categories of 1) Point estimations, which use empirical functions to predict the water retention or conductivity at a certain matric potentials [e.g. Rawls and Brakensek, 1982; Gupta and Larson, 1979]; 2) Parameter predictions, which describe the empirical equations of $\psi(\theta)$ and $k(\theta)$ with a certain number of parameters and estimate the function parameters with regression model from available soil databases [e.g. Cosby et al., 1984; Vereecken, et al., 1989; Wösten, 1999]; and 3) Physical-conceptual PTFs, which derive hydraulic properties based on physical attributes [e.g. Arya and Paris, 1981; Arya et al., 1999]. The physical-conceptual PTFs require detailed soil inputs which are too difficult to obtain and thus are normally not to be considered in climate models.

LSMs generally use the parameter-estimation PTFs. Numerous mathematical functions have been derived to express the retention curve and hydraulic curve in analytical form. Hillel [1998] reviewed some of them. The most widely used schemes in

the LSMs are those proposed by Brooks and Corey [1964], Campbell [1974], and van Genuchten [1980]. Table 2.1 lists the mathematical formulations of the three hydraulic schemes. Among them, the model of Campbell is the most popular, e.g. LSMs of the CLM [Dai et al., 2003], the BATS [Dickinson et al., 1993], the SSiB [Xue et al., 1991]; the NCAR LSM [Bonan, 1996], the MIT [Entekhabi and Eagleson, 1989], the BEST [Pitman et al., 1991] and the CLASS [Verseghy, 1991].

Four parameters of the Campbell's model need to be determined before it can be applied to a specific soil. These are the Clapp and Hornberger parameter b, the saturated hydraulic conductivity k_{sat}, the air-entry potential ψ_0 and the soil porosity θ_{sat}. The last three are fitting parameters to fix the $k(\theta)$ and $\psi(\theta)$ curves and were chosen because the measurements at the saturation point are the most available for many field studies so that their values can be used at the measurement site. They however need to be estimated in the LSMs because their measurement for a large area can not be established. Different schemes to estimate the parameters from basic soil data were usually derived based on different soil databases. Schemes from soil data from one region may not be valid for soils in other regions [Tomasella et al., 2000; Tomasella and Hodnett, 1998]. Schemes containing more soil attributes as predictors are generally better than those containing less [Tietje and Tapkenhinrichs, 1993; Wagner et al., 2001; Cornelis et al., 2001; Pachepsky and Rawls, 1999]. Most LSMs estimate the hydraulic parameters from soil texture alone, i.e. percentage of clay and sand because that the soil texture is the most commonly measured soil attributes across the world.

The Campbell's model and the other popular hydraulic schemes in the LSMs are for soils with uni-mode pore-size distributions, i.e. the sizes of individual pores in a soil

can be described by a single-distribution function such as lognormal or normal distribution. The uni-mode distribution is adequate for soils containing none or few aggregates. However, undisturbed natural soils usually form a substantial amount of aggregates. The pore-size distributions of such soils can not be adequately captured by a uni-mode curve [Zhang and van Genuchten, 1994; Durner, 1994; Chen et al., 1993; Poulsen et al., 2002]. These soils often have a network of large inter-aggregate pores or cracks that are significantly larger than the pores within the aggregates or soil matrix and cause an inflection on the retention and conductivity curves when near saturation. In addition, the macropores depend strongly on the soil structure instead of the soil texture. Hence, the widely used uni-mode distribution-based schemes and the texture-based parameter estimations can not adequately estimate the hydraulic properties in the whole moisture range, and in particular, near saturation.

Significant efforts have been devoted to improve the traditional hydraulic models with better representation of the soil-structural effect [Clapp and Hornberger, 1978; Saxton et al., 1986; Nimmo, 1997; Ross and Semttem, 1993; Durner, 1994]. Nevertheless, few LSMs have been taken into account the effect of soil aggregates and macropores for estimating the soil hydraulic properties. Given that the soil moisture is non-linearly depended on the soil hydraulic properties, the lack of consideration of soil macropores can result in serious errors in modeling the soil moisture, which can affect the surface hydrology including runoff generation and ET. The runoff and ET schemes in the LSMs would also be affected by errors in the simulated soil moisture and its transport.

The following two sections validate the role of soil macropores in the CLM and

enhance its representation in the LSMs.

Table 2.1. Generally used soil-water retention and hydraulic conductivity relationships in the LSMs.

Model	Function	Parameters
Brooks-Corey (1964)	$\theta(h) = \begin{cases} \theta_s & if \quad h \geq h_b \\ \theta_r + (\theta_s - \theta_r)\left(\frac{h_b}{h}\right)^{\lambda} & if \quad h < h_b \end{cases}$	θ_r = residual water θ_s = saturated water or porosity h_b = air entry potential λ = pore-size index S_e = degree of saturation
	$K(S_e) = \begin{cases} K_s & if \quad h \geq h_b \\ K_s S_e^{\frac{2}{\lambda}+3} & if \quad h < h_b \end{cases}$	$S_e = \frac{\theta - \theta_r}{\theta_s - \theta_r}$
Campbell (1974)	$\theta(h) = \begin{cases} \theta_s & if \quad h \geq h_b \\ \left(\frac{h_b}{h}\right)^{1/b} & if \quad h < h_b \end{cases}$	b = constant
	$K(\theta) = \begin{cases} K_s & if \quad h \geq h_b \\ K\left(\frac{\theta}{\theta_s}\right)^{2b+3} & if \quad h < h_b \end{cases}$	
van Genuchten (1980)	$\theta(h) = \theta_r + \frac{\theta_s - \theta_r}{\left(1 + (\alpha h)^n\right)^m}$	α = constant n = constant $m = 1 - 1/n$
	$K(S_e) = K_s S_e^{0.5}\left[1 - \left(1 - S_e^{1/m}\right)^m\right]^2$	

2.2 Use of a two-mode soil pore size distribution to estimate soil water transport in a land surface model

2.2.1 Introduction

In previous section, we introduced the potential effects of the soil structure on soil hydraulic properties. This section explores how such effects may influence the prediction of the soil moisture and through it affects the surface water flux. A new hydraulic scheme developed by Ross and Semttem [1993] for predicting the hydraulic properties of well-structured soils with multiple-mode pore-size distributions is implemented into the CLM. The basic idea is to separate the soil pores into two bins, the macropores and the "fine" pores. Each such group has its own distribution function, and the distribution of the whole pore system can be represented as a linear combination of these two distributions. The hydraulic properties are inferred from the combined distribution. Therefore, the effect of macroporosity is included into the CLM to estimate the hydraulic properties in a physically realistic manner. We then test the new scheme at a forest site and compare its results with that of the standard CLM and field measurements to show by example that how the inclusion of well-aggregated soils influences the simulation of soil moisture. This section also appears as Liu and Dickinson [2003].

2.2.2 Pore size distribution for soils with heterogeneous pore systems

The pore size (i.e. pore radius) distribution as a function of matric potential is commonly expressed as [Ross and Semttem, 1993; Durner, 1994].

$$f(\psi) = dS/d\psi \quad , \tag{2.3}$$

where S is the soil specific moisture and ψ the soil matric potential. For soils with heterogeneous pore systems, the distribution function can be constructed by the linear combination of the distributions of each pore system [Ross and Semttem, 1993], i.e.,

$$S(\psi) = \sum_{i=1}^{n} W_i S_i(\psi) \quad , \tag{2.4}$$

$$f(\psi) = \sum_{i=1}^{n} W_i f_i(\psi) \quad , \tag{2.5}$$

$$\sum_{i=1}^{n} W_i = 1,$$

where W is the weight of each pore size density group given by the relative contribution of each pore system to total pore volume, and n in this case is two. The relative hydraulic conductivity $k_r = k(\psi)/k_s$, where k_s is the saturated hydraulic conductivity, is computed from the above equations based on Mualem's [1976] model:

$$k_r(\psi) = S^{0.5}[g(\psi)/g(0)]^2 \; ; \tag{2.6}$$

where,

$$g(\psi) = \int_{-\infty}^{\psi} \frac{1}{\psi} f(\psi) d\psi \quad . \tag{2.7}$$

For a soil with non-interacting pore systems, i.e. when water in the macropores moves independently of that in the micropores,

$$k(\psi) = \sum_{i=1}^{n} k_{si} k_{ri}(\psi) \quad , \tag{2.8}$$

$$k_{ri}(\psi) = S^{0.5}[g_i(\psi)/g_i(0)]^2 \quad . \tag{2.9}$$

2.2.3 Two-mode pore size distribution in the CLM

In the CLM, the current matric potential retention and the hydraulic conductivity functions are in the form of Campbell's model [1974]:

$$\psi = \psi_{sat} S^{-b} \quad ; \tag{2.10}$$

$$k = k_{sat} S^{2b+3} \quad . \tag{2.11}$$

ψ_{sat} and k_{sat} are the air-entry potential and the saturated hydraulic conductivity respectively. ψ_{sat} , k_{sat} and b are defined by texture Pedo-Transfer Functions (PTFs) [Cosby et al.1984].

$$\psi_{sat} = -10 \times 10\text{^}(1.88 - 0.013(\%sand)) \quad , \tag{2.12}$$

$$k_{sat} = 0.0070556 \times 10\text{^}(-0.884 + 0.0153(\%sand)) , \tag{2.13}$$

$$b = 2.91 + 0.159(\%clay) \ . \tag{2.14}$$

Because such retention curves are not continuous, to avoid numerical inconsistency, we use that of van Genuchten [1980] instead:

$$S = (1 + (-\alpha\psi)^n)^{-m} \quad . \tag{2.15}$$

α, m, n are parameters. According to Ross's theory, we can take a well-aggregated soil as a two-mode pore distribution system: one distribution by macropores, the other by the micropores. We further assume that these two groups of pores don't interact with each other. Therefore, we have:

$$S = W(1 + (-\alpha_1\psi)^{n_1})^{-m_1} + (1-W)(1 + (-\alpha_2\psi)^{n2})^{-m2} \quad , \tag{2.16}$$

$$f = Wf_1 + (1-W) f_2 \quad , \tag{2.17a}$$

$$f_i = \alpha_i m_i n_i (1 + (-\alpha_i\psi)^{n_i})^{-(m_i+1)} . \tag{2.17b}$$

The two sets of parameters (with subscript 1 and 2 respectively) denote the effect of each pore system on the hydraulic properties. Using equation (2.6), (2.8) and (2.17), the hydraulic conductivity can hence be written as:

$$k = k_{s1} S^{0.5} [I(S^{1/m_1}; m_1 + 1/n_1, 1 - 1/n_1)]^2 + k_{s2} S^{0.5} [I(S^{1/m_2}; m_2 + 1/n_2, 1 - 1/n_2)]^2 \quad , \tag{2.18}$$

where *I()* represents the incomplete beta function.

Once the parameters in equation (2.16) are given, we can generate the $\psi(S)$ by fitting the dataset (S, $\log(-\psi)$) with the nonlinear least squares interior-reflective Newton algorithm to an equation of the form $\log(-\psi) = \frac{a_1 + b_1 S + c_1 S^2 + \cdots}{a_2 + b_2 S + c_2 S^2 + \cdots}$. (2.19)

$\psi(S)$ and $k(S)$ are the matric potential and the hydraulic conductivity for soils that has the two-mode pore size distribution function.

2.2.4 Numerical testing

The CLM is interpreted with modified hydraulic properties ($k(S)$ and ((S)) using datasets from a tropical forest site, i.e. the ecological forest reserve, Reserva Jaru (10(05's, 61(55'W) in Ji-Parana, Rondonia, southwestern Amazonia. Atmospheric forcing data are provided by an automatic weather station. The average clay and sand percentages over the simulation depth are 24% and 65% respectively. Based on Young et al. [1998], the Amazon forest soil has a two-mode pore-size distribution; more than 25% of the porosity was contributed by macropores of sizes >0.1 (m. Such structure indicates good water infiltration and storage. Hodnett's study [1996] showed that no surface runoff is observed in that region even after very heavy rain, which also implies well-aggregated soil in the modeled area. Therefore, we add a second distribution of pore sizes to represent the

existence of the macropores. The values given by Ross and Semttem [1993] are used as the macropore parameters (parameters with subscript 1). The weight of the macropores here is set to 0.3 according to its contribution to the total porosity. Parameters for fine pores (parameters with subscript 2) are generated by fitting the Campbell function-generated values to the van Genuchten's function, i.e. equation (2.15). The standard CLM parameters are used in the Campbell functions. The fitted van Genuchten distribution is illustrated in figure 2.3. The parameters are listed in table 2.2.

Table 2.2. Parameters describing hydraulic properties of aggregated soil.

W	α_1	n_1	m_1	α_2	n_2	M_2
0.3	35	3.90	$1-1/n_1$	5.4042	1.156	0.135

The $\psi(S)$ using the fitting method mentioned above is:

$$\log(-\psi) = 7.151 \times \left(\frac{1 + 3.4843S - 9.235S^2 - 5.354S^3}{1 + 27.639S - 5.592S^2 + 10.865S^3}\right). \quad (2.20)$$

Figure 2.4a-2.4c shows the two-mode distribution and hydraulic properties. The k(S), ((S) and their partial derivatives in the CLM are replaced with equations (2.18) and (2.20) and their partial derivatives. Whenever a second function is necessary, the modified method can be applied to calculate the hydraulic properties.

2.2.5 Result and discussion

We run the CLM with both the modified scheme of the hydraulic properties and compare with the original scheme with the same saturated hydraulic conductivity at the chosen site with regards simulated soil moisture and latent heat flux. In this section, ORG represents the original run case, MOD the run case with the modified scheme and OBS the

measurements. Since the only modification of the CLM is its hydraulic properties, the differences between the simulated results of the two cases should result primarily from the differences of matric potential and unsaturated hydraulic conductivities.

Figure 2.5a is the measured precipitation and 2.5b is the measured and simulated soil moisture for 0 – 2 m over the two simulation years. Simulated values are daily-averaged. Water storage by MOD shows good agreement with OBS over the complete time period, but ORG has distinctly lower water storage in 0-2 m than OBS. Given in figure 2.5c is the soil water storage from the surface to the lowest soil layer down to 3.4 m. The shape of the simulation by the MOD is still closer to that by the OBS than the simulation by ORG although the difference between the simulation and the measurements are larger than that of the upper soil layer, probably because water table variations at the site causes large fluctuations of soil water storage in the 2 – 3.4 m layers. An important consequence of the new scheme MOD is its increase of the total water storage in the soil.

Figure 2.6 and figure 2.7 compares the simulated evapotranspiration (ET) rates with observation. Because the fluxes are not continuous over the whole time period of simulation, the longest continuous period of observation, from day 94 to day 207 in 1993, is selected for comparison. The precipitation is concentrated in the first part of this period. We distinguish a wet period from the beginning to day 160, and a dry period from day 160 to day 207. ET predicted by both MOD and ORG shows a good agreement with the observations during the wet period. Observed ET doesn't decrease or increase much during the whole period, but the simulation by ORG falls sharply from the point at which the wet period ceases, and continues to decrease further with the continuation of the dry period. The ET by ORG almost ceases at the end the comparison period. The ET simulated

by MOD doesn't show much decrease during the whole comparison period, and is in very good agreement with the measurements. Shown in figure 2.8 is the comparison of the ET by MOD and by ORG for the whole two-year period. It's very clear that the no obvious limitation of the ET by the MOD though the ET by ORG is distinctly limited during the dry season. The simulated ET by the MOD is consistent with the conclusion by Hodnett [1996] that no transpiration restriction occurred even during the severe dry season of this region.

Evidently, the new scheme gives a much more accurate simulation of the soil moisture and the latent heat flux over the surface for the modeled site than does the old one. The original hydraulic property parameterizations are for soils with almost no aggregates, viz. fine soil. The saturated hydraulic conductivity can be several orders of magnitude smaller than appropriated when the soil is actually well aggregated. The two-mode pore size distribution captures the effects of macropores resulting from soil aggregation. The consequent hydraulic properties are thus more accurate than those by the original scheme. The better estimation of the soil moisture indicates the improvement of the simulation of hydraulic properties.

2.2.6 Conclusion

The existence of macropores greatly affects the estimation of hydraulic properties. Their influence can be included into land models by adding a second function to the pore-size distribution. With inclusion of the soil macropore effect on soil hydraulic conductivities, the estimation of the soil moisture at a well-structured soil is much more accurate by allowing more water percolate down into soil column instead of being lost as

surface runoff during the wet season. The increased water storage during wet season supplies the dry season evapotranspiration with an extended period and less limitation.

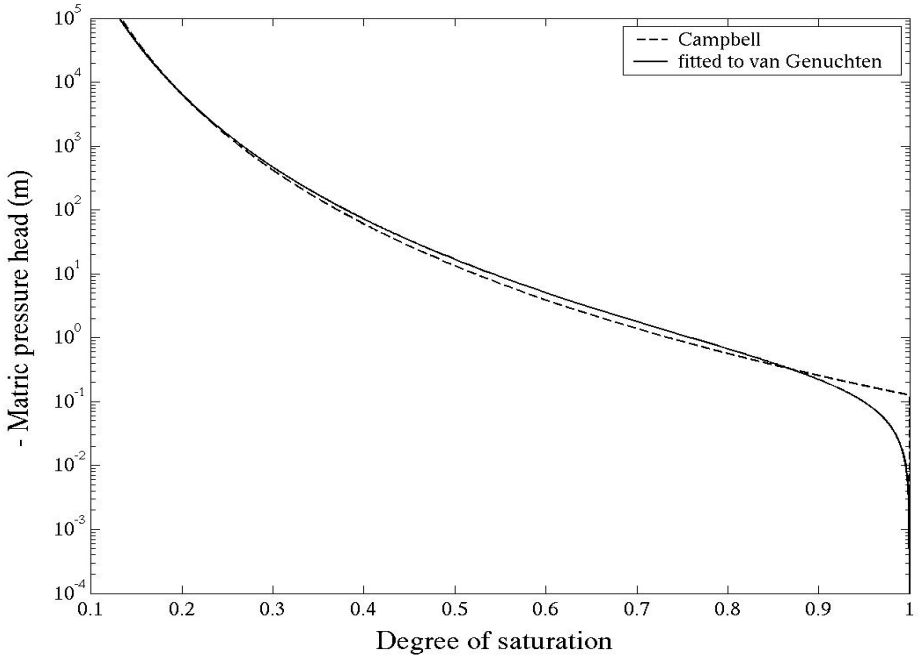

Figure 2.3. Water retention curve by Campbell (dashed) and that fitted to van Genuchten (solid).

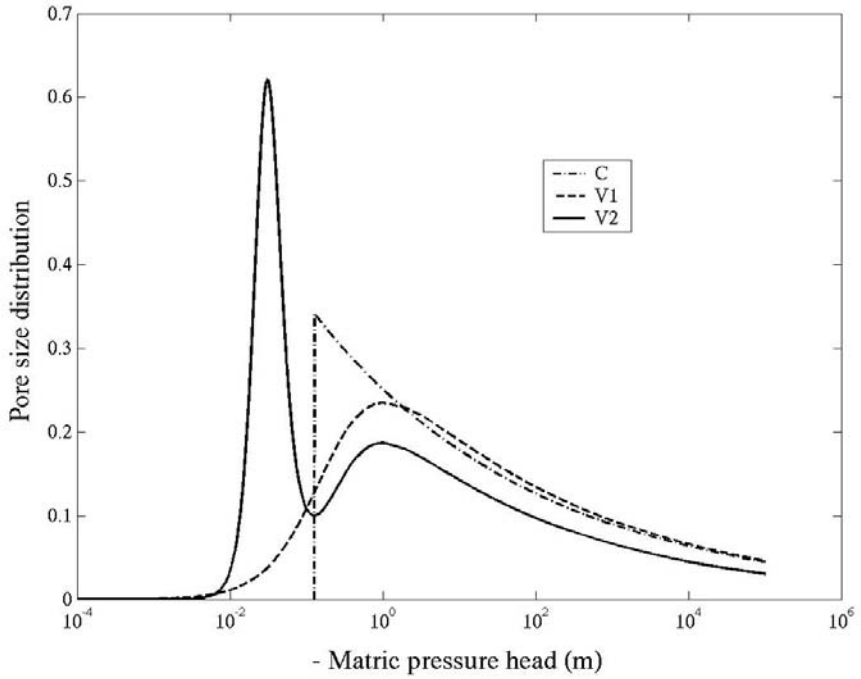

Figure 2.4.a. Pore size distributions based on Campbell model (dash dot (C)), based on van Genuchten(dashed(V1)) model and on two-mode van Genuchten(solid (V2)).

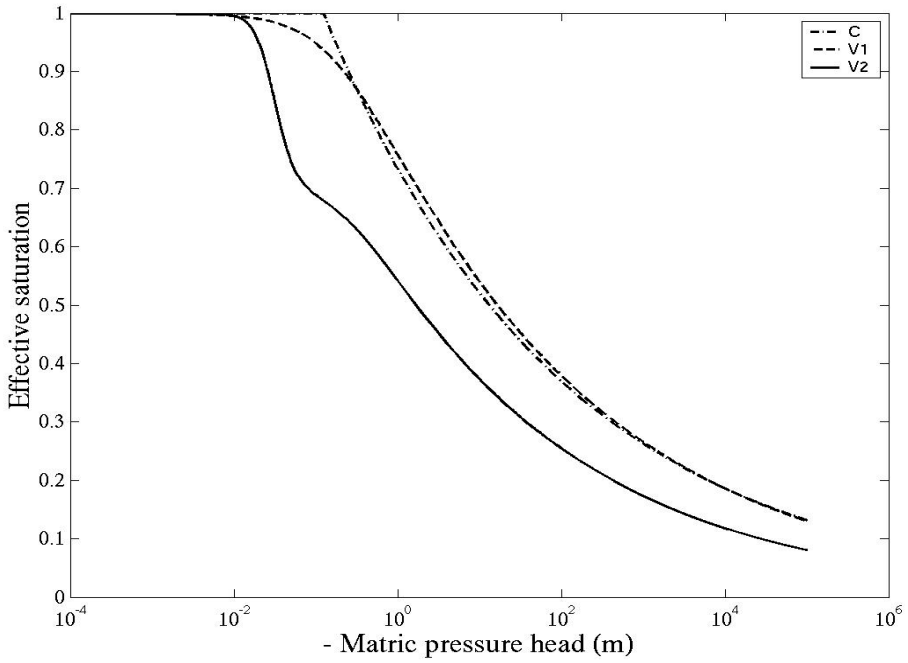

Figure 2.4.b Water retention curve. Legend as figure 2a.

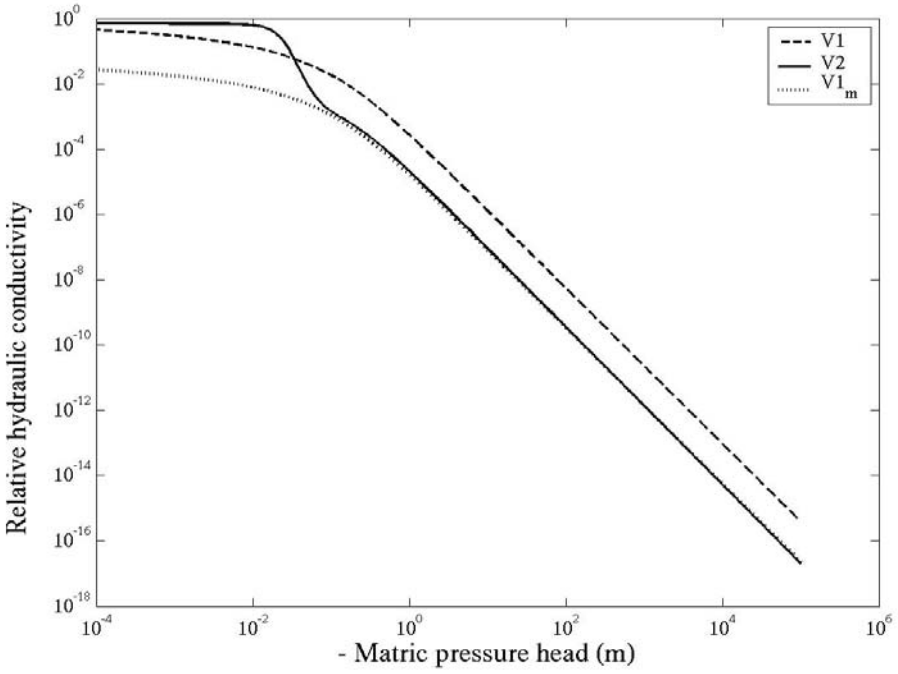

Figure 2.4.c Relative conductivity for a uni-mode pore system (dashed (V1)) and for a two-mode pore system (solid (V2)). By matching V2 to V1 when matric potential is at -100m, we can get the saturated hydraulic conductivity for the two-mode system.

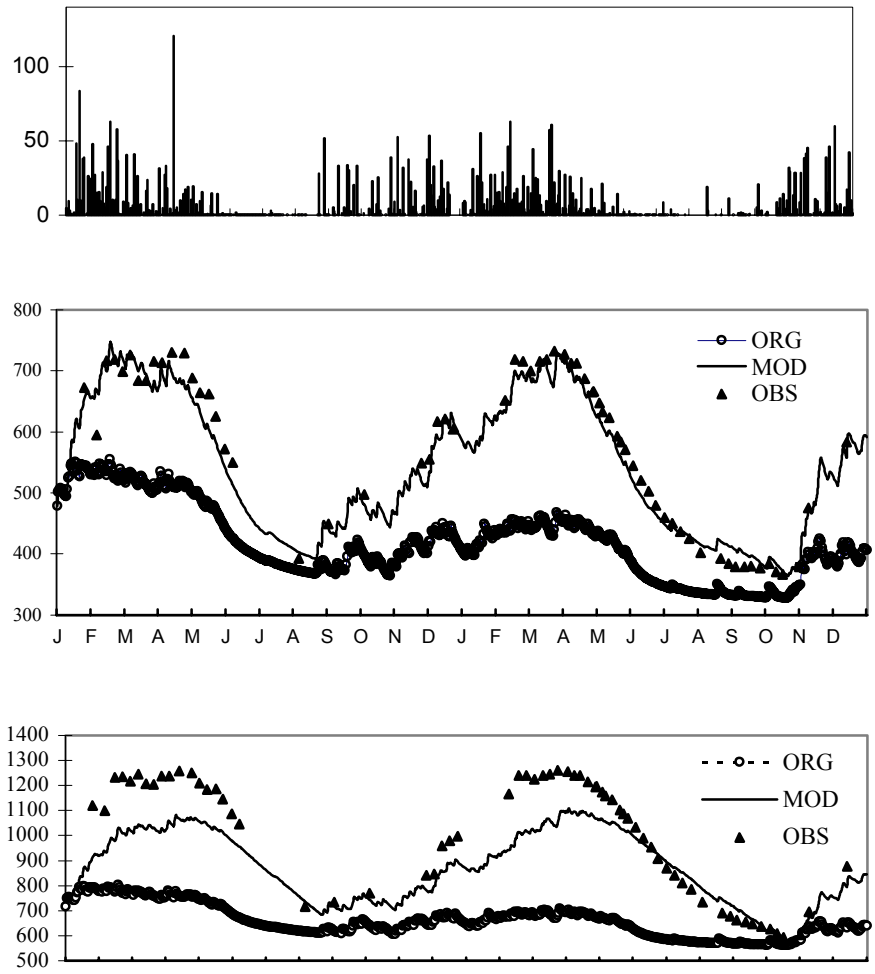

Figure 2.5.a. (upper panel) Precipitation in mm; 2.5b. (middle panel) 0-2 m soil water content in mm from Jan 1992 to Dec 1993; 2.5c. (bottom panel) 0-3.6m soil water content in mm from Jan 1992 to Dec 1993.

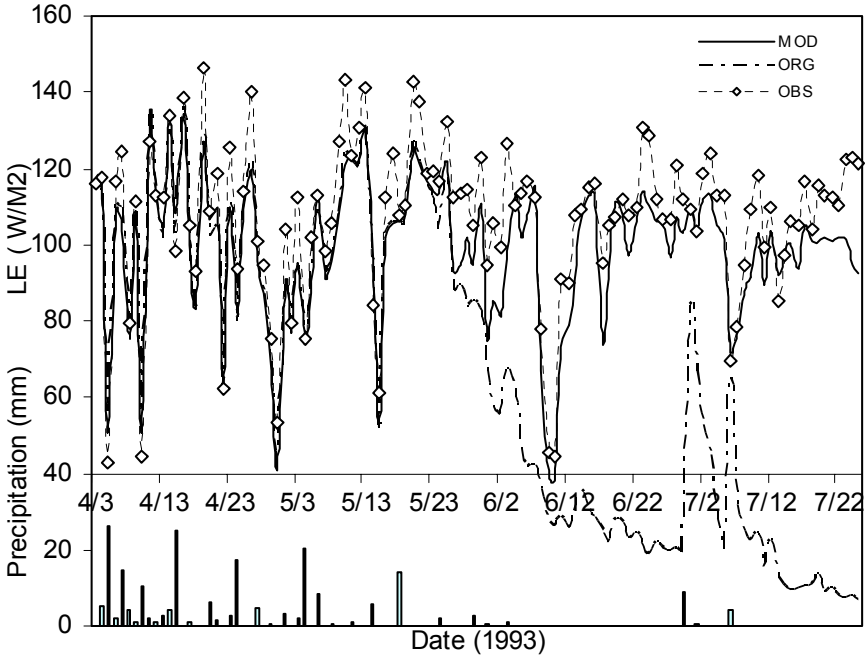

Figure 2.6. Latent heat fluxes from April 4 to July 26 in 1993.

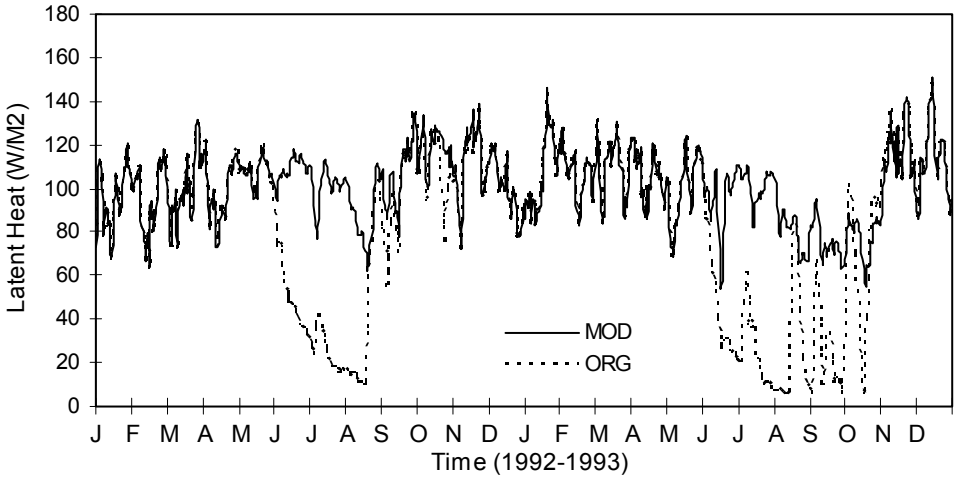

Figure 2.7. Latent head Fluxes from Jan 1992 to Dec 1993.

2.3 A new hydraulic scheme with soil structural effects for global modeling

2.3.1 Introduction

The previous section showed that the neglect of soil macropores in describing the hydraulic properties in the LSMs can cause substantial error in the predicted soil moisture for well-structured soils. The surface hydrological and energy balances of these soils can also be affected significantly. Consideration of soil macropores can improve the soil moisture simulation significantly. Therefore, effects of soil macropores should be included in LSMs.

Although the two-mode pore-size distribution scheme used in the previous section can efficiently capture some of the effects of macropores on soil hydraulic properties, it requires a significant number of inputs to determine its fitting parameters, hence is hard to apply to large scale simulations because the currently limited data sources. Since the existence of macropores primarily causes inflection of the hydraulic curves in near-saturation, a more practical treatment is to separate the inflected retention and conductivity curves into different regions so that each can be described by relatively simple equations. Such approaches have been shown to work in many soil-hydrological applications [e.g. Poulsen et al., 2002; Saxton et al., 1986; Chen et al., 1993]. It is also physically sound to divide hydraulic curves into different regions because the water in general fills soil pores in a systematic manner from smaller to bigger ones for equilibrium conditions. Hence which region a specific water-content belongs can be determined.

We present in this section is a newly derived hydraulic scheme in such a multiple region approach. The total soil porous area is conceptually divided into the matrix volume and the macropore volume. The hydraulic properties for each volume can be

denoted by simple equations. Instead of combining such simple equations into a single complicated one, we determine which equation to use according to the water content given that the water always fill the matrix pores first. Therefore, until the soil-water content exceeds the matrix volume, the macropores will have no effect on the flows in the soil. Through such an approach, the conventional uni-mode schemes and their texture-based parameter estimations can still be used for estimating the hydraulic properties of the water in the matrix domain, and the uncertainties introduced by the additional macropore-domain equations will not affect the estimation accuracy of the hydraulic properties for water content below the matrix volume.

It remains challenging work to quantify the parameters for the macropore hydraulic equations especially when for a large-area application. Nevertheless, the development of global soil databases in recent years can provide some useful information. Here, we also provided the parameter estimation based on globally available soil-measurement attributes from several global soil databases, i.e. the Data and Information System of the International Geosphere Biosphere Programme (IGBP-DIS) [Tempel et al., 1996], the Unsaturated Soil Database (UNSODA) [Leij et al., 1996] and the World Inventory of Soil Emission Potential (WISE), version 1.1 at International Soil and Reference Information Centre (ISRIC) [Batjes, 2002], in order to use the proposed scheme in climate models.

We then implemented the new scheme in the CLM and performed a global offline simulation with atmospheric forcing. An arbitrary hydraulic conductivity decay factor previously needed in the CLM to derive correct runoff is eliminated with the introduction of vertically distributed soil macropores. The simulated results are compared with that

from a standard CLM run with the same initial conditions and atmospheric forcing.

2.3.2. Scheme description

Soil matrix and macropores usually have different hydraulic effects on water in them. The soil pore space can be separated conceptually into matrix and macropores domains so that the total porosity can be represent as the sum of them as

$$P_{tot} = P_{ma} + P_{mi}. \tag{2.21}$$

where, P_{tot}, P_{ma} and P_{mi} are volumetric soil total porosity, macroporosity and microporosity respectively. The microporosity is taken as the portion of soil porous space that can be adequately explained by soil primary particles, the macroporosity the space that involves other soil properties such as aggregates that are dominated by factors other than soil texture. The partitioning can be either based on the value of matric potential, e.g. -10 kPa by Saxton et al. [1986], or their volumetric water content, e.g. 0.3 cm^3/cm^3 by Nimmo, [1997]. Here, we use the water content as the partitioning criterion.

The derived porosity based on the observed bulk density provided by the database of IGBP-DIS [Tempel, 1996] and a particle density of 2.65 g/cm^3 is used to evaluate the suggested value of 0.3 by Nimmo [1997]. The IGBP-DIS contains chemical and physical soil data derived from ISRIC's Soil Information System (ISIS) and the CD-ROM of the Natural Resources Conservation Service (ISDA-NRCS) for 131,472 samples, originating from 20,920 profiles that cover all the soil textural classes. All samples containing valid porosity are first extracted from the database. The samples are then grouped into difference texture classes according to the USDA criterion as shown in figure 2.1. The computational software package, the Trixcel, was used to determine the texture class a soil belongs to with any given percentages of the sand, silt and clay. The initially

extracted samples that have porosities more than two standard deviation away from the average porosity of that texture class are excluded. Finally, we retained 29923 samples for analysis. The basic statistics of the porosities of these samples are listed in table 2.3. The microporosity for soils in each texture class should be within the range of measured porosity but toward the low end of it [Nimmo, 1997]. The values are shown to increase with increased clay content except that of silt. It is reasonable to use a clay fraction related equation instead of a universal value as the critical point to partition the pore domain for different soils. Here, we propose

$$P_{mi} = 0.32 + 0.2 \cdot f_{clay}, \tag{2.22}$$

where, f_{clay} denotes the clay fraction of the soil and ranges from 0 to 1. This estimation gives a threshold water content value of about 0.32 cm^3/cm^3 for sand soils and about 0.42 for clay soils. The rest of the porosity is attributed to soil macropores with a maximum value of 0.25 for each texture class as the largest difference.

Theoretically, the capillary force makes P_{ma} remain zero until water in the matrix is saturated or $\theta \geq P_{mi}$, where θ is volumetric water content. Hence, the relative saturation of in matrix S_{mi} and in macropores S_{ma} can be represented as

$$S_{mi} = \frac{\theta}{P_{mi}}, S_{ma} = 0 \text{ , when } \theta \leq P_{mi} \text{; and} \tag{2.23}$$

$$S_{ma} = \frac{\theta - P_{mi}}{P_{ma}}, \; S_{mi} = P_{mi}, \text{ when } \theta > P_{mi} \tag{2.24}$$

Because the power functions by Campbell [1974] give reasonable descriptions of the retention and hydraulic conductivity relationships of water in compacted soils, thus are generally accepted to be adequate to describe the hydraulic properties in the matrix region [Clapp and Hornberger, 1978; Cosby et al., 1986; Saxton et al., 1986]. Here, we

Table 2.3. Basic statistics of the IGBP-DIS porosity sample for each soil texture class.

Texture class	Sample size	Average clay percentage	Average (range)	Standard deviation
Sand	725	3.1%	0.408 (0.321-0.577)	0.049
Loamy sand	1506	5.4%	0.430 (0.321-0.649)	0.071
Sandy loam	5776	10.4%	0.451 (0.321-0.638)	0.071
Loam	4384	18.7%	0.472 (0.325-0.638)	0.069
Silt Loam	5391	17%	0.478 (0.325-0.660)	0.065
Sandy clay loam	1716	26.1%	0.436 (0.325-0.577)	0.057
Clay loam	2590	32.6%	0.487 (0.342-0.619)	0.057
Silty clay loam	2851	33.1%	0.475 (0.343-0.608)	0.047
Sandy clay	326	40%	0.438 (0.332-0.558)	0.058
Silt	158	7.7%	0.488 (0.358-0.645)	0.061
Silty clay	1398	46.1%	0.495 (0.351-0.690)	0.057
Clay	3102	56.3%	0.518 (0.404-0.638)	0.056
Total	29923			

use them to estimate the hydraulic properties of water in this range, so that when $\theta \le P_{mi}$, retention curve and hydraulic curves can be represented as

$$\psi_{mi}(S_{mi}) = \psi_{mis} \cdot (S_{mi})^{-b}, \tag{2.25}$$

$$k_{mi}(S_{mi}) = k_{mis} \cdot (S_{mi})^{2b+3}, \tag{2.26}$$

where, ψ_{mis} and k_{mis} are the matric potential and conductivity at $\theta = P_{mi}$ respectively.

The current knowledge of hydraulic relationship of water in macropores is still limited due to the sparse measurements of field soils and the large variation of the available data. The hydraulic relationships of the water in the macropore domain are usually arbitrarily given. E.g. Clapp and Hornberger [1978] proposed a parabola to describe the ψ-S relationship for relative saturation S above 0.9. Saxton et al. [1986] suggested a linear ψ-θ relationship for soil domain above -10 kPa matric potential. Chen et al. [1993] used a linear k-θ relationship for the macropore domain. Since these equations give totally different curve shapes in describing the soil water hydraulic properties in the macropore region, it appears that how the matric potential and hydraulic conductivity drops with the decreases of soil water-content is not as critical as the determination of boundary values, i.e., the upper and lower limits. This is reasonable because the quick drop of matric potential and conductivity is over a small macropore moisture-range.

The UNSODA contains comprehensive measurements of the unsaturated soil hydraulic properties from contributions by individual scientists across the world [Leij, 1996]. Based on the general shape of the retention and hydraulic curves at the moisture range above P_{mi} as determined by equation (2.22) for most soil samples (not shown), the following retention and hydraulic functions are assumed

$$\psi_{ma}(S_{ma}) = \psi_{mis} \cdot (1 - \frac{\psi_{mis} - \psi_{mas}}{\psi_{mis}} S_{ma}{}^{2}), \quad \text{and} \tag{2.27}$$

$$k_{ma}(S_{ma}) = k_{mas} \cdot S_{ma}{}^{3}, \tag{2.28}$$

where ψ is the matric potential, k is the hydraulic conductivities. Subscript *mi*, *ma*, *mis* denote water in micropores, in macropores and at micropore saturation. The macropore conductivity, k_{ma}, approaches zero if macropore water content is small and approaches to saturated macropore conductivity, $k_{mas,}$ as macropores are close to saturation. The absolute value of the matric potential drops with increase of the water content in macropores and is only associated with the largest water-filled pores. Thus, the ψ and the k at specific soil-water content can be determined by the formulations of

$$\psi(\theta) = \psi_{mi}(S_{mi}) \text{ , when } \theta \le P_{mi} \text{, and} \tag{2.29}$$

$$\psi(\theta) = \psi_{ma}(S_{ma}) \text{, when } \theta > P_{mi} \tag{2.30}$$

and

$$k(\theta) = \left(\sqrt{k_{mi}} + \sqrt{k_{ma}}\right)^2, \tag{2.31}$$

respectively. The conductivity formula was derived from that of Mualem [1976] and the scheme of Ross and Semttem [1993] as shown in equation (2.5) and (2.6). Here, the k_{ma} equals zero when $\theta \le P_{mi}$ and the k_{mi} equals the k_{mis} when $\theta > P_{mi}$.

2.3.3 Parameter estimation for global application

Practical application of the proposed scheme requires determination of the parameters including the matrix hydraulic curve parameter b in equations (2.25) and (2.26) as well as the fitting parameters of ψ_{mi}s, ψ_{mas}, k_{mi}s, k_{mas} and either two of the P_{mi}, P_{ma} or P_{tot}. For a global application, it is necessary to relate all the parameters to routine

soil survey data. Given the current limitation of the data availability on a global scale, we only consider the soil texture for the matrix property estimation and derive the macropore properties based on a prescribed macroporosity.

The parameters *b*, known as the 'Clapp and Hornberger parameter', is only associated with soil matrix flow. Thus it should be adequately represented by the soil texture. The estimation scheme by Cosby et al. [1984] as shown in equation (2.14), which is the standard estimation scheme for *b* in the CLM, is tested against the value derived from the soil database of the IGBP-DIS. 22,270 of the soil samples that contains valid measurements of both water content at -33 kPa potential (θ_{33}) and water content at -1500 kPa potential (θ_{1500}) are extracted from the IGBP-DIS. For each soil the *b* is estimated from its clay content with equation (2.14). The observational *b* is estimated by its measured θ_{33} and θ_{1500} with the equation

$$b = \frac{\log(1500/33)}{\log(\theta_{33}/\theta_{1500})}. \tag{2.32}$$

The soil samples are then grouped into different textural class using the method described in previous section, and all the *b* values with a texture class are averaged. The comparison of the average of the observational and the estimated *b*'s for each texture class is shown in figure 2.8. The difference of the IGBP-DIS observational *b* and estimated *b* as percentage of the IGBP-DIS *b* is also illustrated. The values are listed in Table 2.4. It is shown that equation (2.14) adequately estimated the average IGBP-DIS value of *b* with a difference less 20% for all textural classes except for silt and silt loam soils. The small *b* value for silt soils is due to the small range of the size of their soil particles. The magnitude of *b* indicates how fast the matric potential will drop when soil wetness decreases. A large *b* means that the change of certain soil-water content involves

particles that cover a large size-range. The silt soils in the sample have narrow range particle-size distributions so that the *b*'s for them should be small. However, the current small sample size for silt soils is inadequate to derive a scheme that is valid for all soil classes. Given that the absolute value of their estimated *b*'s do not differ much from the observed ones because they are small, and silt is not a widespread soil type in nature, we still use equation (2.14) to estimate the constant *b*.

Table 2.4. Comparison of the parameter *b*'s based on observation and estimation for each texture class.

Texture class	Sample size	*b* (based on IGBP_DIS data)	*b* (estimated using Cosby et al. [1984])
Clay	1813	10.35	11.69
silty clay	1077	9.26	10.33
sandy clay	323	10.34	9.26
silty clay loam	1620	6.94	8.17
Silt	132	2.62	4.18
clay loam	2071	7.17	7.56
sandy clay loam	1526	7.06	7.03
silt loam	3383	4.15	5.66
Loam	3997	5.10	5.86
sandy loam	4421	4.26	4.62
loamy sand	1206	4.01	3.79
Sand	701	3.60	3.45

Because the water content of field capacity (θ_{33}) and wilting point (θ_{1500}) are generally measured on a routine basis and they normally fall into the range of matrix, the matric potential for filled micropores, i.e. P_{mi}, can be derived from them using equation (2.25) as

$$\psi_{mis} = -\psi_{sp} \cdot (\frac{P_{mi}}{\theta_{sp}})^{-b}; \tag{2.33}$$

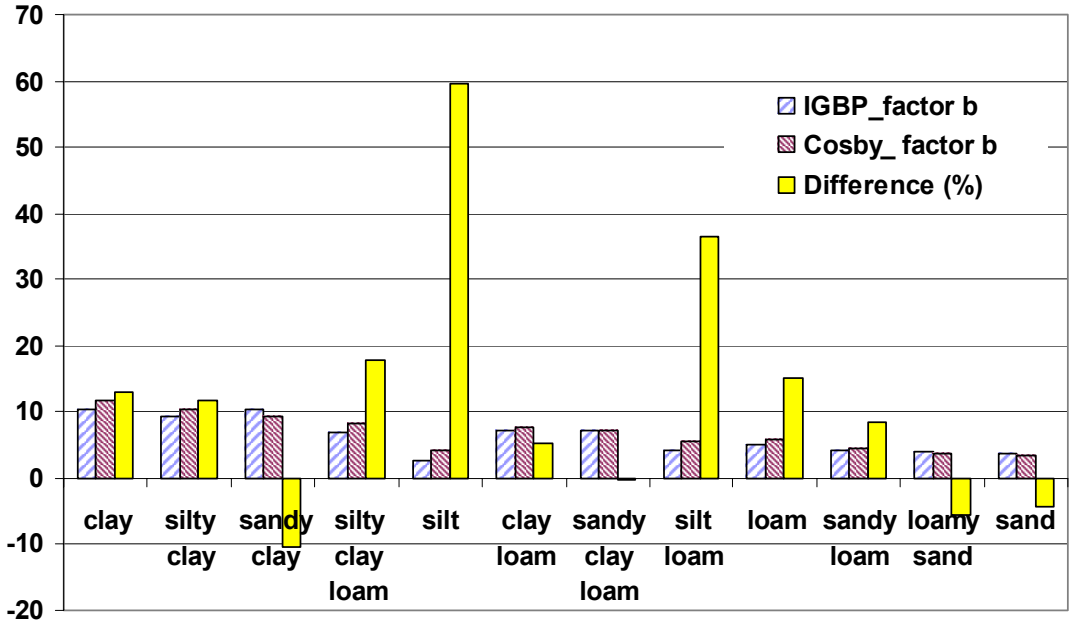

Figure 2.8. Difference of the *b*'s from IGBP-DIS observation and estimation using scheme of Cosby et al. [1984] for each texture class.

where ψ_{sp} and θ_{sp} are a pair of potential and water content values within the matrix range that can be either -33 kPa or -1500 kPa. The advantage is that the water content at lower matric potential, i.e. drier soils, can be estimated more accurately by soil texture that that at higher matric potential [Rawls et al., 1982]. For instance, we use a simple linear regression model with *%sand* and *%clay* as the predictors to estimate θ_{33} and θ_{1500} for 22,270 IGBP-DIS soil samples. The prediction accuracy R^2 is 0.40 for θ_{33} and 0.71 for θ_{1500} respectively. Here, we provide the regression equation for estimating θ_{1500} derived from the IGBP-DIS database

$$\theta_{1500} = 0.0336 + 0.35 \cdot f_{clay}, \qquad [\mathrm{cm}^3/\mathrm{cm}^3] \tag{2.34}$$

where the f_{clay} is the clay mass fraction and scales from 0 to 1.

The equation (2.13) is used in the CLM to estimate the saturated hydraulic conductivity k_{sat}. It was originally derived based on the laboratory-measured k_{sat}'s of

1448 soil samples taken from 35 locations in 23 states in the United States by Cosby et al. [1984]. Comparing its geometric average values for each textural class with values provided in Rawls et al. [1982], equation (2.13) overestimated saturated hydraulic conductivities for clayey soils significantly, e.g., its average value for clay is 12 times larger than that in Rawls et al. [1982]. The values in Rawls et al. [1982] range over a four orders of magnitude from 1.7×10^{-4} mm/s for clay to 7×10^{-2} mm/s to sand and these can be taken as the range of conductivity at micropore saturation. We fit these values with a simple equation to reproduce the same order of magnitude for each texture class using the middle value of the clay and sand fractions of each texture class,

$$k_{mis} = 5\times10^{-3}\cdot\exp(2.05\cdot f_{sand} - 7.37\cdot f_{clay}) \ . \ \text{[mm/s]} \tag{2.35}$$

The microporosity has been defined as in equation (2.22). Either the total porosity P_{tot} or the macroporosity P_{ma} also need to be determined. Many schemes have been proposed to estimate the total porosity from soil texture and other soil attributes [e.g., Cosby et al., 1986; Rawls and Brakensiek, 1982; Vereecken et al., 1989; Saxton et al., 1986]. The macroporosity can be taken as the difference between the total porosity and the microporosity. However, large discrepancies exist between the estimated P_{tot} using different schemes. Those derived from compacted soil should not be used for the well-structured soils. Table 2.5 presents the estimated average total porosity for IGBP-DIS soil samples that containing valid porosity measurements for each soil texture class using the scheme in Cosby et al. [1984], which is

$$P_{tot} = 0.489 - 0.126\cdot f_{sand} \tag{2.36}$$

where the f_{sand} is sand fraction scaled from 0 to 1. The equation (2.36) is the standard porosity estimation in the CLM. Compared to the measured values listed in table 2.3, the

Table 2.5. Statistics of the estimated porosities for the IGBP-DIS soil samples using the scheme by Cosby et al. [1984] for each soil texture class.

Texture class	Sample size	Average sand percentage	Average (range)	Standard deviation
Sand	725	91.5%	0.373 (0.364-0.381)	0.004
Loamy sand	1506	81.3%	0.386 (0.377-0.400)	0.005
Sandy loam	5776	64.1%	0.408 (0.384-0.434)	0.01
Loam	4384	41.1%	0.437 (0.423-0.46)	0.008
Silt Loam	5391	18.8%	0.466 (0.429-0.489)	0.014
Sandy clay loam	1716	56.3%	0.407 (0.384-0.434)	0.01
Clay loam	2590	31.6%	0.449 (0.432-0.464)	0.009
Silty clay loam	2851	8.9%	0.477 (0.464-0.489)	0.007
Sandy clay	326	50.2%	0.425 (0.413-0.432)	0.005
Silt	158	7.5%	0.479 (0.466-0.488)	0.005
Silty clay	1398	7.1%	0.48 (0.464-0.489)	0.006
Clay	3102	17.8%	0.467 (0.432-0.489)	0.014
Total	29923			

Cosby scheme gives a much narrower within-class porosity range and generally underestimates the total porosity.

The volume of macropores is primarily associated with the shape, size, amount and distribution of the soil aggregates, which can not be adequately represented by soil texture. Additional predictors to account for soil structure have to be included in order to produce accurate estimation of the soil porosity for well-structured soils. A common way is to use the content of soil organic matter (OM) or organic carbon (OC) as an indicator of the macropores [e.g. Vereecken et al. 1989; Rawls and Brakensiek, 1989; Wösten, et al., 1999]. Normally, the higher the soil organic carbon content, the higher the macroporosity because the soil OC increases the soil aggregation and associate pore space [Holis et al., 1977; Paustian et al., 2000; Six et al., 2000]. Nevertheless, we could not establish any credible relationship between the OM content and the porosity quantitatively from their measured values in the IGBP-DIS database. Perhaps the soil porosity is affected by too many other factors such as the earth-worm activity [Hendrix et al., 1986; Young and Ritz, 2000], tillage condition [Six et al., 2000] and location of the soil on a hill-slope [Mohanty and Mousli, 2000], and incorporation of plant material [Oyedele et al., 1999]. Some of these factors may have been correlated with the measured OM as many of the above factors can change the OM content in soils, but apparently not all. Hence, we can still regard OM as a strong indicator of soil structure but only in a qualitative fashion. An accurate value of macroporosity should be based on direct measurement. When such is not available, it should be based on the availably statistical information and assigned a value between 0 and 0.25, which is based on the range of the measured soil porosities in the IGBP-DIS. For large scale applications, it is plausible to

link the soil macropores directly with the local biological activity and climate conditions. Although it is difficult to validate such an assumption quantitatively as yet, it is plausible to use it in the absence of more information.

The saturated conductivity for water in soil macropores k_{mas} is close to zero if a soil contains only a few macropores, but can be in orders of magnitude larger than the k_{mis} of that soil if the macropore amount is substantial. The UNSODA database provides 234 soil samples with measured saturated-conductivity. The largest value is around 1.5 mm/s associated with a substantial OM content of above 20% of the soil mass. The value can be taken as the k_{mas} of soils with the largest possible macroporosity of 0.25. A simple function is proposed to link the k_{mas} to the P_{ma} directly as

$$k_{mas} = (\frac{P_{ma}}{0.2})^2, \quad [\text{mm/s}] \tag{2.37}$$

so that k_{mas} is 1.5 mm/s for a P_{ma} of 0.25 and 0 for a P_{ma} of 0.

The ψ_{mas} is the air entry potential of the largest soil pores. It should equal the ψ_{mis} if P_{ma} is zero, otherwise higher than ψ_{mis}. The ψ_{mas} is inversely proportional to the radius of the largest pores according to the capillary relation

$$\psi = -\frac{2\gamma \cos\alpha}{r}, \tag{2.38}$$

where r is the effective pore radius, γ the surface tension between water and the air and α the contact angle. The combined term of $2\gamma cos\alpha$ is about 0.13 mm kPa for soils [Nimmo, 1997; Chen and Schnitzer, 1976], i.e., the matric potential is equivalent of -0.13 kPa when water fills a pore with radius of 1 mm. Shown in table 2.6 is the summary of observed air-entry suction classified by soil texture. The within-class variation is much larger than the between-class variation, indicating that the air-entry suction (negative of

the potential) is much more dependent on macroporosity than in texture. Thus, we propose an equation below for deriving the ψ_{mas} from the $P_{ma,}$as

$$\psi_{mas} = \frac{\psi_{mis}}{1. + 50\sqrt{P_{ma}}} \quad . \tag{2.39}$$

so that a P_{ma} of 0.25 can lower the air-entry suction to 1/25 of its matrix saturation suction.

Table 2.6. Air-entry potential classified by soil texture.

Texture class	Sample size	Geometric mean, cm	±one standard deviation about the mean, cm
Sand	762	7.26	1.36-36.74
Loamy sand	338	8.69	1.80-41.85
Sandy loam	666	14.66	3.45-62.24
Loam	383	11.15	1.63-76.40
Silt Loam	1206	20.76	3.58-120.4
Sandy clay loam	498	28.08	5.57-141.5
Clay loam	366	25.89	5.80-115.7
Silty clay loam	689	32.56	6.68-158.7
Sandy clay	45	29.17	4.96-171.6
Silty clay	127	34.19	7.04-166.2
Clay	291	37.30	7.43-187.2

From Maidment [1992] p. 5.14

2.3.4 Simulation of unsaturated hydraulic conductivities

The above scheme is proposed for a large scale application, so it is preferable to be validated with global datasets. The retention curve determines the field capacity, permanent wilting point as well as the available water content for plant to extract. The parameter b is the most important determinant for these attributes. As it has been validated in previous section, we do not further discuss the retention scheme.

The measurements of unsaturated hydraulic conductivities are used to test the hydraulic scheme. The field-measured pairs of hydraulic conductivity k and soil

volumetric water content θ of 4071 points from 192 soil profiles are extracted from the UNSODA database. Each extracted soil contains at least 10 pairs of measured *k*-θ. The number of the extracted soil samples is listed in table 2.7.

Table 2.7. Number of the samples extracted from the UNSODA database.

DATA	Sandy soils	Loamy soils	Clayey soils
UNSODA, 192 soils	57	92	43

Sandy soils: sand;
Loamy soils: loamy sand, sandy loam, loam, silt loam, and silt;
clayey soils: sandy clay loam, silty clay loam, clay loam, sandy clay, silty clay, and clay.

Figure 2.9 compares the estimated *log(k)* based on the standard CLM scheme, i.e., equations (2.10) to (2.14), with the measured values. Figure 2.10 compares the estimated *log(k)* using the two-region scheme (TRS) describe in previous section with the measured *log(k)* at measured water-content points of selected soils. Prediction accuracy was evaluated using the measured hydraulic conductivity data from UNSODA. The root mean square error (RMSE) was used as the measure of prediction accuracy.

$$RMSE = \sqrt{\frac{1}{N}\sum_{i=1}^{N}(X_{i,measured} - X_{i,predicted})^2} \quad . \tag{2.40}$$

The smaller the RMSE, the higher the prediction accuracy. The prediction by the TRS (RMSE = 3.15) is some what better than that of the standard CLM scheme (RMSE = 3.79).

The largest error of the TRS came from the estimation of the k_{mis}. If we derived the k_{mis} by fitting a measured value in the matrix range ($\theta < P_{mi}$), the prediction accuracy can be improved substantially (RMSE = 1.48) as shown in figure 2.11. Figure 2.12 shows the estimated *log(k)'s* by TRS in the moisture range larger than P_{mi}. The conductivities in the macropore range are controlled by the relative water content in macropore as well as

the saturated conductivity of the matrix flow. The P_{ma} and k_{mas} for each soil use its maximum measured values, and k_{mis} derived from a mid-point measurement. 771 points from 90 soils are extracted. The proposed equation (2.28) fits to the measurement hydraulic curve adequately with a prediction parameter $R^2 = 0.82$.

The above results indicate 1) the TSR captures the conductivities in the high moisture range reasonably, 2) it reduces the error in estimating the hydraulic conductivities at the drier moisture range as well compared to the Cosby scheme and 3) a more accurate k_{mis} description would increase the prediction accuracy substantially.

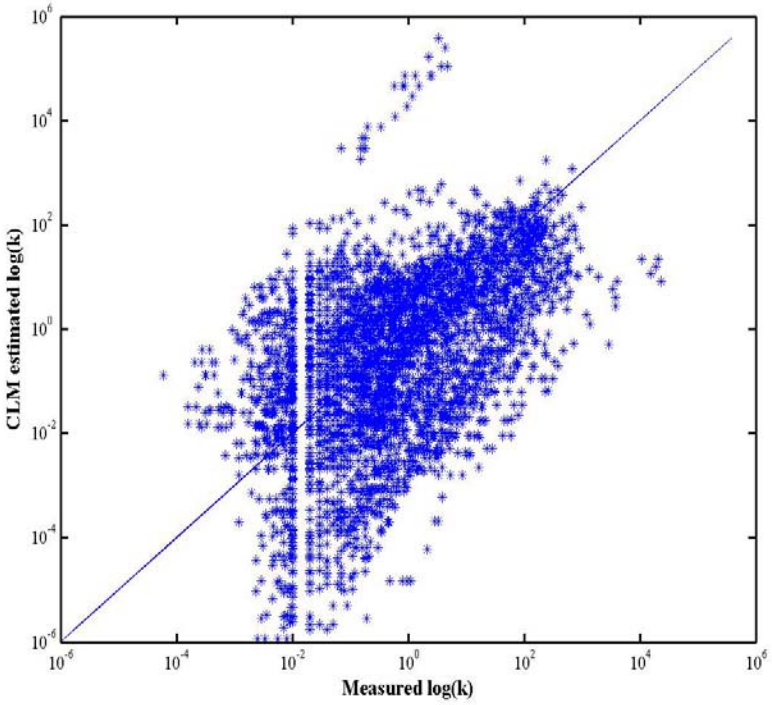

Figure 2.9. Estimated versus measured hydraulic properties for the 4071 water content versus k points of 192 UNSODA soil samples using the scheme of Cosby et al. [1984].

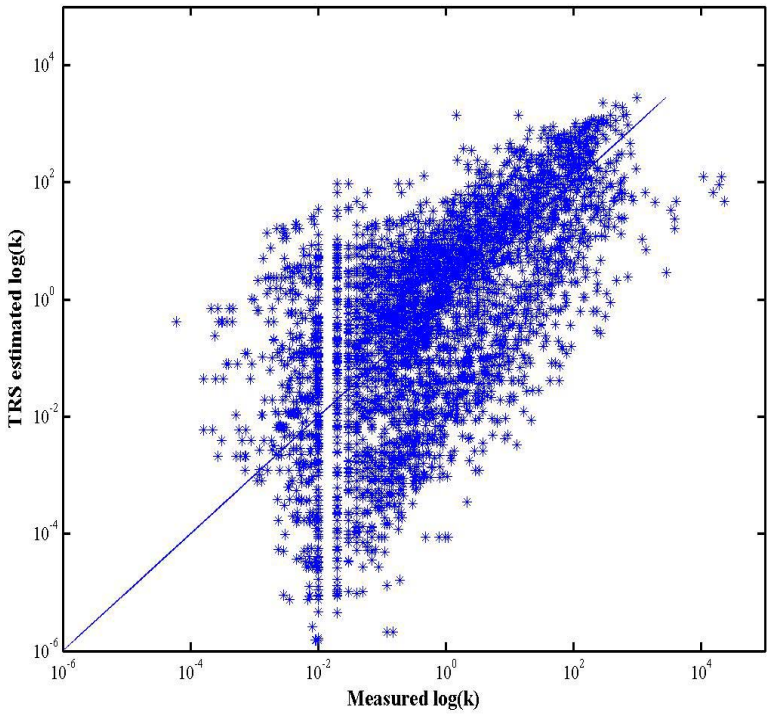

Figure 2.10. Estimated versus measured hydraulic properties for the 4071 water content versus k points of 192 UNSODA soil samples using the scheme proposed in this section.

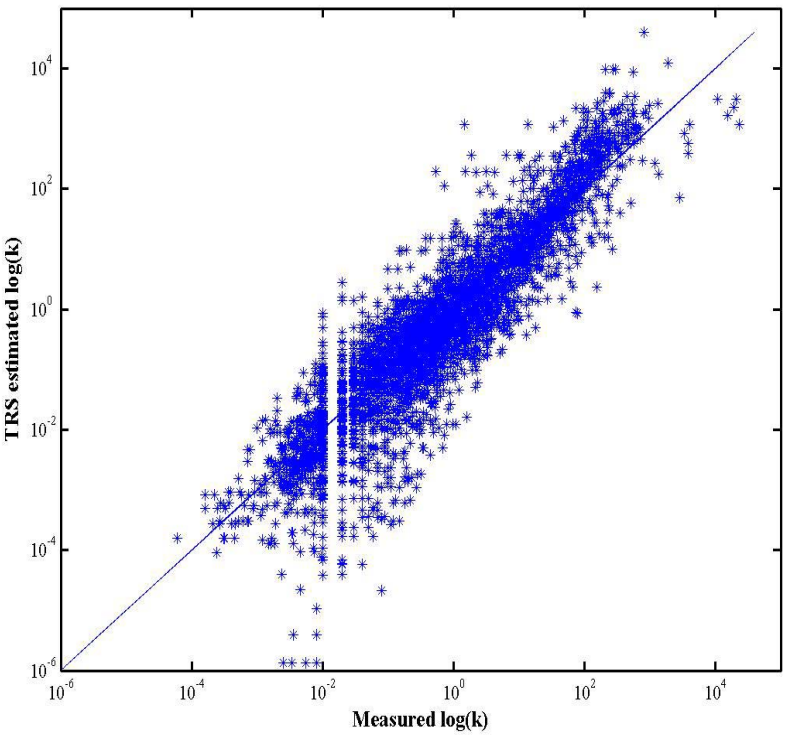

Figure 2.11. The same as figure 2.10 but for each soil sample using a random fitting point in the matrix moisture range.

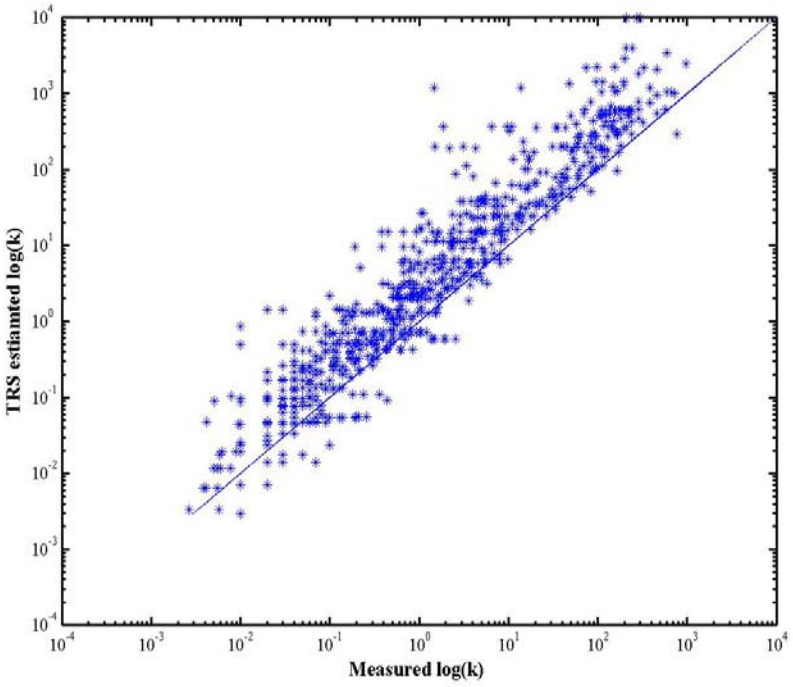

Figure 2.12. Measured versus observed hydraulic conductivities for moistures larger than the microporosity (771 points from 90 soils).

2.3.5 Preliminary results from inclusion of the new scheme into the CLM

We implement the proposed scheme into the CLM. The CLM has a 10-laryer soil with various thicknesses for each layer. Its current hydraulic scheme uses equation (2.10) to (2.14) based on the hydraulic model in Campbell [1974] and parameter estimation in Cosby et al. [1984]. For each grid cell, the soil texture is needed as input. The global distribution of soil texture for each soil layer was derived from the Global Soil Data Task [2000]. The CLM introduced a TOPMODEL concept-based runoff scheme [Dai et al., 2003]. The saturated hydraulic conductivity is assumed to decrease exponentially along the soil depth with a prescribed decay factor as

$$k_{sat} = k_{sat,surface} \exp(-\frac{z}{z^*}) \tag{2.41}$$

where k_{sat} is the saturated hydraulic conductivity at depth z, $k_{sat,surface}$ is the saturated conductivity at the surface, and z^* is the length scale for the k_{sat} decrease and is assumed 500 mm in the CLM. The exponential vertical-decay of the k_{sat} is a prerequisite TOPMODEL assumption as to constrain water to flow laterally down hill-slopes. However, such an arbitrary constraint, although it can produce correct runoff generation on a catchment scale, may underestimate the vertical transport of water in soil for surface evapotranspiration. It is preferable to replace such an arbitrary factor with a meaningful physical description. The k_{sat} vertical decay assumption is associated with the fact that soil macropores are abundant at the surface but sparse in deep soils. A proper description of the vertical profile of the soil macroporosity would capture the vertical decay feature of k_{sat} more realistically.

Application of the TRS globally requires a prescription of the distribution of soil macropores for each soil layer. We have discussed earlier that the abundance of soil

macropores is associated with soil organic matter content which is determined largely by the biological activities and root penetration [Young and Ritz, 2000]. Thus, a connection could be inferred between the soil macropores and the root properties. To assess such a connection, The World Inventory of Soil Emission Potentials (WISE) soil database developed at the International Soil Reference and Information Centre (ISRIC) [Batjes, 2002] is used. The WISE database contains complicated data and profile description for 4382 soil profiles from 123 countries. Each measured soil property consists of several classes. A one-way analysis of variance (ANOVA) was performed for the surface dry bulk density, which indicates the total porosity, to determine if it varies significantly over the classes of roots and soil texture. Two root properties, the overall size of the roots and the abundance of the roots, are examined using a code [FAO/ISRIC, 1990 p. 63] as shown in Table 2.8. The texture classes are according to the USDA definition as shown in figure 2.1.

Table 2.8. Class description of the presence of roots in the WISE databases.

a)Abundance of roots (expressed as number of roots per square decimeter)

Code	Quantity	Description
O	No roots	0
V	Very few	1-20
F	Few	20-50
C	Common	50-200
M	Many	>200

b) Description of root sizes.

Code	Description	Diameter (mm)
V	Very fine	< 0.5 mm
F	Fine	0.5 - 2 mm
M	Medium	2 – 5 mm
C	Coarse	> 5 mm
X	All	Very fine roots to coarse

Table 2.9. ANOVA for dry bulk density.

Bulk density by classes of	Root sizes	Root abundance	Soil texture
F factor	22.68	64.01	11.33
P values	<0.0001	< 0.0001	<0.0001

Table 2.10. The statistics of bulk density for each root-abundance class.

Bulk density by root abundance	N	Mean	SD	SE
C	1226	1.423	0.227	0.0065
F	1895	1.484	0.237	0.0054
M	1011	1.346	0.263	0.0083
O	161	1.494	0.248	0.0195
V	335	1.415	0.259	0.0141

The results are shown in Table 2.9. The *F* is the ratio of the parameter variance between groups to the parameter variance within groups. A large value of *F* indicates a significant change in the parameters distribution from class to class of the descriptor. A small *p* value indicates that the class to class variations of the bulk density are much stronger than the within class variations. Based on the resulting *F* and *p* values, the bulk density varies the most significantly over different class of "root abundance". Table 2.10 shows the statistics of the bulk density for each root-abundance class. The increase of root abundance, i.e. from Many (M) to No roots (O), is associated with decrease of bulk density, and thus increase of soil porosity. Given that the microporosity is determined primarily by soil texture and there is no obvious correlation between the soil texture and root abundance being found (not shown), large portion of the variation of the bulk density is thus contributed mainly by the macroporosity. Therefore, it is plausible to define the macroporosity of a soil based on its roots. To confirm such a hypothesis, we apply the same statistical analysis to the soil organic carbon content (table 2.11 and table 2.12). The

root abundance is the strongest factor to affect the OC content, and the magnitude of the OC content for root-abundance class of many roots (M) is above 4 times of that for class of no roots (O). Given the strong correlation between the soil macropores and the soil organic matter, Our hypothesis holds.

Table 2.11. ANOVA for soil OC content.

OC by classes of	Root sizes	Root abundance	Soil texture
F factor	17.07	132.81	6.21
P values	<0.0001	< 0.0001	<0.0001

Table 2.12. The statistics of soil OC content for each root-abundance class.

OC by root abundance	N	Mean	SD	SE
C	1226	1.070	1.481	0.0423
F	1895	0.718	1.233	0.0283
M	1011	2.016	2.329	0.0732
O	161	0.472	0.814	0.0642
V	335	0.523	0.639	0.0349

Neither the abundance nor the sizes of roots has been explicitly described in climate models. They can be inferred by the root biomass which is associated with the above-ground biomass and biomes as grasses < semi-shrubs < shrubs < trees [Schenk and Jackson, 2002; Jackson et al., 1997]. Based on it, we currently simply assign the macroporosity as 0.2 cm^3/cm^3 for forests soils, 0.1 cm^3/cm^3 for grasses and crops soils, 0.05 for shrubs soil, and 0 for bare soils. Such a simple assignment can be refined later when more information about the soils and roots is available.

In the CLM, a conceptual vertical distribution of roots is incorporated to better simulate the water available for plant extraction [Zeng et al., 1998]. We assume a similar vertical distribution of the macroporosity of a soil based on this root distribution pattern,

i.e. vertically decay along the soil depth. It is given as

$$P_{ma}(z) = p_{ma}(0)\exp(-\frac{z}{a}), \tag{2.42}$$

where $P_{ma}(z)$ is the macroporosity at soil depth z, $P_{ma}(0)$ is the surface macroporosity, a is a decay factor. It is now assumed that $a = 150$ mm for all soils. The assumption of a vertical decay of soil macroporosity is consistent with the observed vertical decay of soil organic carbon whose distribution is affected by the vertical root distribution [Jobbágy and Jackson, 2000].

We perform two global offline runs forced by the atmospheric data from the NCEP/NCAR Reanalysis [Kalnay et al., 1996; Kistler et al., 2001] to assess the effect in surface hydrology by the new hydraulic scheme. One is the standard CLM2 and the other is the CLM2 with the proposed TSR. For simplicity, we denote the standard CLM2 run as "ORG" and the other as "MOD" in the following. Results for 7 years from January 1985 to December 1995 are produced from both runs. The initial condition for both uses the equilibrium state of MOD which was obtained by a 10-yr spinup period. All the output variables are monthly averages.

Figure 2.13 shows differences between the estimated surface porosity using the original scheme versus that using the modified scheme. The surface porosities by MOD are distinctly larger than that by ORG in regions dominated by forests, i.e. the Amazon basin and the Congo basin, by above 0.15 cm^3/cm^3 of difference, showing the contribution of soil macropore contribution to the total porosity in MOD. Because the macroporosity decays rapidly with the soil depth, at 1 m soil depth, the porosity by MOD becomes slightly lower than that by ORG by about 0.05 cm^3/cm^3 in most regions except in the tropics. The difference is attributed to the different porosity-soil textural

relationship of ORG and that of MOD.

Table 2.13 compares the annual water budget at the land surface by MOD and ORG respectively for 14 vegetated land regions. The values presented are 3-yr averages from 1992 to 1994. The simulated canopy evaporation and ground evaporation differ little between the two cases. The evaporation over Amazon, i.e. 50% of annual precipitation, is overestimated due primarily to the treatment of precipitation as large scale precipitation. Such a treatment overestimates canopy intercepted water amount during raining period, thus exaggerates the canopy surface evapotranspiration. Compared to ORG, MOD generally decreases the runoff generation and increases the transpiration through the canopy. The most prominent changes are in tropical regions that have the highest annual precipitations, e.g. Amazonia, central Africa and Brazil, in which about 4% of annual precipitation that is lost as runoff in the ORG is contributed to increase transpiration. MOD increases the annual transpiration in the Amazonia by about 50% of that of the ORG. Regions outside of the tropics show much less difference in all their hydrological fields in the two runs as expected fro lower annual precipitation because soil macropores have little effect on water if the soil moisture is less than the microporosity.

The Amazon basin and the Congo basin are selected for further discussion. The Amazon simulated values are the averages of the simulated points within the squares of 10˚S to equator latitude and 70˚W to 50˚W longitude. The Congo basin values are the averages within 10˚S to 5˚N and 70˚E to 50˚E. Both have a primary vegetation type of evergreen forest with fractional coverage larger than 85%, so that both have increased porosity at the surface contributed by macropores in MOD.

The annual pattern of the precipitation forcing over the Amazon (figure 2.14)

shows an alternative dry season, i.e., from May to September, and wet season, i.e., from October to April. The precipitation seasonality is substantial with a monthly average rate above 9 mm/day in the wet season rate and below 3 mm/day in the dry season. The

Table 2.13. Comparison of the annual regional surface water budget by ORG and by MOD averaged over 1992 to 1994. ET and runoff are presented as fraction of the precipitation.

	Precipitation	Canopy evaporation Fraction of P		Canopy transpiration Fraction of P		Ground evaporation Fraction of P		Total runoff Fraction of P	
	(mm/yr)	**ORG**	**MOD**	**ORG**	**MOD**	**ORG**	**MOD**	**ORG**	**MOD**
Eastern Siberia	376.652	0.27	0.27	0.12	0.13	0.24	0.23	0.39	0.38
Western U.S.	350.183	0.15	0.15	0.12	0.15	0.48	0.47	0.30	0.29
Central U.S.	720.309	0.27	0.27	0.19	0.24	0.36	0.35	0.21	0.18
Eastern U.S.	994.739	0.28	0.28	0.16	0.19	0.25	0.25	0.32	0.29
Europe	718.446	0.21	0.21	0.18	0.21	0.23	0.21	0.39	0.38
Central America	1845.494	0.40	0.40	0.07	0.10	0.22	0.22	0.31	0.29
Amazonia	2080.385	0.50	0.50	0.07	0.11	0.15	0.15	0.28	0.23
Central Africa	1567.411	0.50	0.50	0.10	0.15	0.24	0.24	0.16	0.12
Brazil	1306.866	0.43	0.42	0.12	0.17	0.28	0.27	0.18	0.13
Sahel	948.389	0.30	0.30	0.09	0.12	0.41	0.42	0.20	0.17
Southern Africa	752.602	0.39	0.39	0.13	0.18	0.37	0.36	0.13	0.10
Indochina	1527.966	0.25	0.25	0.07	0.11	0.39	0.38	0.29	0.27
Sahara Desert	78.931	0.03	0.03	0.01	0.01	0.98	0.97	0.16	0.14
Australia	242.409	0.08	0.08	0.13	0.14	0.73	0.76	0.11	0.09

precipitation in the Congo Basin shows two peaks in a year with a very severe dry period around June and a less severe dry period in December and January. The wet periods are between the two dry periods. The second annual wet period of about 6 mm/day has slightly higher precipitation than the first one.

Figure 2.15 compares the simulated transpiration by MOD and ORG respectively for the two regions. CLM determines transpiration to occur only through dry leaves so that its monthly average during wet periods is smaller than that during dry periods. MOD show larger transpiration rates as well as extended transpiration period in both regions compared to the ORG for all simulation years. The Amazon has a maximum monthly value around 1.5 mm/day in MOD and around 1 mm/day in ORG while the Congo has around 1mm/day and 0.6 mm/day respectively. The increase of their maximums is consistent with their increase of annual transpiration.

Compared to the ORG, The surface runoff (figure 2.16) in both regions are reduced by MOD. The decrease of runoff is less evident in Congo than in Amazon and is most prominent during periods of highest precipitation in both in a year. The reduction of surface runoff indicates that MOD allows more water to penetrate into soil in the wet season. This is associated with the increased porosity and the saturated hydraulic conductivity at the surface provided by MOD.

Shown in figure 2.17 and 2.18 are the simulated soil water storage for upper layers (surface - 1 m depth), and lower layers (2 m – 4 m depth) from MOD and ORG for both regions respectively. The upper water store in MOD is higher than that in ORG during wet periods and is comparable or lower during dry periods in both regions. The higher water storage is associated with the increased total porosity contributed by

macropores, so that more water can be loaded into the surface soil at saturation during precipitation. The slightly decrease in surface water store in dry periods is attributed to the slightly lower value of the water content at the permanent wilting point in MOD than that in ORG as to match the global observation data in the IGBP-DIS database. The lower water storages from MOD and ORG show much larger difference than that of the upper layers. In both regions, the storage throughout the simulation period is substantially larger in MOD than that in ORG. The initial water storage is too high for the ORG run, so it keeps decreasing until reaches a lower equilibrium content after about 3 years. The increased lower-layer storage is attributed to the increased hydraulic conductivity after eliminating the conductivity decay-factor in MOD, so that water can reach deeper soil and store longer for plant extraction in dry season instead of lateral drainage. In the case of ORG in both regions, their lower-layers are maintained at constant low water contents, far lower than the field capacity. That is not available to plants.

Figure 2.19 compares the subsurface runoff from both runs for both regions. The subsurface runoff occurs below the soil surface and depends on both soil moisture and hydraulic conductivity. The annual pattern of both runs in good agreement with each other, but the peak values of a year are decreased by MOD by a small amount in Amazon and by more one in Congo basin, which is associated with its smaller increase in the total soil water storage than that in Amazon. The less intensive precipitation during dry period in Congo also contributes to its larger decrease of runoff. In Amazon, years, e.g. 1992 and 1993, with less precipitation have a larger decrease in subsurface runoff than have normal years.

The above results show that the new scheme captures the net effect of soil

macropores to allow the water incident at the surface to penetrate downward faster and be retained longer in deeper soils where the macropores are rare. The surface runoff is thus decreased. The increased soil water penetration increases both wet and dry season water storage and makes more water available for transpiration especially during the dry season. Although the simulated runoff generation is decreased by the new scheme, its annual cycle and magnitude is still reasonably captured by the assumed macropore profile along the depth. The new scheme gives a more realistic description of the effects of soil macropores on the soil hydrology than does the original scheme.

2.3.6 Conclusion

The section proposes a practical scheme to represent the effect of soil macropores on the soil-water hydraulic properties for use in climate models. This scheme is based on the basic idea that the macropores introduce an inflection in the soil-water retention and conductivity curves in the moisture range near saturation and that the water fills soil pores systematically from the smallest to the largest according to the capillary theory. The whole soil porous space is divided into two regions: the matrix region and the macropore region, each with its own porosity. The retention and conductivity for each are calculated separately and combined in a logical way. The introduced parameters were either derived from global soil databases or arbitrarily defined based on current qualitatively analysis. Its application in the CLM shows reasonable results.

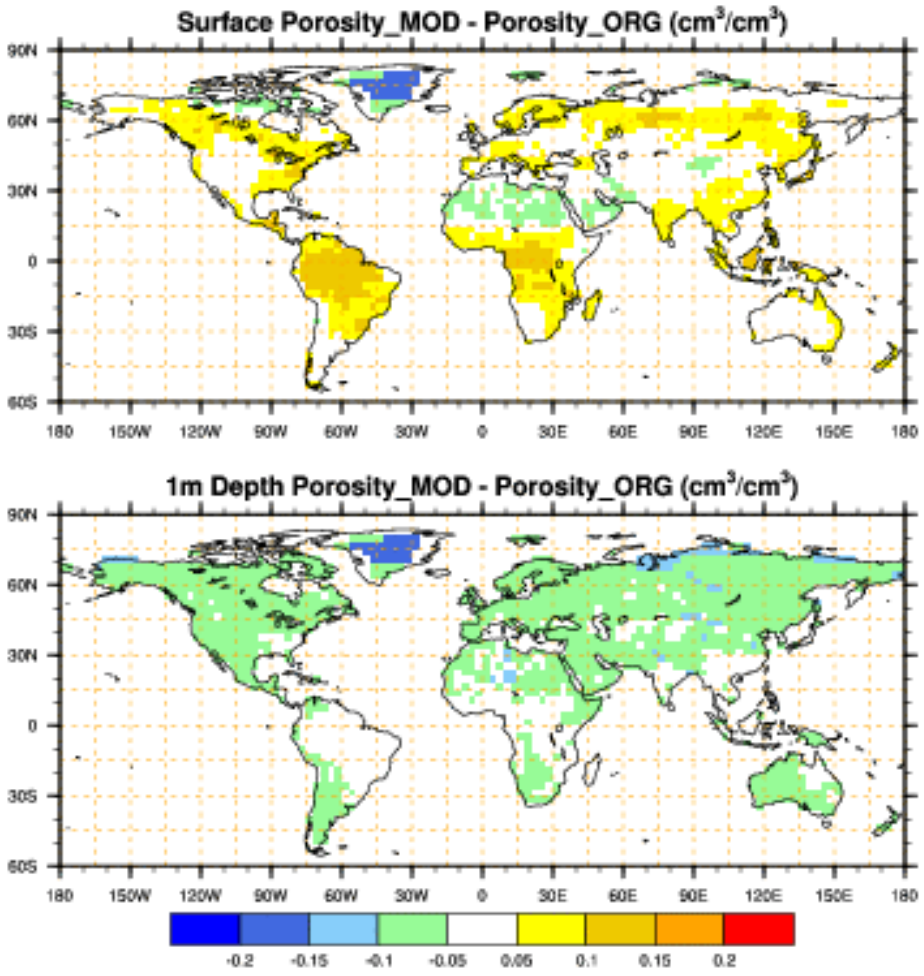

Figure 2.13. Differences of the estimated surface (upper) and 1m depth (lower) volumetric soil porosity by the original (ORG) and modified (MOD) cases.

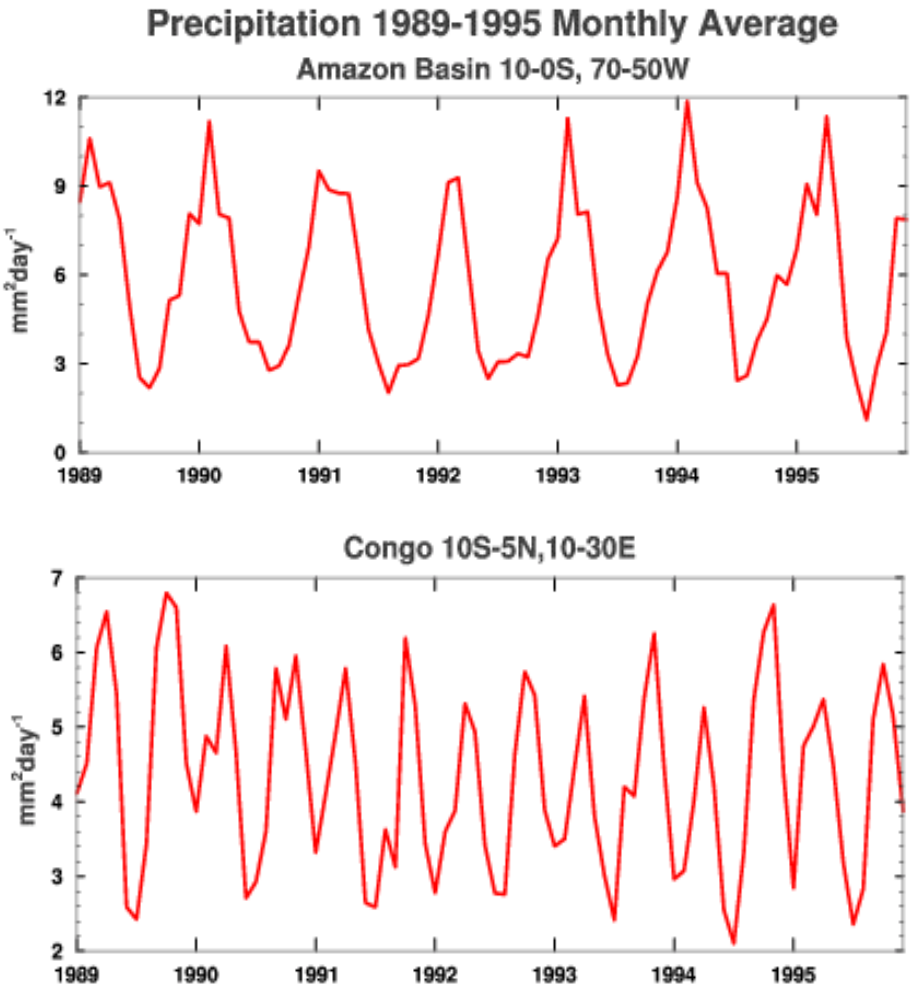

Figure 2.14. Monthly mean of precipitation for the Amazon basin (upper) and the Congo basin (lower)

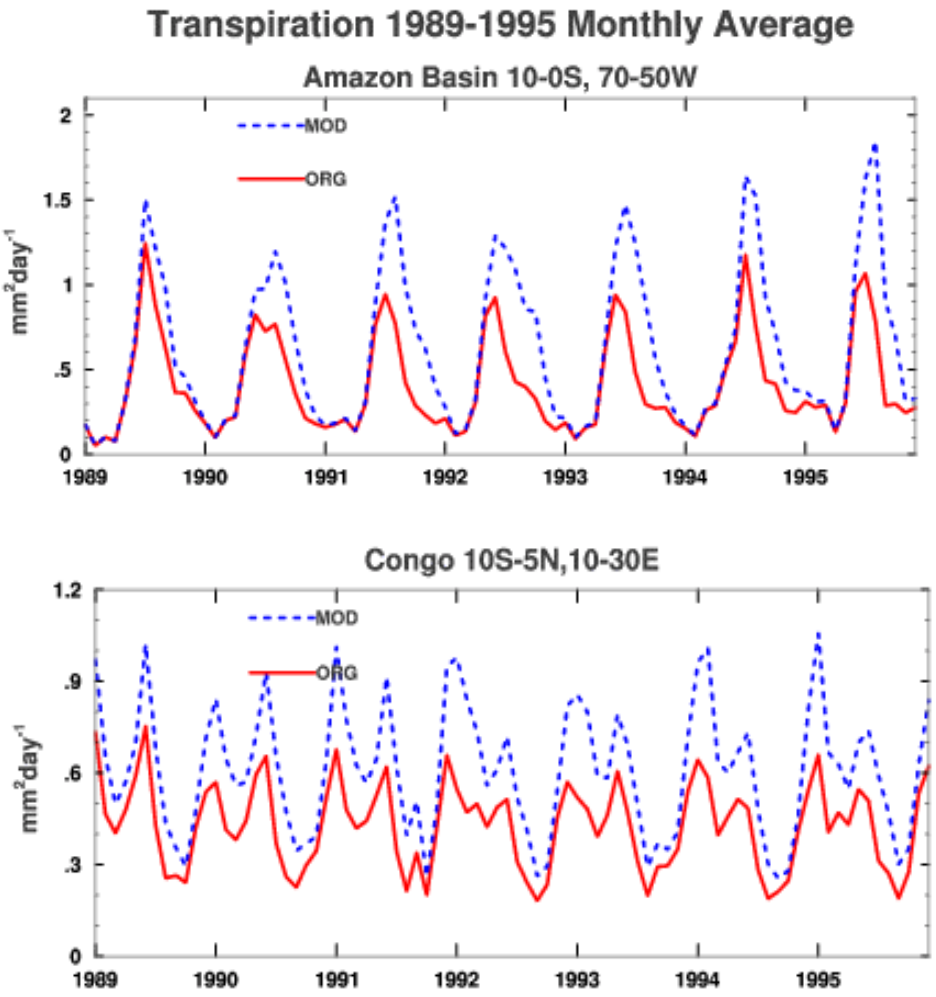

Figure 2.15. Comparison of canopy transpirations by MOD and ORG.

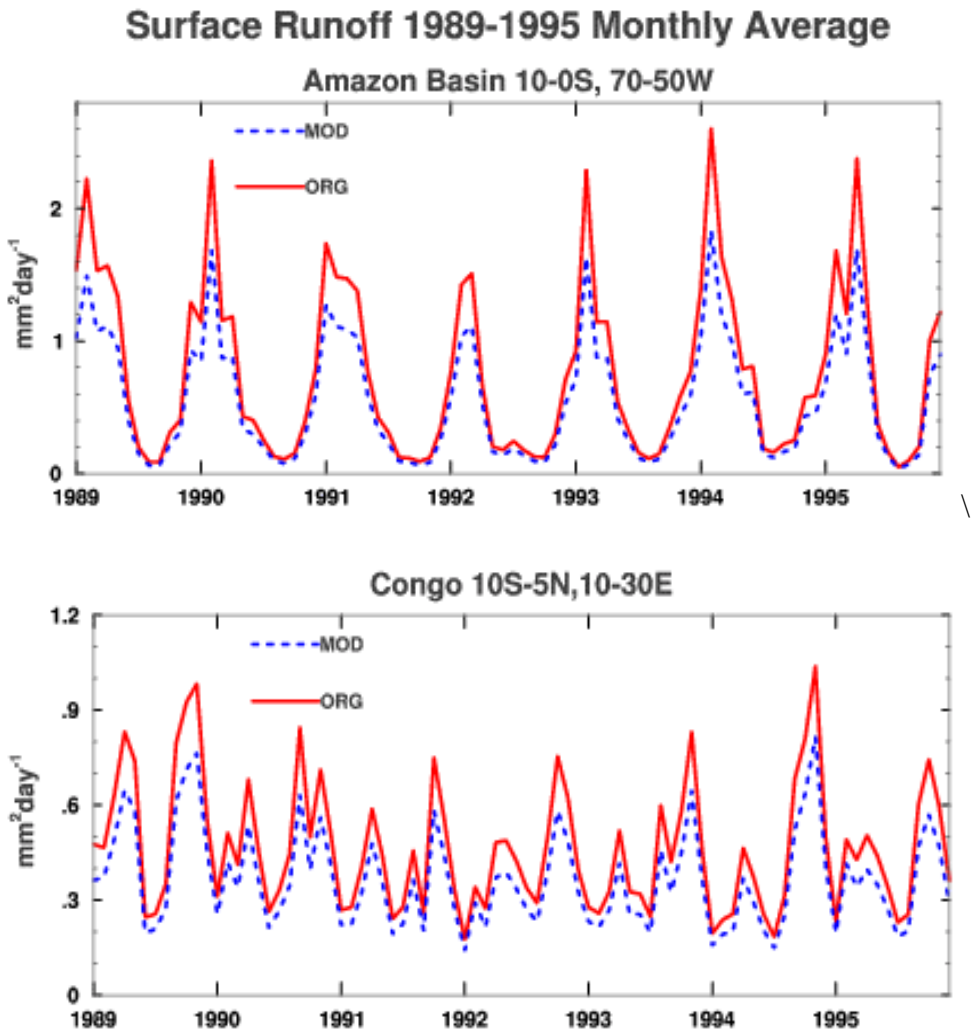

Figure 2.16. Comparison of surface runoff.

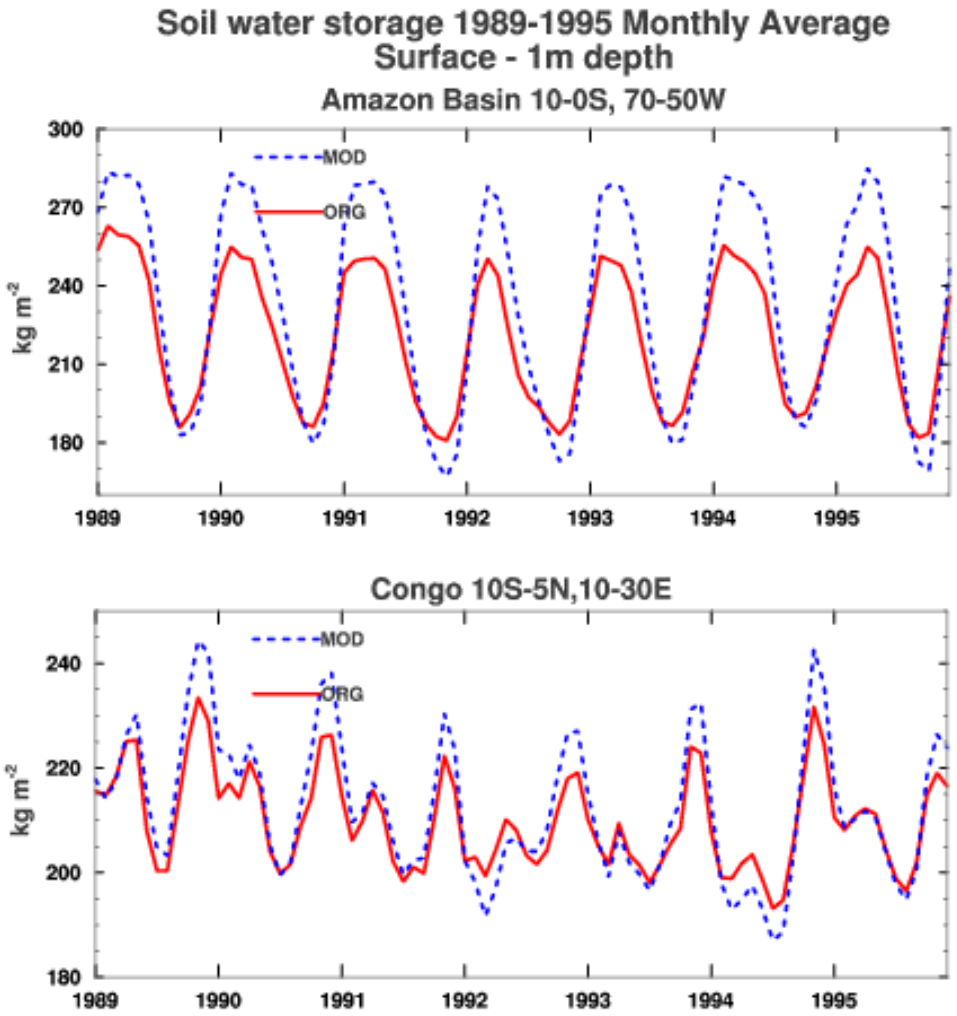

Figure 2.17. Comparison of soil water storage for upper soil layers (surface to 1m depth)

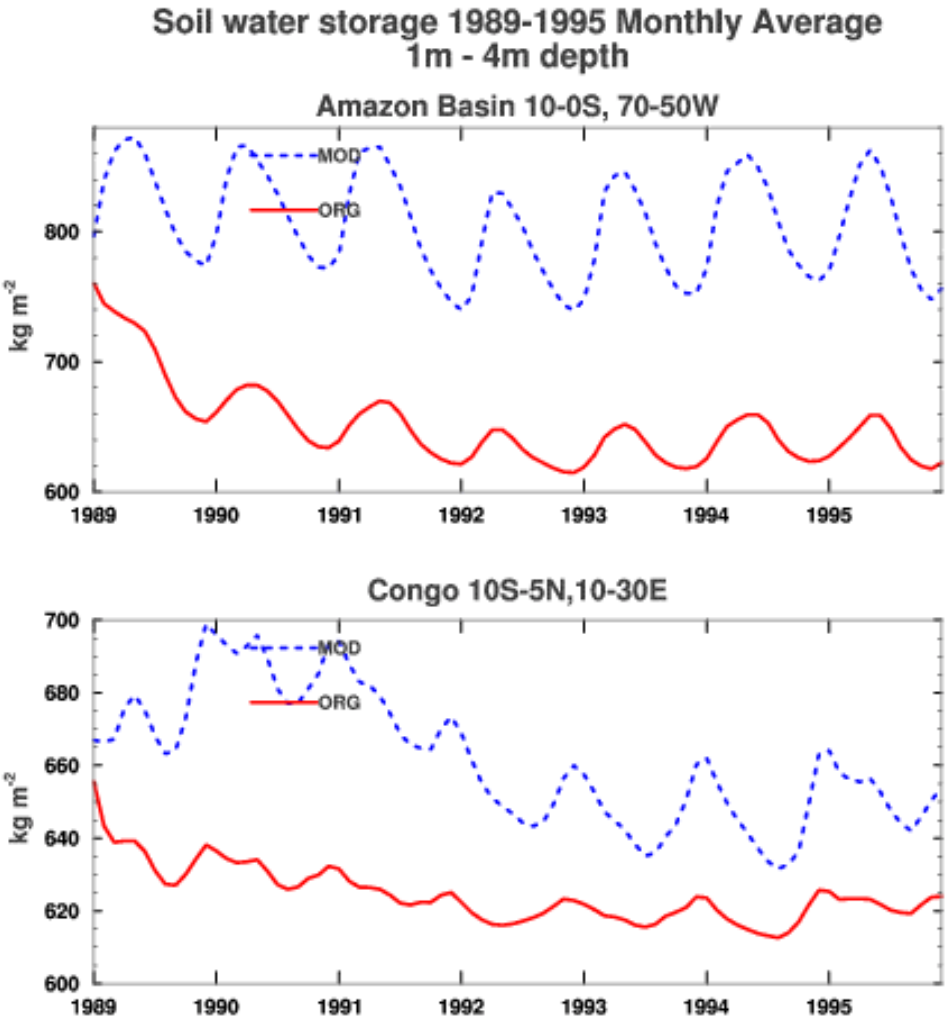

Figure 2.18. Comparison of soil water storage for lower soil layers (1m to 4m depth).

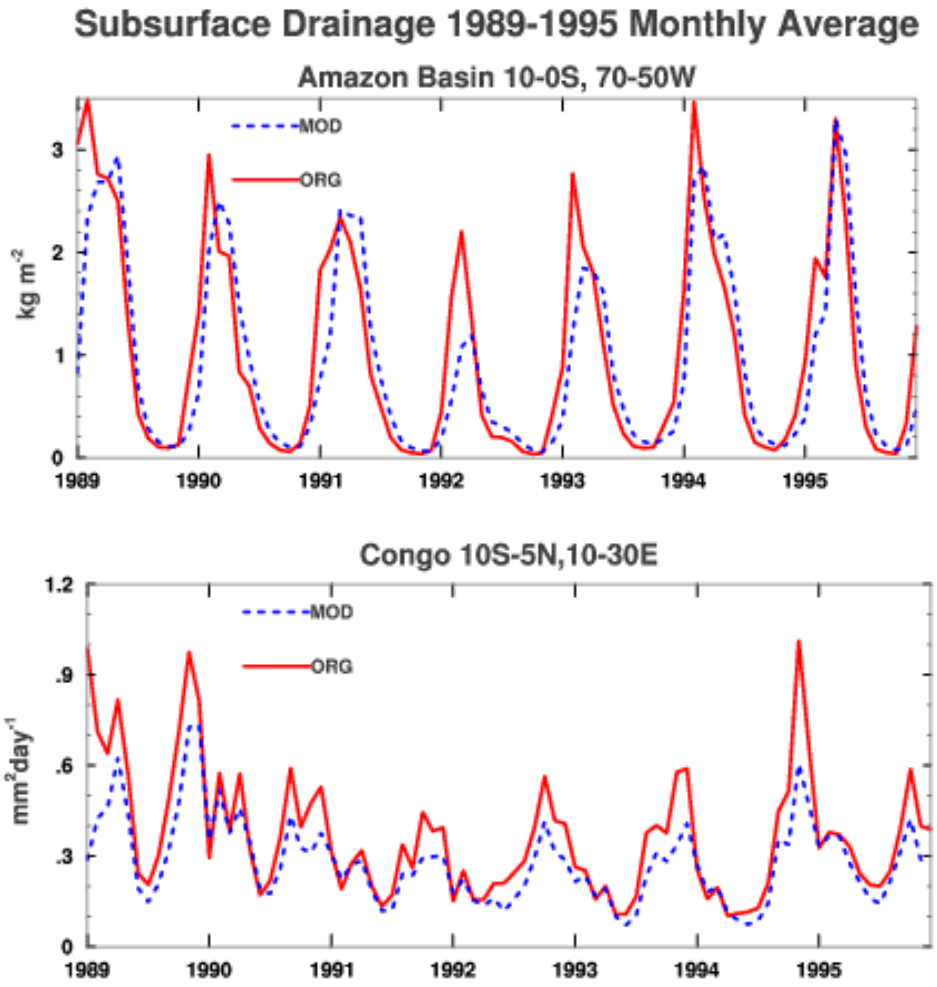

Figure 2.19. Comparisons of subsurface Drainage.

CHAPTER 3

Development of an integrated land/ecosystem model

3.1 Introduction

The land surface-atmosphere interactions are realized not only through the effect of the biophysical and physiological properties of the vegetation and soils on the surface energy, water and momentum exchanges but also through their exchange of greenhouse gases such as the carbon dioxide as well as the dynamic responses of the land ecosystems to the changing environment. These aspects need to be considered together in climate models to capture the feedbacks between the biosphere and the atmosphere.

Land surface models usually prescribe the dynamics of the vegetation and soil properties as model inputs. Simulating the ecosystem processes, on the other hand, requires climate conditions to model the ecosystem functioning and the vegetation structure. Dickinson et al. [1998, 2002] modified the previous Biosphere-Atmosphere Transfer Scheme (BATS) with the ecosystem carbon and nitrogen cycling processes that occur on time scales of weeks to seasons. Through these ecosystem processes dynamic features of the leaf canopy and photosynthesis are provided interactively for the surface physical system.

In this study, we adopt the ecosystem descriptions in Dickinson et al. [1998, 2002] to the recently developed Community Land Model (CLM) and to assess in the

framework of a climate system model the simulation accuracy of the ecosystem carbon and nitrogen cycles as well as the impact of the enhanced considerations of the ecosystem responses to environment on the land surface climatology variables.

The developed model is named CLM-C/N. The next section introduces the fundamental model-structure of the CLM-C/N and the parameterizations of the simulated land surface processes. The physiological and ecological processes are reviewed in detail while the surface physical processes are summarized in a simple manner.

During the last several years, the establishment of global or regional inter-disciplinary experiments, such as the FLUXNET and the Anglo-Brazilian Amazonian Climate Observation Study (ABRACOS), has led to numerous sites with flux-tower measurements across the world. Many of these sites provide measured surface flux data of both energy and carbon over continuous periods and make it possible to test the integrated land/ecosystem models such as the CLM-C/N against observations more extensively over a large geographic area. The new model was first tested at four selected sites representing different ecosystems and climate regimes. Associated adjustments were made to its ecosystem parameterizations. It is then coupled with the NCAR Community Climate System Model, version 2 (CCSM2) [Blackmon et al., 2001] using observed sea surface temperature to assess the effect of the better description on the climatology of land surface variables. The simulated global carbon cycle and nitrogen cycle using the coupled model are also presented.

3.2 Model description

3.2.1 Model structure

The code architecture of the CLM-C/N is based on the standard structure of the CLM for easy implementation in the CCSM. All codes were written in Fortran90 computing language. The model consists of two relatively independent modules: the biophysical-physiological module (BPM) and the ecosystem module (EM). The BPM contains parameterizations of the surface physical processes including the energy, water and momentum balances and parameterizations of the physiological processes. The EM contains the ecosystem carbon and nitrogen cycling processes taking the carbon assimilation and climate attributes that affect the ecological processes such as the leaf and soil temperature, soil moisture and the light-limited rate of the carbon assimilation as input from the BPM. The computed LAI and the content of the Rubisco nitrogen are output to the BPM from the EM at each simulation timestep to provide the biophysical and biochemical feature of the vegetation needed for calculation of the surface energy and water balances. The BPM and the EM are coupled in a synchronous manner. Their schematic coupling is shown in figure 3.1. Keeping the biophysical and biochemical simulations in separate modules allows the ecological aspects to be switched on or off conveniently. If we use prescribed LAI and photosynthesis capacity (V_{max}) instead of predicting them based on the outputs of the EM, the coupling is removed and the coupled model reverts back to the previous CLM.

The simulation structure for physical attributes uses the approach in the CLM version 2 as described in Dai et al. [2003]. In summary, the vertical structure consists of one vegetation layer, 10 unevenly spaced vertical soil layers, and up to 5 snow layers.

Each soil layer can have its own temperature and moisture. Horizontally, every surface grid cell can be subdivided into any number of tiles. Each tile contains a single land cover type with an area fraction of the gird cell. There is no lateral interaction between tiles. The simulation of the ecological attributes uses a simplified soil vertical structure to consider an integrated soil layer around the roots.

Physical prognostic variables include the temperatures of canopy and each soil layer, and the moisture of each soil layer. Ecological prognostic variables include the carbon and nitrogen state of each defined C/N pool. They are calculated for each tile and areally-weighted averages are computed for each grid. The model needs grid averaged atmospheric forcing of surface pressure, air temperature, precipitation, solar and long-wave radiation, wind velocity and air humidity as the driving force. Some soil and vegetation properties are needed to be prescribed for each tile to determine soil and vegetation type related parameters. The required surface-data include the soil texture, vegetation type and the fraction of that vegetation type in each tile. The LAI does not need to be prescribed in the CLM-C/N.

3.2.2 The biophysical-physiological module

This module describes the surface water and energy balances and their transfer processes. These are primarily based on the parameterizations of the CLM, version 2 (CLM2) except for the simulation of the stomatal resistance and the photosynthesis. Detailed descriptions of the CLM2 formulations were presented in Dai et al. [2003]. In the following, we first briefly review the major model physical algorithms. The modified physiological scheme in the CLM-C/N is then described in detail.

The energy and water balances are calculated for the canopy and for each soil

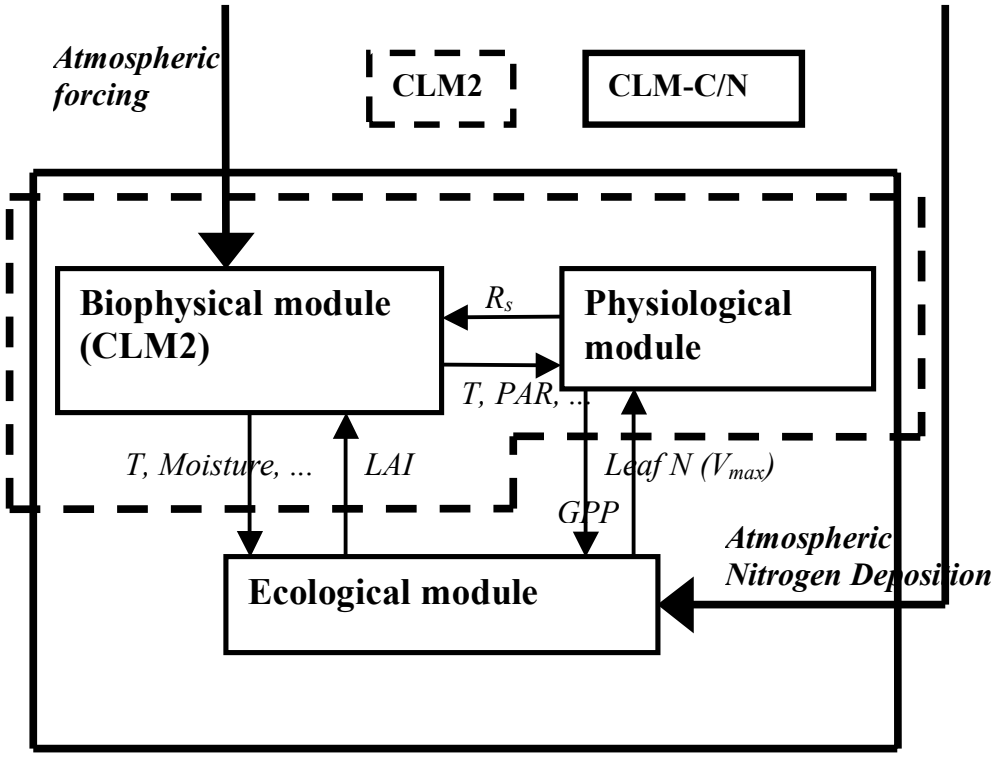

Figure 3.1. Schematic of the CLM-C/N coupling structure.

layer. Precipitation is initially intercepted by canopy according to the canopy density. Part of the intercepted water is evaporated back to the atmosphere. The water that reaches the ground as through-fall or drop-fall from canopy is partly lost as surface runoff and partly percolates downward, according to surface hydraulic conductivities. The downward water transport in the soil is computed using Richard's equation. The soil water is returned to the atmosphere by either evaporation from the soil surface or by transpiration through root uptake. The calculations of the surface and subsurface runoff incorporated the TOPMODEL [Beven, 1982] concept as the approach by Stieglitz et al. [1997]. The resistance diagram is used to calculate the evapotranspiration. The transpiration rate is determined by the leaf boundary resistance and the stomatal resistance, which is calculated in the physiological sub-module and is linked to leaf photosynthesis based on an empirical relationship. Solar radiation is balanced by the sensible and latent heat flux at canopy and by soil heat conduction. The temperatures of foliage and each soil layer are computed as results of the energy balance.

The CLM calculates the photosynthesis and stomatal resistance in a manner similar to the NCAR LSM [Bonan, 1995] and SiB2 [Sellers et al., 1996b] using parameterizations of photosynthesis and empirical relationships between carbon assimilation and stomatal resistance to infer stomatal resistances. The CLM-C/N adopts the calculation in Dickinson et al. [2002] as it fits to data not only for stomatal resistance but also for carbon assimilation rates. The detailed formulations used in the CLM-C/N are presented in the following.

a) The leaf-level stomatal resistance and photosynthesis

The leaf stomatal resistance is calculated from carbon assimilation as

$$\frac{1}{r_s} = m\frac{A_n}{C_s}\frac{1}{(1+0.05\cdot V_{pd})}P_s + \frac{1}{r_{s\max}}, \tag{3.1}$$

where r_s is the leaf stomatal resistance, m an empirical parameter assumed 9 for all species, A_n leaf photosynthesis, C_s the CO_2 concentration at the leaf surface in Pa, V_{pd} the water vapor pressure deficit in millibar, p_s atmospheric pressure at surface (Pa) and r_{smax} the maximum stomatal resistance when $A_n = 0$.

The leaf carbon assimilation is based on the biochemical approach of Farquhar et al. [1980] and Collatz et al. [1990, 1991], i.e., the net assimilation rate is determined by the minimum of three rates determines leaf carbon assimilation: the light-driven rate w_j, and the Rubisco catalysis and photosynthate export rates, w_c and w_e, respectively as well as the leaf light respiration and is expressed as

$$A_n = \min(w_j, w_c, w_e) - R_{leaf\_dm}. \tag{3.2}$$

The light-driven rate w_j is assumed to be linear in absorbed visible light, as most appropriate for low-light levels, and so the only form of light saturation included is that implied by the Rubisco-controlled rates. Hence,

$$w_j = w_{j0} * \varphi_{PAR}\ , \tag{3.3}$$

where φ_{PAR} is the absorbed PAR by leaves, w_{j0} is a coefficient to covert the light to photosynthesis with a light use quantum efficiency of 8%. The w_{j0} is also a leaf temperature dependent and is expressed in μmoles/J as

$$w_{j0} = 0.425 \times \frac{1-0.1f(t_{lef})\cdot\kappa}{1+0.2f(t_{lef})\cdot\kappa}, \tag{3.4}$$

where, the constant "0.425" is the units conversion coefficient times the quantum efficiency of 0.08. κ is the ratio of CO_2 of a prescribed reference concentration at leaf

surface to that at the Rubisco site, calculated by balancing carbon fluxes with carbon assimilation from the Ball-Berry relation with a prescribed transfer conductance for diffusion through the leaf as given in Poorter and Evans (1998). The internal resistance is assumed proportional to leaf thickness, which is given by the parameter "specific leaf area (SLA)". The value of κ is typically between 1 and 2 and smaller for larger SLA values. Its relationship to the SLA for some a prescribed conditions is shown in figure 3.2.

The leaf temperature t_{lef} dependency uses the general Q_{10} with a Q_{10} value of 2.2 as

$$f(T) = \exp[0.08 \cdot (T - 25°C)]. \tag{3.5}$$

Q_{10} is a commonly-used term describing the relative increase in the rate of a biological process for a temperature increase of 10˚C.

The rate at which Rubisco can assimilate carbon w_c at 360 ppmv atmospheric CO_2 mixing ratio is given as

$$w_c = V_{\max} \frac{1 - 0.1 \cdot f(t_{lef}) \cdot \kappa}{1 + 2 \cdot f(t_{lef}) \cdot \kappa}, \tag{3.6}$$

where V_{max} is the maximum assimilation rate possible at the ambient CO_2 concentrations. It is defined as a function of leaf Rubisco-related nitrogen and the leaf temperature as

$$V_{\max} = a_s \cdot N_{rub} \frac{f(t_{lef})}{1 + 0.04 f(t_{lef})^3}, \tag{3.7}$$

The a_s is the slope for correlating the V_{max} with Rubisco-related leaf nitrogen in units of g/m^2, specified as 200 μmol C/g N. The temperature dependence of the V_{max} to leaf temperature is shown in figure 3.3.

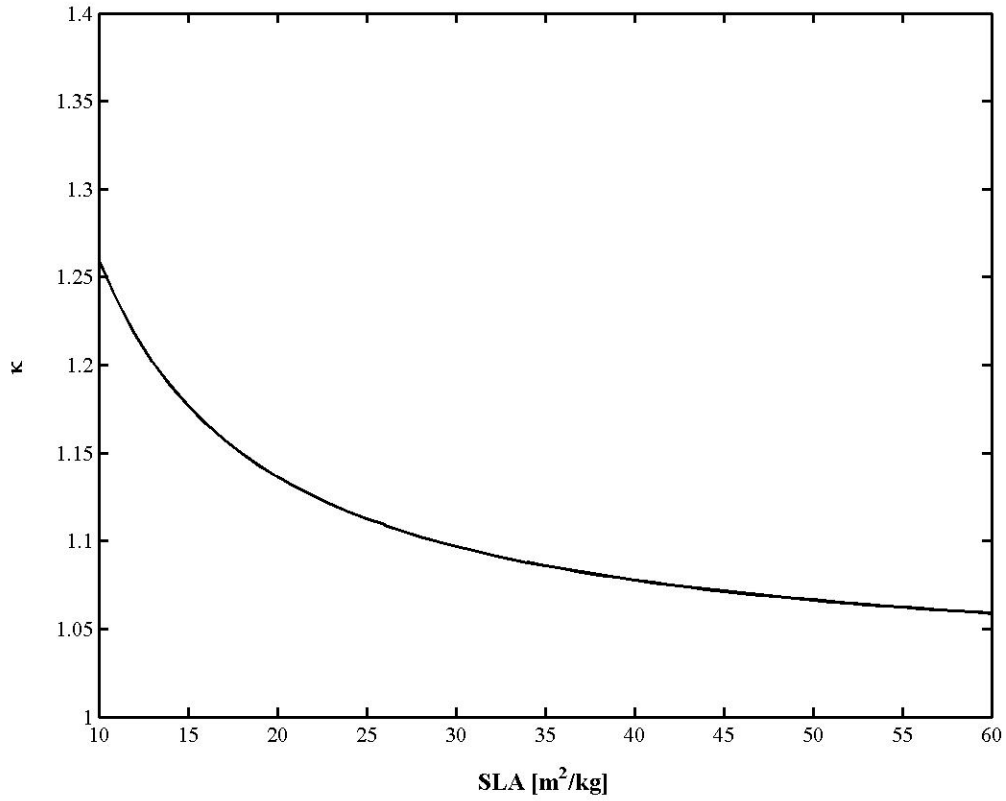

Figure 3.2. The dependence of the parameter κ in equation (3.4) on specific leaf area under condition that $C_i = 0.7\ C_a$, air temperature of 25˚C and V_{max} of 40 umole/m^2/s.

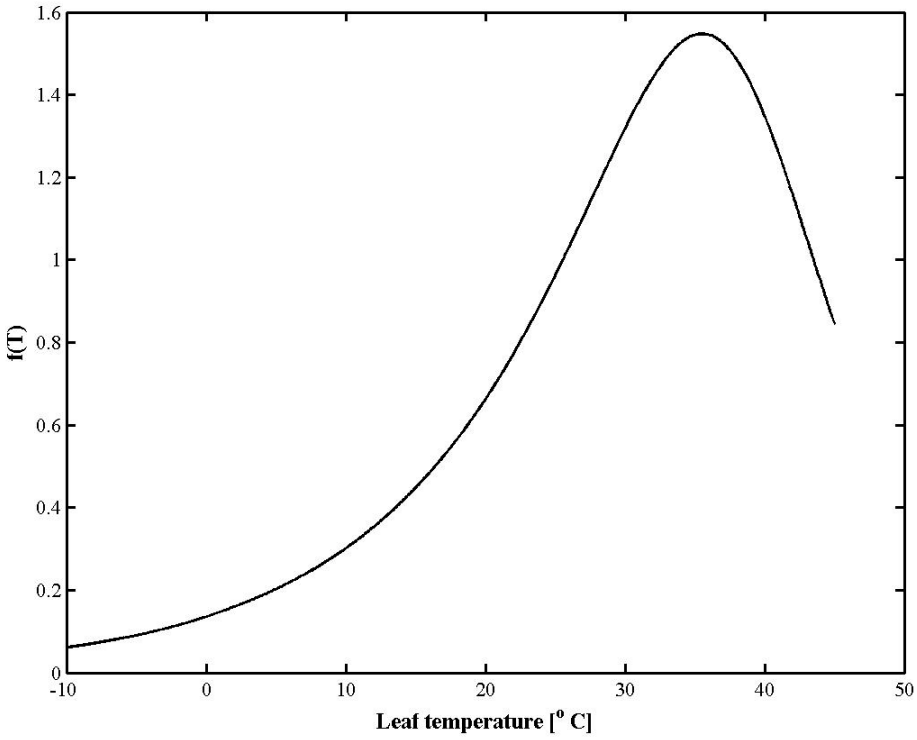

Figure 3.3. Leaf temperature dependence of V_{max}.

The export-limited rate w_e is assumed to be the same as used by Collatz et al. [1991],

$$w_e = 0.5 \cdot V_{\max} . \tag{3.8}$$

The description of the daytime leaf respiration (R_{leaf_dm}) is to be given in next section as in equation (3.27).

b) Scaling from leaf level to canopy level

The CLM treats a canopy as a single layer with varying sunlit and shaded fraction. The scaling of the V_{max} is the same as the scaling of light within the canopy. As the V_{max} is associated with the canopy nitrogen distribution, which doesn't acclimate to the radiance immediately, the CLM-C/N uses the layered canopy structure with different treatments for the leaves exposed to direct solar and the leaves in shade when scaling up the leaf-level photosynthesis and stomatal conductance to the canopy level as referred to Dickinson et al. [1998]. The canopy is divided into four layers with a spherical distribution for the leaf orientation. A fraction of attenuated direct sun is transformed in the canopy to downward scattered radiation using a downward scattering coefficient of 0.1. The sunlit fraction leaf area in each canopy layer is integrated into a single canopy fraction according to

$$f_{sun} = \frac{1}{L}\int_0^L e^{-\lambda \cdot x} dx = \frac{1}{\lambda \cdot L}(1 - e^{-\lambda \cdot L}), \tag{3.9}$$

where L is the leaf area index (LAI); λ is the canopy transmission coefficient to direct beam of the photosynthetically active radiation (PAR) and is assumed as

$$\lambda = 0.5 / \eta , \tag{3.10}$$

where η is the cosine of solar zenith angle; 0.5 is the average leaf cross-section per LAI. The shaded fraction of each layer is the layer fraction of canopy excluding the sunlit fraction in each layer and is given by

$$f_{sha,i} = \frac{1}{4} - f_{sun,i}, \tag{3.11}$$

where $f_{sun,i}$ is the scaled sun fraction of each layer based on the direct solar attenuation profile. The canopy profile of the Rubisco-related nitrogen is assumed as

$$N_{rub,L} = N_{rub,0} \cdot e^{-k_n L}, \tag{3.12}$$

where $N_{rub,0}$ is the Rubisco-related nitrogen content at top of the canopy, $N_{rub,L}$ that under leaf area index L, and k_n is a nitrogen extinction coefficient and is assumed 0.6 for all vegetation. The average N_{rub} content per leaf area for each canopy fraction is calculated based on the nitrogen profile from the total canopy N_{rub}. Thus the canopy level net carbon assimilation X_c can be calculated according to

$$X_c = L \cdot (\sum_{i=1}^{4} f_{sha,i} A_{n,sha,i} + f_{sun} A_{n,sun}). \tag{3.13}$$

Figure 3.5 compares the simulated mean leaf stomatal resistance and the photosynthesis rate by the standard CLM photosynthesis scheme with those by the scheme described above for a canopy under the same environmental conditions. The simulated stomatal resistances by both agree well with each other. The CLM estimated photosynthesis under the given condition is higher than that by the modified scheme in particular around noon when the solar radiance has been saturated in the modified case but not in the CLM case. Another reason for the different in the two schemes is that the CLM does not take into account the light respiration while the modified scheme does. The scheme prescribed in this paper is more realistic than that in the CLM.

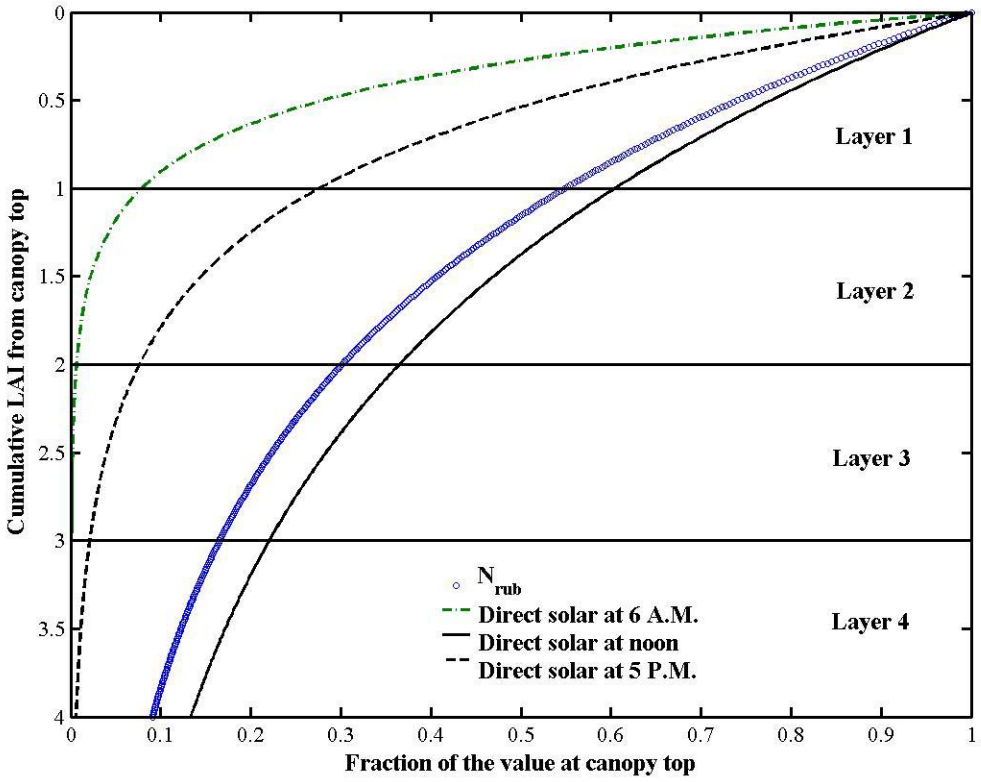

Figure 3.4. Distributions of direct solar and leaf Rubisco-nitrogen within canopy during the course of a day at a specific condition (30˚N in May 01, 1998 with LAI = 4 m^2/m^2).

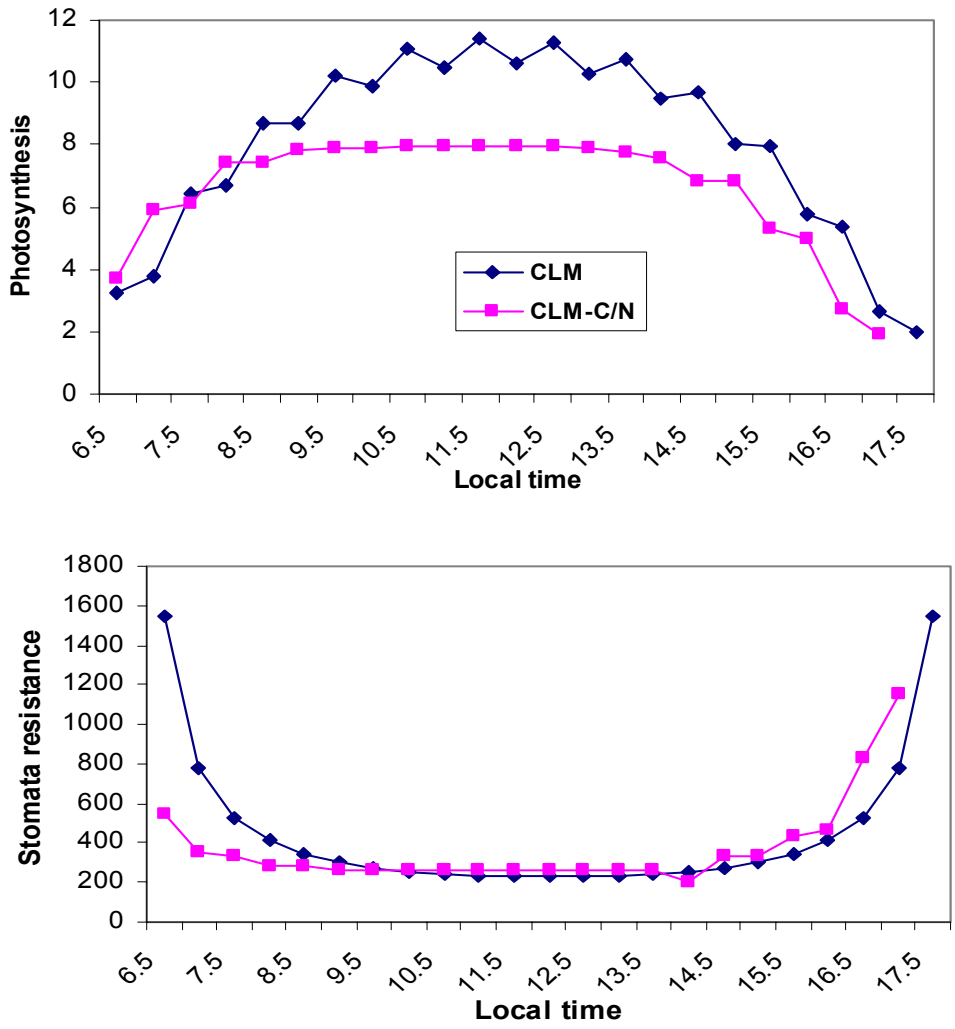

Figure 3.5. Comparison of the Calculated photosynthesis (upper) and stomatal resistance (lower) by canopy scaling scheme by CLM2 and by CLM-C/N under conditions of PAR = 300 W/m^2 at noon, LAI = 4, Vmax = 40 umoles C/m^2/s, and leaf temperature of 25˚C and air relative humidity of 0.7.

3.2.3 The ecological module

The ecological module consists of box-model approach of coupled ecosystem carbon cycle and nitrogen cycle and is adopted primary from Dickinson et al. [1998, 2002] but with some modifications. For each vegetated model tile, the states of each carbon and nitrogen pool and the fluxes between these pools are computed at every timestep. A summary of their original descriptions and formulations is presented first in the following. The modification made to the original parameterization is given afterward.

3.2.3.1 Carbon cycle

The atmospheric CO_2 as the carbon source enters the ecosystem carbon cycle through leaf photosynthesis. The carbon assimilation integrated over canopy is calculated in the biophysical-physiological module and input into the ecosystem module at each simulation timestep. The assimilated carbon is partly released back to the atmosphere and partly allocated into different plant compartments to increase biomass. Meanwhile, plant tissues die or fall by many environmental factors. The debris of plants and soil organic carbon release carbon to the atmosphere through soil respiration. The atmospheric CO_2 is assumed constant for timescales of interest, i.e. several hours to several years. Long term cycling of global carbon are not taken into account in this study. The difference between the ecosystem carbon gain and carbon release is the net exchange of carbon between the ecosystem and the atmosphere. The simulated carbon-cycling processes between the carbon pools used here are described below.

a) Carbon reservoir and allocation

Five reservoirs for the ecosystem carbon cycle are defined. They are photosynthate, leaf, wood, root and soil organic carbon. The soil carbon is divided into a

fast and slow pool. The latter has a lifetime that is long compared to a year and is taken to be inert, and serves as a net carbon sink. The conceptual photosynthate pool accounts for all the plant respiration to avoid an unrealistic day-night fluctuation in LAI when the net leaf carbon assimilation becomes negative because of dominance of respiration. It also provides a rapid leaf growth at the beginning of a growing season by converting stored starches back to sugars. The transfer of photosynthate to leaf structure is given as,

$$C_{p\_l} = k_p \cdot F \cdot C_p , \tag{3.14}$$

where k_p is a maximum convert coefficient, F is a regulating factor as

$$F = (1 - f_p)\exp(-LAI)\frac{1}{1 + S_{cd}} , \tag{3.15}$$

where f_p is the fraction of assimilated carbon that is allocated to photosynthate pool and is formulated as

$$f_p = \frac{\left[\left(1 - \exp(-LAI)\right)\cdot \exp(-\frac{C_p}{C_{p0}}) + S_{cd}\right]}{1 + S_{cd}}, \tag{3.16}$$

where the dependence on LAI allows the allocation to go directly to the leaves in the limit of small LAI and the C_{p0} is a reference photosynthate constant to allow the C_p for full canopy to equilibrate to a value at which about half of carbon assimilation is needed to pay respiratory costs.

According to the equation (3.16), the initial development of leaves, i.e., small LAI, consumes photosynthate for maximum growth. After a full canopy is developed, such conversion ceases because further leaf production beyond maintenance would be wasted as much or more incremental carbon loss by respiration as that gained by

photosynthesis. S_{cd} is a parameter of combined cold stress S_c and drought stress S_d as given by

$$S_{cd} = S_c + S_d \ , \tag{3.17}$$

$$S_c = \exp(-(t_{leaf} - t_{leaf\,0})) \, , \tag{3.18}$$

$$S_d = \exp(100 \cdot (W_s - 1)) \, , \tag{3.19}$$

where, t_{leaf} is canopy temperature, t_{leaf0} is a critical value below which leaf loss by cold stress is rapid, and W_s is a water stress term, estimated from the energy status, i.e., the matric potential of soil water as

$$W_s = \frac{\psi(\theta) - \psi_0}{\psi_{wilt} - \psi_0} \, , \tag{3.20}$$

where, $\psi(\theta)$ is the matric potential at current water content θ, ψ_0 is the air-entry potential and ψ_{wilt} is the soil wilting potential (= -1500 kPa). At values of W_s above 1, permanent wilting occurs for vegetation. These stress terms, equations (3.18) to (3.20) have been reformulated to give more realistic results as discussed in section 3.2.3.4.

The fraction of carbon to leaf is given as according to the leaf area index LAI,

$$f_l = (1 - f_p) \cdot \exp(-0.2L) \cdot S_n \, . \tag{3.21}$$

The allocation to leaves decreases with increasing LAI to limit leaf growth to values near the maximum observed. S_n is a nitrogen stress factor that converts a fraction of 1-S_n of leaf to root allocation, and is given as,

$$S_n = 1 - \frac{(1 - h_p)^2}{2} \, , \tag{3.22}$$

where h_p is a factor to reduce soil ion uptake by light-limited canopy, and is assumed to have the form of

$$h_p = 1 - \exp(-\max(0.1, \frac{w_j}{w_c})), \tag{3.23}$$

where w_j and w_c are the carboxylation rate limited by light and by Rubisco respectively and are defined by equations (3.3) and (3.6), such that root physiological uptake of nitrogen ion is reduced at low light or equivalently, high Rubisco, to 10% of it high light value.

The allocation of the rest of assimilated carbon to roots and wood is according to a relative fraction of the carbon allocated to wood versus root f_{rw} as

$$f_{rw} = \frac{\exp(-b_f R_{wr} \frac{C_r}{C_w})}{b_f}, \tag{3.24}$$

where C_w is the wood carbon storage, C_r is the root carbon storage, R_{wr} is the predefined approximate ratio of wood to root carbon as inferred from observations, and b_f is an adjustable constant close to but less than 1.0 (here b_f = 0.9). With equation (3.24) the ratio of carbon allocated to wood versus roots approaches $1/b_f$ when $\frac{C_w}{C_r} << R_{wr}$ and approaches small values for $\frac{C_w}{C_r} >> R_{wr}$, hence, in general, forcing the ratio of $\frac{C_w}{C_r}$ to approach R_{wr}. The root and wood allocations of the net assimilated carbon are thus expressed as,

$$f_r = (1 - \frac{f_l}{S_n} - f_p) \cdot f_{rw} + (1 - S_n) \frac{f_l}{S_n}, \text{ and} \tag{3.25}$$

$$f_w = (1 - \frac{f_l}{S_n} - f_p) \cdot (1 - f_{rw}), \tag{3.26}$$

respectively.

b) Plant autotrophic respiration

The assimilated carbon is in part released back to atmosphere through the autotrophic respiration. The autotrophic respiration is the respiration cost to support the needs of plant. It can be divided according to the functional usage of the released energy into two different physiological processes: growth respiration R_g and maintenance respiration R_m. Growth respiration is defined as the amount of carbohydrates respired in processes that result in a net gain in plant mass. Maintenance respiration is the respiration needed to provide energy to support all other plant functioning. The growth respiration is modeled as proportional to the net carbon assimilation. The proportionality is assumed to be 30% for plants in the current model. Different maintenance-respiration parameterizations are used for different vegetation parts. The leaf respiration during the day R_{leaf_dm} is assumed a function of leaf nitrogen content. The leaf respiration during the evening R_{leaf_nm} is assumed slightly higher than that during the day with a Rubisco-related consumption. Their average leaf-level rates in μmole/m^2/s are expressed as,

$$R_{leaf\_dm} = R_{leafc} \cdot f(t_{leaf}) \cdot N_l , \tag{3.27a}$$

and,

$$R_{leaf\_nm} = R_{leaf\_dm} + 2 \cdot R_{leafc} \cdot f(t_{leaf}) \cdot N_{rub} , \tag{3.27a}$$

respectively.

The maintenance respiration rate of the roots R_{root_m} is based on the root nitrogen content N_r as,

$$R_{root\_m} = R_{rootc} f(t_{soil}) \cdot N_r , \tag{3.28}$$

where R_{rootc} is a constant coefficient. Its soil-temperature t_{soil} dependence uses the Q_{10} of 2.2 as defined in equation (3.5). The wood respiration is

$$R_{wood\_m} = R_{woodc} f(t_{leaf}) \cdot C_w . \quad (3.29)$$

The plant autotrophic respiration is the sum of the growth respiration and the maintenance respiration,

$$R_{auto} = R_g + R_m , \quad \text{where} \quad (3.30)$$

$$R_g = 0.3 \cdot X_c , \quad \text{and} \quad (3.31)$$

$$R_m = R_{leaf\_m} + R_{root\_m} + R_{wood\_m} , \quad (3.32)$$

where, R_{leaf_m} is R_{leaf_dm} during the day and R_{leaf_nm} during the night.

c) Soil heterotrophic respiration

The fast soil carbon accumulates the carbon that is lost from the plant by leaf and root turnover, and by leaf loss from cold and drought stress, and is lost by soil heterotrophic respiration. The heterotrophic respiration R_{hetero} is the release of CO_2 to the atmosphere from decay and breakdown of litter and soil organic matter. It is estimated from the soil organic content C_s and a coefficient R_{soilc} that is regulated by soil temperature and moisture,

$$R_{hetero} = R_{soilc} \cdot C_s , \text{ and} \quad (3.33)$$

$$R_{soilc} = R_{soilc0} f(t_{soil}) \cdot (1 - \exp(-R_{sdryc} \cdot S_{soil}) \quad (3.34)$$

where R_{soilc0} is a constant coefficient, and the soil temperature dependence $f(t_{soil})$ uses equation (3.5). The last term represents the dryness of soil in limiting the soil respiration. The R_{sdryc} is a coefficient denoting degree of drying that reduces soil respiration and is assumed a constant value of 40; S_{soil} is the root zone soil water relative saturation. The

exponential form indicates that the soil respiration rate will not be affected by the soil moisture until soil gets extremely dry, i.e., when S_{soil} is below 0.1.

d) Plant carbon loss and phenology

While plants gain carbon by forming new tissues, they also lose carbon through processes including herbivory or mechanical loss, death by senescence and death by environmental stresses such as cold and drought stresses and harvest removal for agricultural systems. The losses by senescence, herbivory or mechanical means are grouped into a turnover coefficient for each plant parts. The leaf turnover coefficient is given as

$$k_{lt} = k_{lt0} \cdot [0.3 + 0.01 \cdot L_c \cdot (0.5 \cdot N_{rub} + 1)], \tag{3.35}$$

where k_{lt0} is a prescribed rate and L_c is the specific leaf area (SLA). The above description allows for the shorter lifetimes of thinner leaves, i.e., leaves with larger specific leaf area, and the greater attractiveness of high-nitrogen leaves to herbivores. The root turnover coefficient is defined as a prescribed value that is regulated by soil temperature as

$$k_{rt} = k_{rt0} \cdot \sqrt{f(t_{soil})}, \tag{3.36}$$

where the temperature dependence $f(t_{soil})$ uses equation (3.5). The wood turnover coefficient k_{wt} is prescribed as a constant to account for natural turnover as well as loss through lumber extraction.

Agricultural removal coefficients of leaf k_{lh} and root k_{rh} are prescribed as non-zero constants for agricultural systems and zero for natural systems. Agricultural loss serves as a net sink of the ecosystem carbon cycle. Leaf loss coefficients of cold and drought stress

are formulated as a constant coefficient k_s multiplied by a stress factor S_{cd} as given in equation (3.17).

e) Carbon cycling equations and ecosystem carbon budget

The active carbon pools include photosynthate carbon C_p, carbon stored in leaves C_l, carbon in wood C_w, carbon in roots C_r and fast soil carbon C_s. Their states are prognostic variables and updated at each timestep according to the following equations,

$$\frac{dC_p}{dt} = f_p \cdot X_c - C_{p\_l} - R_{auto} \quad ; \tag{3.37}$$

$$\frac{dC_l}{dt} = f_l \cdot X_c + C_{p\_l} - (k_s \cdot S_{cd} + k_{lt} + k_{lh}) \cdot C_l \, ; \tag{3.38}$$

$$\frac{dC_r}{dt} = f_r \cdot X_c - (k_{rt} + k_{rh}) \cdot C_r \, ; \tag{3.39}$$

$$\frac{dC_w}{dt} = f_w \cdot X_c - k_{wt} \cdot C_w ; \tag{3.40}$$

$$\frac{dC_s}{dt} = (k_s \cdot S_{cd} + k_{lt}) \cdot C_l + k_{rt} \cdot C_r - R_{hetero} . \tag{3.41}$$

The ecosystem level carbon uptake during photosynthesis is termed gross primary production GPP. GPP is partly lost during autotrophic respiration. The rest is the net carbon uptake by plant, or the net primary production NPP. NPP if positive is used to produce new plant tissues and increase plant biomass. The continuous positive NPP period of a year is referred to as the "growing season". The ecosystem carbon budget in different terms can be represented as,

$$GPP = X_c ; \tag{3.42}$$

$$NPP = GPP - R_{auto} ; \tag{3.43}$$

$$NEE = NPP - R_{hetero} . \tag{3.44}$$

The NEE is the net ecosystem carbon exchange. The cumulative NEE over a long term, e.g., over a year, represents the net increase of the carbon storage of the ecosystem.

The LAI L is determined by the leaf carbon multiplied by the SLA L_c as

$$L = C_l \cdot L_c . \tag{3.45}$$

3.2.3.2 Nitrogen cycle

The ecosystem nitrogen cycle and carbon cycle are tightly coupled with nearly fixed C/N ratios for each organ of vegetation and the soil organic material. There is also a close relationship between nitrogen supply and increase in biomass. The energy and the molecular structures need the incorporation of nitrogen which is derived from carbon metabolism and photosynthesis. The photosynthesis is dependent on nitrogen-containing compounds such the Rubisco, as has been addressed in the previous section.

a) Nitrogen reservoirs and plant uptake

Three nitrogen reservoirs are models for the nitrogen cycling processes: the plant nitrogen N_p, soil organic nitrogen N_s and soil mineral nitrogen N_m. Vegetation utilizes inorganically bound nitrogen. Nitrogen is taken up from the soil as either nitrate (NO_3^-) or ammonium ions (NH_4^+). The nitrogen uptake coefficient is assumed as

$$k_m = k_{m0} \times \min(\lambda_r, \lambda_t) , \tag{3.46}$$

where k_{m0} is a base uptake rate, and λ_r, λ_t are nondimentional rates of ion uptake by high and low affinity transport at the root interface, and by physical transport by ion diffusion and bulk flow respectively. The rate λ_r is assumed the same form for all species and for both ions (NH_4^- and NO_3^+) and is expressed as

$$\lambda_r = h_p\left(\frac{C_r}{C_{ro}}\right) \times \left(\frac{r_{ref}}{r_r}\right) \times \frac{\left(I_{\max}/N_m + K_l\right)}{\left(1 + K_m/N_m\right)} , \tag{3.47}$$

where r_{ref} is a reference root radius and r_r is the characteristic root radius assumed here to be r_{ref}, and where C_r and C_{ro} are the root carbon and a reference value, N_m is either the concentration of NH_4^- or NO_3^+ normalized by 1.0 g/m^2, and $K_{m,}$ K_l and I_{max} are nondimensional root physiological parameters, and h_p represents reduction of root uptake by light-limited canopy, and is formulated as in equation (3.23). The transport term λ_t is defined separately for each ion to be of the form

$$\lambda_t = \lambda_d + \lambda_{et}, \tag{3.48}$$

where for a soluble ion, such as nitrate, the diffusion transport rate, λ_d is assumed to be

$$\lambda_d = 0.4 w_r \cdot \frac{C_r}{C_{r0}} \cdot \frac{D_i}{D_{ref}} \cdot \left(\frac{r_{ref}}{r_r} \right)^2, \tag{3.49}$$

where D_i is ion diffusion coefficient in saturated soil here assumed to be D_{ref}, which is a reference value. w_r is the root zone soil relative saturation so that it ranges from 0 to 1 with smaller roots needing less mass for the same diffusion uptake. The product of root carbon and inverse radius squared is proportional to root length. The ET-driven bulk flow rate is given by

$$\lambda_{ET} = 0.2 \cdot \frac{ET}{w_r \cdot ET_0}, \tag{3.50}$$

where ET_0 is a reference value for the rate of transpiration ET. Because ammonium is less soluble, it is crudely allowed for here by multiplying the ammonium concentrations by 0.3.

b) Plant nitrogen sub-pools and the loss of plant nitrogen

The nitrogen taken up by roots is carried to leaves and incorporated into carbon compounds in amino groups, forming amino acids and amides. The nitrogen balances and

carbon balances are strongly interdependent. Thus, nitrogen content of a plant is linked to carbon content with a nearly fixed C/N ratio for each plant part. Four plant nitrogen sub-pools are defined: leaf structural nitrogen N_{ls}, leaf Rubisco nitrogen $N_{rub,}$ leaf nitrogen other than structural and Rubisco N_{lo} and root nitrogen N_r. The leaf structural and root pools are determined from leaf and root carbon as

$$N_{ls} = r_{ncl} \cdot (1 - f_n) \cdot C_l \ , \text{ and} \tag{3.51}$$

$$N_r = r_{ncr} \cdot (1 - f_n) \cdot C_r \, , \tag{3.52}$$

where r_{ncl} and r_{ncr} are ratio of nitrogen to carbon for leaf structure and for root respectively, and f_n is the fraction of the leaf structural and root nitrogen that has been moved to the N_{rub} pool because of shortage, and is assumed

$$f_n = 0.2 \exp(-2 \cdot N_{rub}) \, . \tag{3.53}$$

The Rubisco nitrogen N_{rub} pool is assumed the difference between the total plant nitrogen and the leaf structural plus root nitrogen regulated by ratio of leaf structural nitrogen to total leaf nitrogen N_l,

$$N_{rub} = (N_l - N_{ls}) \frac{N_{ls}}{N_l} \, , \tag{3.54}$$

where, $N_l = N_p - N_r$. This expression assumes that all nonstructural leaf nitrogen is put into Rubisco when total leaf nitrogen is not much larger than that needed to supply the minimum structural requirement, otherwise only part is put in Rubisco. Such treatment is to avoid extra cost of respiration through overloading of Rubisco nitrogen when the LAI and structural nitrogen requirement is small at the beginning of growing season.

The loss of plant nitrogen to litter and soil denoted as ΔN_s is associated with the plant carbon loss, i.e., leaf and root turnover as well as the leaf stress loss,

$$\Delta N_s = k_{rt} \cdot N_r + \gamma_r \cdot (k_s \cdot S_{cd} + k_{lt}) \cdot (N_{ls} + N_{rub}), \quad (3.55)$$

where, N_r and N_l are root and leaf nitrogen respectively, $1\text{-}\gamma_r$ is a re-translocation coefficient for leaves (i.e., fraction of recapture into the plant when the leaf dies), assumed to be 0.5 following Aber et al. [1997], k_{rt} and k_{lt} are the root and leaf turnover rates, and $k_s \cdot S_{cd}$ is the cold and drought mortality rate.

c) Soil organic N mineralization

The N mineralization ΔN_m is the converting rate of soil organic nitrogen to soil mineral nitrogen. This process recycles the nitrogen in litter into active form and is given by

$$\Delta N_m = R_{soilc} \times I_{mob} \times N_s, \quad (3.56)$$

where R_{soilc} is the soil fast carbon pool respiration rate coefficient and I_{mob} reduces mineralization of N through the immobilization by bacteria for low ratios of N_s/C_s, that is, the N_s is largely recaptured by bacteria when N_s is less than 0.05 of C_s. This effect is parameterized by

$$I_{mob} = \exp\left(-0.05 \cdot \frac{C_s}{N_s}\right). \quad (3.57)$$

d) Nitrification and denitrification

The mineral nitrogen of nitrate and ammonium ion can convert their forms to each other through nitrification and denitrification. Their coefficient are formulated as,

$$k_{ni} = k_{ni0} \times f(t_{soil}) \times \frac{w_s(1-w_s)}{(0.25 + 1/NH_4^+)}, \quad (3.58)$$

$$k_{dn} = k_{dno} \times f(t_{soil}) \times {w_s}^b, \quad (3.59)$$

where $f(t_{soil})$ is the rooting-zone soil-temperature dependence using equation (3.5), w_s is the root-zone soil-water relative saturation and b is the Clapp-Hornberger parameter, such that equation (3.59) scales with the inverse of the soil water potential. Equation (3.58) hypothesizes that at low NH_4^+ the rate becomes small and proportional to NH_4^+. Although the denominator of equation (3.58) is speculative in detail, some such slowing of nitrification at low ammonium levels may be needed in natural systems to reduce nitrogen loses to maintain observed levels of soil nitrogen.

e) Nitrogen sources and sinks

The annual supply of N in natural systems at present is about half natural and half anthropogenic. The major nitrogen sources include the atmospheric deposition, the biological fixation and fertilization. The major sinks are the ammonia volatilization and leaching of nitrate ions through runoff. The rate of sources and sinks are defined in a simple manner.

Fertilizer production and consumption is assumed an average anthropogenic source term for the dry-land and irrigated agricultural grid squares, taking for these

$$S_{fert} = 2.5\times10^{-7}\, g m^{-2} s^{-1} \quad . \tag{3.60}$$

Natural systems are assumed to be fertilized by microbiological fixation, with an assumed supply (at 298K and low-nitrate concentrations) of $S_{bf} = 1.\times10^{-7}\, g\ m^{-2} s^{-1}$, and to a lesser extent, by a constant rate wet and dry deposition from the atmosphere of

$$S_{wd} = 1.5\times10^{-8}\, g\ m^{-2} s^{-1}, \tag{3.61}$$

$$S_e(natural) = \left[S_{wd} + S_{bf}\sigma_f \times (1-f_p)\times f(T)\times \exp(-\beta_f \times NO_3^-)\right]. \tag{3.62}$$

The nitrogen fixation varies with fractional vegetation, with the fraction of assimilated carbon not put into the photosynthate pool, and with a simple negative feedback response to excess soil nitrate with $\beta_f = 0.5$. Fixation ceases during periods of drought when the photosynthate carbon reservoir is unable to provide the energy cost.

The ammonia volatilization rate is assumed to have a small constant coefficient of 10^{-9} s^{-1}. Such slow volatilization holds for natural systems. The larger agricultural losses to ammonia emission are lumped with the prescription of the agricultural net source term. The runoff loss rate is estimated for nitrate ions

$$k_{ro} = R_{off} / W_0 \quad , \tag{3.63}$$

where R_{off} is the runoff in units of mm s^{-1}, and W_0 = 200 mm is an assumed average soil water store. Runoff loss of ammonium ions and loss from biomass burning are neglected.

f) Nitrogen cycling equations

The cycling equations for prognostic variables of plant nitrogen N_p, soil organic nitrogen N_s and soil mineral nitrogen (NH_4^+ and NO_3^-), and are given

$$\frac{dN_p}{dt} = k_m N_m - \Delta N_s ; \tag{3.64}$$

$$\frac{dN_p}{dt} = k_m N_m - \Delta N_s ; \tag{3.65}$$

$$\frac{dNH_4^+}{dt} = S_e + \Delta N_m - (k_m + k_v + k_{ni}) NH_4^+ ; \tag{3.66}$$

$$\frac{dNO_3^-}{dt} = k_{ni} NH_4^+ - (k_m + k_{dni} + k_{ro}) NO_3^- . \tag{3.67}$$

3.2.3.3 Changes in the ecological module from Dickinson et al. [1998, 2002]

The coefficient of the cold and drought caused leaf death is formulated in Dickinson et al. as an assumed value of $2\times10^{-7}\,s^{-1}$ multiplied by a stress factor of cold and drought as given in equations (3.18) and (3.19). The stress term partly controls the phenology of the carbon cycle in particular of deciduous vegetation species. The exponential terms introduce strong stress-effect when the temperature or soil moisture is below critical values as to cause substantial drop of leaf mass in a quite short period of time, e.g., with a temperature below critical value for 10˚C, the full canopy of foliage will die within 4 minutes. The drought caused leaf death is even more abrupt. However, it has been found that forests have strong capability to tolerate short term environmental stresses including both cold and dry stresses [Larcher, 1995].

The instantaneous critical leaf temperature is replaced by daily average leaf temperature so that occasional night time coldness or a short-term of cold weather will not affect the leaf mass and the leaf area index too immediately.

The drought stress term is replaced by the soil-water regulation term on leaf carbon assimilation adopted from the CLM2. The photosynthesis capacity as in equation (3.7) is multiplied by this factor given as

$$P(\theta)=\frac{\psi_{wilt}-\psi(\theta)}{\psi_{wilt}-\psi_0}, \tag{3.68}$$

where, P is a dryness factor indicating the reduction of the carbon assimilation and ranges between 0 for stomata fully closed to 1 for no water limitation. ψ and θ are soil-water matric potential and soil volumetric water content respectively. ψ_{wilt} is the matric potential at permanent wilting point. It is a constant of -1500 kPa. ψ_0 is the air-entry

potential. Compared to the original scheme provided by Dickinson et al. [1998] that assumes a rapid increase of leaf mortality by soil water stress, the above modified scheme lets the soil moisture to affect the rate of carbon assimilation and hence influence the leaf biomass gradually through the unbalances between the carbon assimilation and carbon release, so that a sudden change of LAI under temporary drought can be avoided. The modified scheme is more consistent with some measured features as shown in figure 3.6 than the previous treatment.

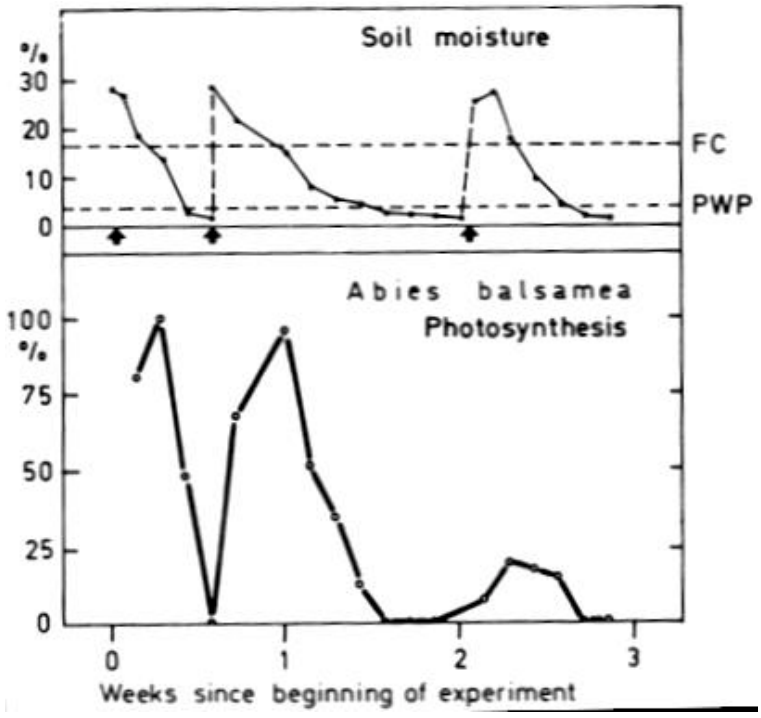

Figure 3.6. Effect if drought on the net photosynthesis of one-year-old seedlings of *Abies balsamea* (after Larcher [1995]).

3.2.4 Model parameters

All the biophysical parameters use values provided in the standard CLM as listed

in Dai et al. [2003] and Bonan et al. [2002]. The parameters required for both the ecological module and the physiological sub-module of the CLM-C/N are primarily referred to Dickinson et al. [2002] and summarized below.

a) Vegetation type independent parameters

Table 3.1 List of coefficients and fluxes for carbon and nitrogen pools.

Symbol	Definition	Value
Coefficients for carbon pools in s^{-1}		
k_{lt}	Leaf turnover coefficient	Eq. (3.35)
k_{lt0}	Characteristic value to calculate k_{lt}	3×10^{-8}
k_{rt}	Root turnover	Eq. (3.36)
k_{rt0}	Characteristic value to calculate k_{rt}	4×10^{-8}
k_{wt}	Wood turnover	1×10^{-9}
k_{lh}	Leaf harvest	6×10^{-8}
k_{rh}	Root harvest	3×10^{-8}
k_s	Base value to calculate coefficient of leaf loss due to cold and drought stresses.	2×10^{-7}
R_{soilc}	Soil respiration coefficient	Eq. (3.33)
R_{soilc0}	Base value to calculate R_{soilc}	4×10^{-8}
R_{leafc}	Base value to calculate leaf maintenance respiration coefficient.	5×10^{-6}
R_{rootc}	Base value to calculate root maintenance respiration coefficient.	4×10^{-6}
R_{woodc}	Base value to calculate wood maintenance respiration coefficient.	5×10^{-10}
k_p	Maximum coefficient of photosynthate transfer from pool to leaf as used.	5×10^{-6}
Coefficients for nitrogen pools in s^{-1}		
k_m	N uptake coefficient for $NO3^-$ and $NH4^+$	Eq. (3.46)
k_{m0}	Base value to calculate k_m	5×10^{-6}
k_{ni}	Nitrification coefficient for $NH4^+$	Eq. (3.58)
k_{ni0}	Base value to calculate kni	1×10^{-6}
k_dni	Denitrification coefficient for $NO3^-$	Eq. (3.59)
k_{dn0}	Base value to calculate kdni	2.5×10^{-6}

k_v	Ammonium ion volatilization coefficient	1×10^{-9}
Prescribed rates of nitrogen sources in g N /m²/s		
S_{bf}	N biological fixation rate at 25˚C	4×10^{-7}
S_{wd}	N wet and dry deposition	1.5×10^{-8}
S_{fert}	N fertilizer for agricultural lands	2.35×10^{-7}

Table 3.2 Prescribed parameters for calculating physiological and ecological processes.

Parameters to calculate leaf photosynthesis and stomatal resistance			
Symbol	Definition	Value	Units
M	"Ball-Berry" factor to compute stomata resistance from photosynthesis	9	-
r_{smax}	Maximum stomatal resistance	20000	s/m
Other prescribed parameters			
r_{ncl}	Leaf structural N to C ratio	0.03	-
r_{ncr}	Root N to C ratio	0.024	-
C_{ro}	Characteristic root mass used in Eq. (3.47)	250	g C/m²
ET_0	Characteristic transpiration used in Eq. (3.50)	1.5×10^{-4}	mm/s
γ_r	Fraction of leaf of N not retranslocated used in Eq. (3.55)	0.5	-

b) Vegetation type-related parameters

Three parameters need to be defined as type-specific: the specific leaf area (SLA) L_c, the wood to non-wood ratio R_{wr} and the critical leaf temperature, t_{leaf0}, below which leaf dies rapidly. L_c for forests and crops plant function types is derived from values for associated biomes in Dickinson et al. [2002], and for grasses and shrubs are from White et al. [2000]. R_{wr} is assumed constant of 30 for forests, 3 for shrubs and 0 for grasses and crops as defined in Dickinson et al. [2002]. It is used to determine the relative allocation of assimilation carbon to roots versus wood. t_{leaf0} is the primary control of the annual canopy dynamics of deciduous plants.

3.3 Model tests at single sites

The CLM-C/N is first tested at four sites with different plant species from different climate regions before coupled into the climate model. The standard CLM have been evaluated with extensive offline tests using a variety of observational data by Dai et al. [2003] that adequately showed the performance of the physical processes. One

Table 3.3 Plant functional types for CLM2 and their associated parameters.

PFT	L_c (m^2m^{-2})	R_{wr}	t_{leaf0} (k)
Temperate needleleaf evergreen forest	10	30	263
Boreal needleleaf evergreen forest	10	30	230
Boreal Needle leaf deciduous forest	30	30	278
Tropical broadleaf deciduous forest	25	30	282
Temperate broadleaf evergreen forest	25	30	263
Tropical broadleaf deciduous forest	30	30	282
Temperate broadleaf deciduous forest	30	30	282
Boreal broadleaf deciduous forest	30	30	272
Temperate broadleaf evergreen shrub	16	3	263
Temperate broadleaf deciduous shrub	25	3	282
Boreal broadleaf deciduous shrub	25	3	272
Arctic C3 grass	40	-	262
Non-arctic C3 grass	40	-	272
C4 grass	50	-	282
Crop	50	-	282

advantage of the CLM-C/N is that it can simulate the surface energy, water and carbon fluxes together. Here, the simulated surface fluxes, the canopy cover and the photosynthetic capacity as well as the ecosystems at four sites representing different forest ecosystems are presented. The simulated fluxes are compared with the flux-tower measurement on both diurnal and annual scales.

3.3.1 Site description

Sites selected in this experiment covers climate regime from boreal to tropical regions and forest function type of evergreen needleleaf, evergreen broad leaf, and deciduous broad leaf. They are standard sites in either the FLUXNET project or the ABRACOS project. The FLUXNET is a global network of micrometeorological tower sites that use eddy covariance methods to measure the exchanges of carbon dioxide (CO_2), water vapor, and energy between terrestrial ecosystem and atmosphere. At present, over 200 tower sites are operating on a long-term and continuous basis. Researchers also collect data on site vegetation, soil, hydrologic, and meteorological characteristics at the tower sites (available online in http://www.eosdis.ornl.gov/FLUXNET/).

a) Oak Ridge (temperate deciduous broadleaf forest)

This is a FLUXNET site. It is located on the Walker Branch Watershed, near Oak Ridge, Tennessee (35˚ 57' N, 84˚ 17' W). It has a mixed-species deciduous broadleaf forest. The start and end date of growing season are late April and mid-October respective with a total length of around 200 days. Its soil is silt loam. This site is simulated for a period of four years from January, 1995 to December, 1998. The annual precipitation is 1682 mm in 1996, and 1435 mm, 1616 mm in 1997 and 1998 respectively. Its annual mean temperature is around 14˚C. Meteorological attributes including air temperature, air humidity, precipitation and wind speed and the surface energy and NEE are continuous measured at a 36 m tower on a half-hour basis during the simulation period. Solar radiation (direct and diffuse) is measured above the canopy. A clay content of 20% and sand content of 24% is provided by Hanson et al. [1998].

b) Tharandt (temperate evergreen needleleaf forest)

The site is located 20 km southwest of Dresden, Germany (50˚ 58' N; 13˚ 34' E). Its dominant vegetation type is evergreen needleleaf. The stand age is approximately 120 years old. The average canopy height is about 26 m. The maximum LAI over a year is generally above 7, e.g. 7.6 in year 2000. The average annual precipitation from 1997 to 1999 is 824 mm. The average air temperature is 7.5˚C. The soil type is loamy brown earth. Both its weather station and eddy covariance measurements are at 42 m. The period modeled in this study is from January 1996 to December 1999 for 3 years. Continuous meteorological and flux measurements for this period are available on a half-hour basis. Soil clay and sand contents of 15% and 30% are estimated based on the soil texture.

c) Boreas NSA (Boreal evergreen needleleaf forest)

This study site is situated on the relatively flat terrain of the Canadian Shield, near the northern edge of the boreal forests, in the zone of discontinuous permafrost. Its forest is dense 10 m tall black spruce. Carbon-rich peat soils underlie the site. The tower above the canopy is located at the latitude of 55˚ 52’ N and longitude of 98˚ 29’ W. The soil clay and sand percentages are estimated from the soil texture of sandy clay. The 3 year period from January, 1995 to December, 1998 for 3 years is simulated. A 30-m tall tower extends 10 m above the canopy. From the tower, eddy-correlation flux measurements for NEE and energy fluxes are collected every half hour.

d) Reserva Jaru (Tropical evergreen broadleaf forest)

Reserva Jaru (10˚ 05' S, 61˚ 55' W) is an ABRACOS site. It is located about 80 km north of Ji-Parana in Rondonia, Brazil and at 120 m above sea level. The site has a pronounced dry season between June and August, often with periods of several weeks

without rain. The wettest period is December to April. The dominant vegetation type is tropical evergreen broadleaf forests. Its forest climate measurements were made from the top of a 52 m high tower since October 1991 [McWilliam et al. 1996; Roberts et al., 1996]. We use the meteorological observation from January, 1992 to December 1993 for 2 years as the simulation period. The timestep is an hour for the site. Its soil clay and sand contents are the averages of measured values at the surface and at 1 m depth [Wright et al., 1996]. The soil is rich in macropores in the surface layers so that its infiltration capacity is high [Yang et al. 2000].

3.3.2 Results and discussions

We run the model at each site with local observed meteorological forcing of air temperature, precipitation, surface net radiation, air humidity and wind speed. The atmospheric CO_2 and O_2 concentrations use 360 ppmv and 21 ppv respectively. The initial values of the soil moisture and the carbon and nitrogen pools use equilibrium values obtained by running the model with the atmospheric forcing repeated for several times. The goal of these simulations is not to match the observation but to validate the model performance. Therefore, all the parameters are based on values given in table 3.1 and 3.2 unless otherwise stated. Site-specific parameters are listed in table 3.4. The running timestep is 30 minutes for the FLUXNET sites and 1 hour for the Reserva Jaru. A full vegetation-coverage is imposed.

The simulated results are presented and discussed specifically for each site. Different experiments were conducted in each case as to explore the model performance and the difference between the simulation and the observation, through which the sensitivity of the model to some important parameters are presented. The long term

evolution, i.e., over a year, of the surface fluxes presented below are 10-day running averages of the daily average to smooth the day to day variation. The short term one uses the values at each timestep.

Table 3.4 Site-specific descriptions and parameters.

	Oak Ridge	Tharandt	Boreas NSA	Reserva Jaru
Site location	35° 57'N, 84° 17'W	50° 58'N, 13° 34'E	55° 87'N, 98° 48'W	10° 05'S, 61° 55'W
Dominant Forests function type	Deciduous broadleaf	Evergreen needleleaf	Evergreen needleleaf	Evergreen broadleaf
Climate region	Temperate	Temperate	Boreal	Tropical
Soil texture (sand%, clay%)	24%, 20%	30%, 15%	39%, 28%	67%, 24%
SLA (m^2/kg)	30	10	10	25
Temperature of cold stress occurs	5 ˚C	-5 ˚C	-5 ˚C	5 ˚C

a) Oak Ridge

Figure 3.7 compares the 4-year modeled and the measured daily averages of the sensible heat (SH), the latent heat (LE), the soil conduction heat fluxes (G) and the net ecosystem exchange of carbon (NEE) which is the net carbon flux between the surface and the atmosphere and when positive indicating net carbon release of the ecosystem and negative net carbon uptake to the ecosystem. The annual cycles of all fields are well captured by the model. The underestimation of the sensible heat flux and overestimation of the soil heat conduction that happen before the beginning of or after the end of the growing season are associated with an underestimated aerodynamic transfer coefficient for less dense canopies as has been discussed by Zeng et al. [2004]. The annual pattern of the simulated LE is primarily controlled by its annual precipitation as well as the dynamics of its canopy cover. The deciduous forests at the site have small LAI during winter time and large LAI during summer time.

The simulated LAI (figure 3.8) captured the phenology of the vegetation at the site very well for each year except that the predicted LAI magnitude in its peak values, e.g., maximum of 7 to 9, overall is overestimated compared to field observed annual maximums, e.g., maximum of 5.5 in 1996 and 6 in 1997 [Wilson and Baldoccih, 2001]. This is due to the difference between the prescribed and the field specific leaf area (SLA), i.e., 30 m^2/kg C versus 13.4 m^2/kg C [FLUXNET web]. The prescribed SLA is based on the average of a plant function type. In reality, it has large varieties between species, stand ages as well as the locations of plants. A larger SLA as in the model indicates larger leaf area produced by the same amount of leaf production and a higher efficiency to assimilate light.

Both the simulated heat and carbon fluxes have large intra-annual fluctuations, in particular in summer 1995 and late fall 1998. Both periods show a large decrease of the LE during a short period of time associated with a large decrease of ecosystem carbon uptake, implying that the photosynthesis during such periods is significantly underestimated. These features are highly unrealistic compared to the observation. The control of soil moisture on carbon assimilation has been found to be the primary contributor to the underestimation as both abovementioned period are corresponded with low values of simulated soil moisture regulation factor P as defined in equation 3.68 (figure 3.9). P at 1 and 0 indicates no soil-water stress on carbon assimilation and full closure of stomates respectively. Given that forests have the ability to uplift deep soil water if its transpiration needs is limited, we assume the P for all forests always above 0.3 to eliminate the extreme dryness caused photosynthesis ceases. Figure 3.10 presents the simulated surface fluxes after the adjustment on P. The intra-annual fluctuations of LE and NEE are largely suppressed and their agreement with observation is much better than as shown in Figure 3.7.

Figure 3.11 and 3.12 show the simulated 4-yr evolutions of each carbon and nitrogen pool respectively to show the model performance to model ecosystems. Each simulated pool has pronounced seasonality and interannual variation. The model captures the equilibrium states of the ecosystem without any significant drift from year to year for each pool. For this temperature deciduous forest site, the leaf, root and wood accumulate carbon during spring to fall and loss carbon in winter. Most of the assimilated carbon is initially allocated to leaf to increase absorption of solar radiation. Thus, the leaf biomass increases very fast at the beginning of each growing season but slows down when a large

leaf mass is achieved. Leaf mortality occurs around November when daily temperature falls below the critical point. The root and wood biomass change more gradually than leaves. The annual turnover of the wood is small compared to that of leaves and roots. The simulated maximum leaf and root pools, i.e. about 250 and 420 g C/m^2 as well as the root increment, i.e. 100–150 g C/m^2/yr are reasonable compared to field measurement, i.e. leaf pool of 230 g C/m^2, root pool of 360 g C/m^2 [Curtis et al., 2002] and root increment of 100 g C/m^2/yr [DeAngelis et al., 1997]. The fast soil carbon pool exhibits a seasonal pattern that reverse of that of the plant. It decreases during the growing season when the soil respiration exceeds the turnover from plants and increases rapidly when growing season ceases corresponding to the mass mortality of leaves.

Because the CLM-C/N links the C and organic N in plant and soil fast pools with a nearly fixed C/N ratio, the simulated Plant N and soil organic N have the same variation as those of C. The simulated soil NH_4^+ and NO_3^+ both show strong dependences on plant uptake with an obvious decease at the beginning of the growing season when the plant requirement for nitrogen is the strongest. Figure 3.13 and 3.14 show the daily average rates sources and sinks of the soil NH_4^+ and NO_3^+ pools respectively for 1998. The NH_4^+ is largely determined by the rate of mineralization, nitrification and plant uptake. The external source term is small compared to the mineralization rate. The annual nitrification is comparable to the annual plant uptake with it being slightly weaker in spring and stronger in fall, as associated with the plant needs and temperature dependence of the nitrification. For the soil nitrate pool, the nitrification and plant uptake are the most critical processes. The external sink of denitrification loss is negligible while the runoff loss is at times substantial. The simulated results show that the recycling of the nitrogen

within the ecosystem is more important to the soil mineral nitrogen than external sources and sinks at the site.

A period of 7 days starting in June 1 in 1998 is presented in figure 3.15 to compare the modeled diurnal evolution of surface fluxes with observations. This short term prediction adequately captures the diurnal evolution of the surface fluxes. However, LE is underestimated around noon-time, in particular in days when solar radiation is strong, e.g. June 1, 3 and 5, associated with underestimation of NEE. This may be a consequence of an underestimation of the ratio of diffuse to direct solar radiation. The model assumes 70% of incident solar as direct radiation and 30% as diffuse because their ratio is not measured, so that there is limited light for leaves under shade to assimilate even at noon when the radiation is strong. The assumed diffuse ratio is likely low for the aerosol laden hazy condition of the southeastern US especially after precipitation and thus likely results in an underestimation of mid-day photosynthesis and transpiration.

b) Tharandt

Figure 3.16 compares the simulated versus observed SH, LE, G and NEE for the 3-year simulation period. Their annual cycles are well captured except in each year there is lower net ecosystem carbon uptake in fall and a slight larger uptake in spring by simulation than observed and the simulated winter time G shows significantly larger fluctuation than observations. The latter occurs during periods when air temperature are below freezing point (figure 3.17) and may be cause by the model treatment of frozen soil. As this is beyond the scope of this study, we do not further discuss it here.

The NEE is the balance of the photosynthesis and respiratory carbon releases by plants and soil. The difference between simulation and observation can be attributed to

either overestimated photosynthesis or underestimated respiration or both. Figure 3.18 shows the daily average carbon fluxes of photosynthesis (GPP) and respiration (R_s) for the 3 simulation years. The modeled R_s lags GPP by about a month, which is the primary cause of the modeled and observed NEE difference because the seasonal pattern of measured GPP and R_s for the site does not show such a lag [Falge et al., 2002]. Compared to measured annual carbon fluxes at the site for year 1998 (table 3.5), GPP and R_s are overestimated with the later overestimated by more than 463 and 635 $gC/m^2/yr$ respectively, which results in an underestimation of the NPP. The simulated leaf area index (figure 3.19) for the site is smaller than the measured values, i.e. maximum of 6 in 1997 to 1999 and 7.6 in 2000 (from FLUXNET website).

Figure 3.20 compares the seasonality of canopy absorption of PAR and the simulated Rubisco nitrogen. Experiments have found that the photosynthetic capacity acclimates to canopy light conditions over periods of 5 to 15 days to maintain optimum assimilation of light [Kull and Jarvis, 1995]. The acclimation of Rubisco nitrogen to light is reasonably simulated by the model.

The diurnal pattern of simulated heat and carbon fluxes are shown in figure 3.21 for a 7 day period starting May 29, 1999. The estimations agree very well with the observations in both raining and clear periods. A slight underestimation of the LE during noon-time is also shown at the site. The NEE simulation adequately captures the diurnal carbon evolution and day to day variation.

c) Boreas NSA

This is a boreal evergreen needleleaf forest site. Simulations for the long term evolution over the four simulation years of the SH, LE and NEE are shown in figure 3.22.

The soil conduction heat flux was not measured for the simulation period. Because the measured net solar radiation can not be balanced by the observed sensible and latent heat fluxes, there are periods in which both LE and SH are overestimated, e.g. winter time and late growing season in each year.

The simulated large carbon release in winter results from the underestimation of snow coverage of the canopy due to the large net radiation forcing. The net ecosystem uptake of carbon during the growing season is considerably overestimated. A comparison of the simulated annual carbon fluxes with field measured value in 1996 (table 3.5) [Goulden et al., 1996], shows the overestimation of the annual net ecosystem uptake is due primarily to the underestimation of the soil respiration. The predicted soil respiration is only about half of that measured, giving an underestimation of 296 g $C/m^2/yr$ while the autotrophic respiration is larger than its measured value by 90 $gC/m^2/yr$. The modeled carbon annual assimilations for each year in 1996 to 1998 are comparable with measurements within 20%. The significant underestimation of the soil respiration results in a considerable net carbon uptake at the site for the simulation period while the measurements show either a source in some years, i.e. in 1995 and 1997, or a small sink in others, 1996 and 1998. Both temperature dependence of soil respiration and neglect of slow soil release of carbon can be attributed to the underestimation of the soil respiration because the slow soil carbon pool is large compared to the fast pool at the boreal forest area [Bajtes, 1996].

Figure 3.23 shows the simulated LAI. The model simulated the LAI dynamics and magnitude very well the field measured values, e.g. maximum value of 4.2 m^2/m^2 in 1994 [Steele et al., 1997]. The modeled LAI is an index of the green leaves that are free of

snow coverage. Its smooth winter pattern indicates that no snow coverage is modeled.

d) Reserva Jaru

This tropical evergreen forest site has alternative dry and wet seasons. Its high temperature maintains a fast turnover rate of the plant and soil organic matter. The soil has many macropores. It has been found that the soil hydraulic scheme in the standard CLM2 causes significant error in estimating the soil water balances at the site. Therefore, we modified the hydraulic scheme to that described in the Liu and Dickinson [2003] for this site. The flux tower observations at this site are not continuous. The simulated surface fluxes are compared to two periods of measurement: August 8 to October 4, 1992 and April 4 to July 26, 1993.

Figure 3.24 presents a comparison of modeled versus observed sensible and latent heat fluxes at each time step of the two experimental periods. The latent heat fluxes are well simulated, but less so the simulation of the sensible heat fluxes. The cause of this problem is unclear but certainly is not related to the ecosystem processes because similar features exist in the standard CLM2 results.

Figure 3.25 shows the short term evolution of the surface carbon fluxes. The observed NEE is the sum of the CO_2 turbulent flux and the within canopy CO_2 storage variation at each time step [Grace et al., 1996]. The diurnal variation is adequately captured by the model. The overestimated mid-day NEEs in some days, i.e. May 27 to 30, are associated with intensive precipitation.

Its simulated annual carbon fluxes are shown in Table 3.5. The annual GPP's of the site are 3435 g C/m^2 for both simulation years. This magnitude is similar to the measurement at a evergreen forest site nearby, i.e. 3249 g C/m^2 [Falge et al., 2002]. Both

sites have similar annual NEE. More than half of the carbon obtained by the leaves are consumed to retain the activity of the plant functioning. The simulated NPP is 1344 and 1339 g C/m^2 for 1992 and 1993 respectively. The simulated net ecosystem exchange of carbon of above 750 g C/m^2 for both years overestimates the net carbon uptake compared to the observed 580 ±100 g C/m^2 in 2000 [Kruijt, 2002].

3.3.3 Conclusion

The CLM-C/N has been tested at 4 forests sites with different environments. The model simulates the seasonal development of vegetation cover reasonably in both its absolute magnitude and seasonal cycle except at the Oak Ridge site, where the assumed SLA is too large compared to the field values, indicating the importance of the SLA for modeling accurate values of the LAI. The dynamics of leaf Rubisco nitrogen as acclimation to environmental irradiant condition is reasonably captured by the model. The simulated latent heat and photosynthesis fluxes are reasonable compared to measured values, indicating also that the predicted value of photosynthetic capacity is reasonable.

The simulated nitrogen cycle shows that majority of the plant nitrogen needs come from its recycling within the ecosystem. The external sources and sinks may play a role in changing the nitrogen cycle in the long run but do not contribute as much to the seasonal variability of the soil mineral nitrogen supply as the recycling. However, the runoff loss of nitrate can be a primary control factor for the soil nitrate ion concentration during wet period.

The carbon assimilation rate under adequate irradiance depends largely on how much of the radiation is direct versus diffuse. Thus, it is important to determine the diffuse fraction of incident solar radiation at top of the canopy in order to estimate the

assimilation rate accurately. The soil moisture dependence of the carbon assimilation is another important issue for proper prediction. An assumption is imposed to the current model to avoid extreme dryness to cease carbon uptake for forest vegetation types given that the strong ability of forests to tolerate drought stresses.

The simulated results also suggest that there are significant discrepancies between the modeled and observed respiration including both plant autotrophic respiration and soil heterotrophic respiration. The current temperature dependence of respiration needs further evaluation.

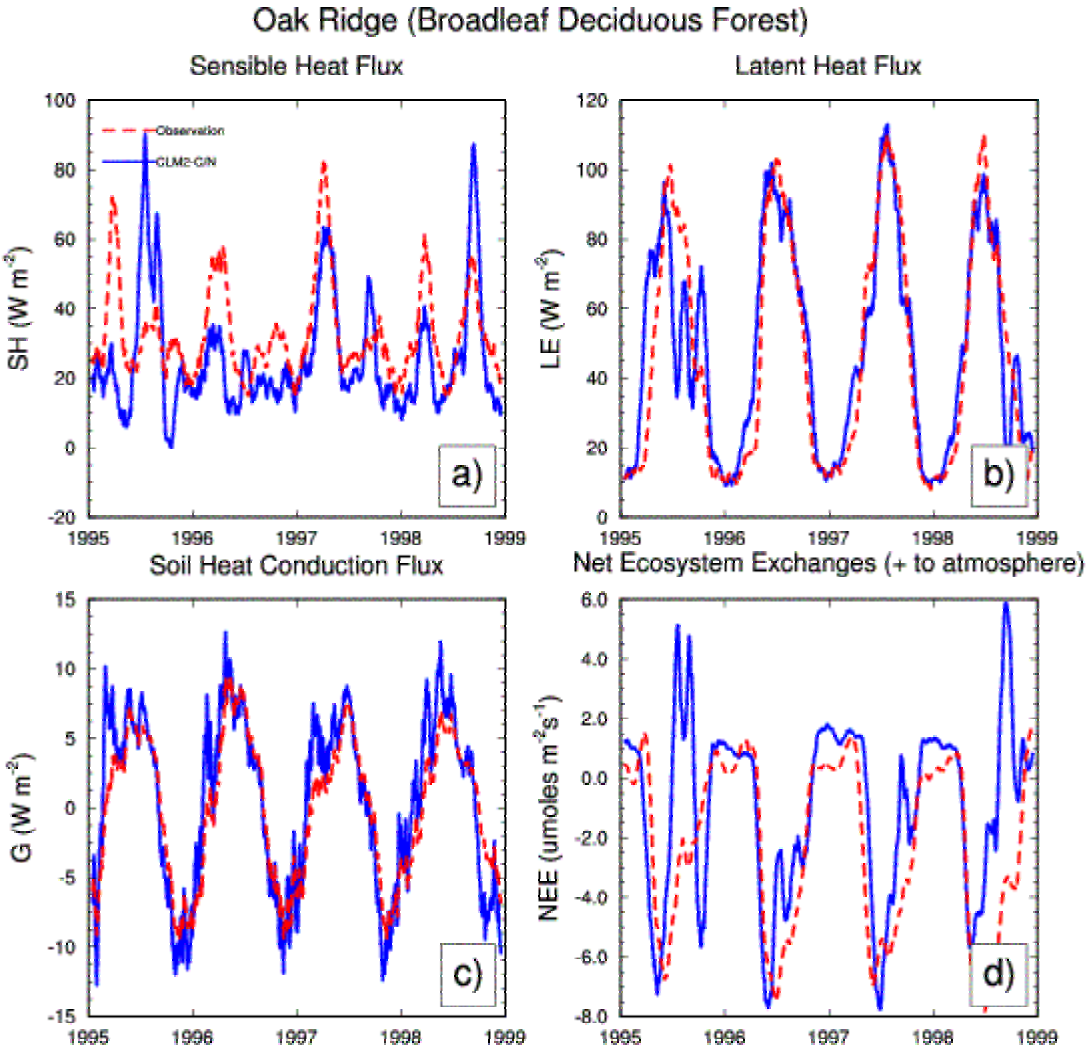

Figure 3.7. Comparison of the long term evolution of observed and CLM-C/N modeled fluxes of surface sensible heat (SH), latent heat (LE), soil heat conduction flux(G) and net ecosystem exchange of carbon (NEE) at Oak Ridge. The presented values are 30-day running average of daily mean.

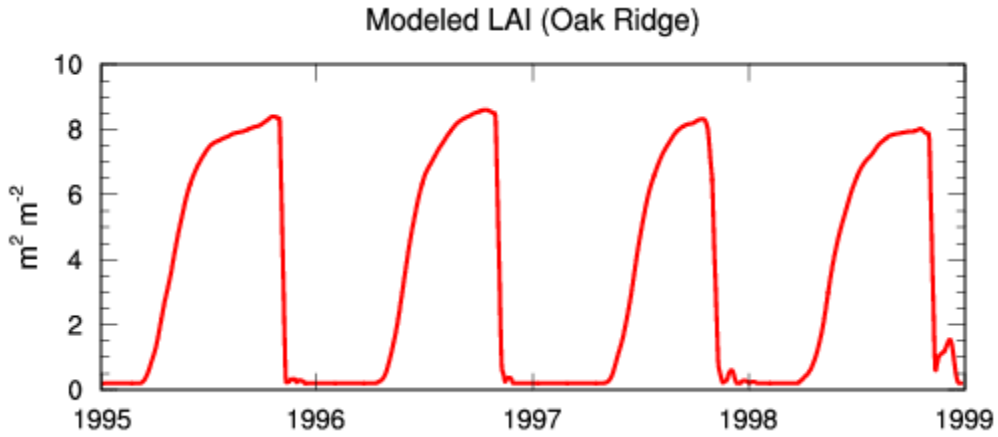

Figure 3.8. Simulated leaf area index at Oak Ridge during the 4-yr period.

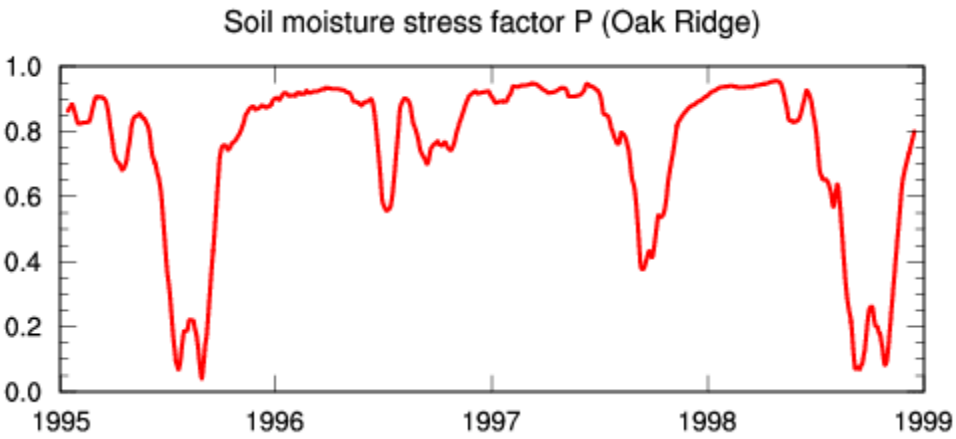

Figure 3.9. The predicted carbon assimilation regulation by soil moisture. Zero indicates extreme soil dryness, corresponded to full closure of stomates and cease of carbon assimilation. One indicates no soil moisture limitation on leaf carbon assimilation.

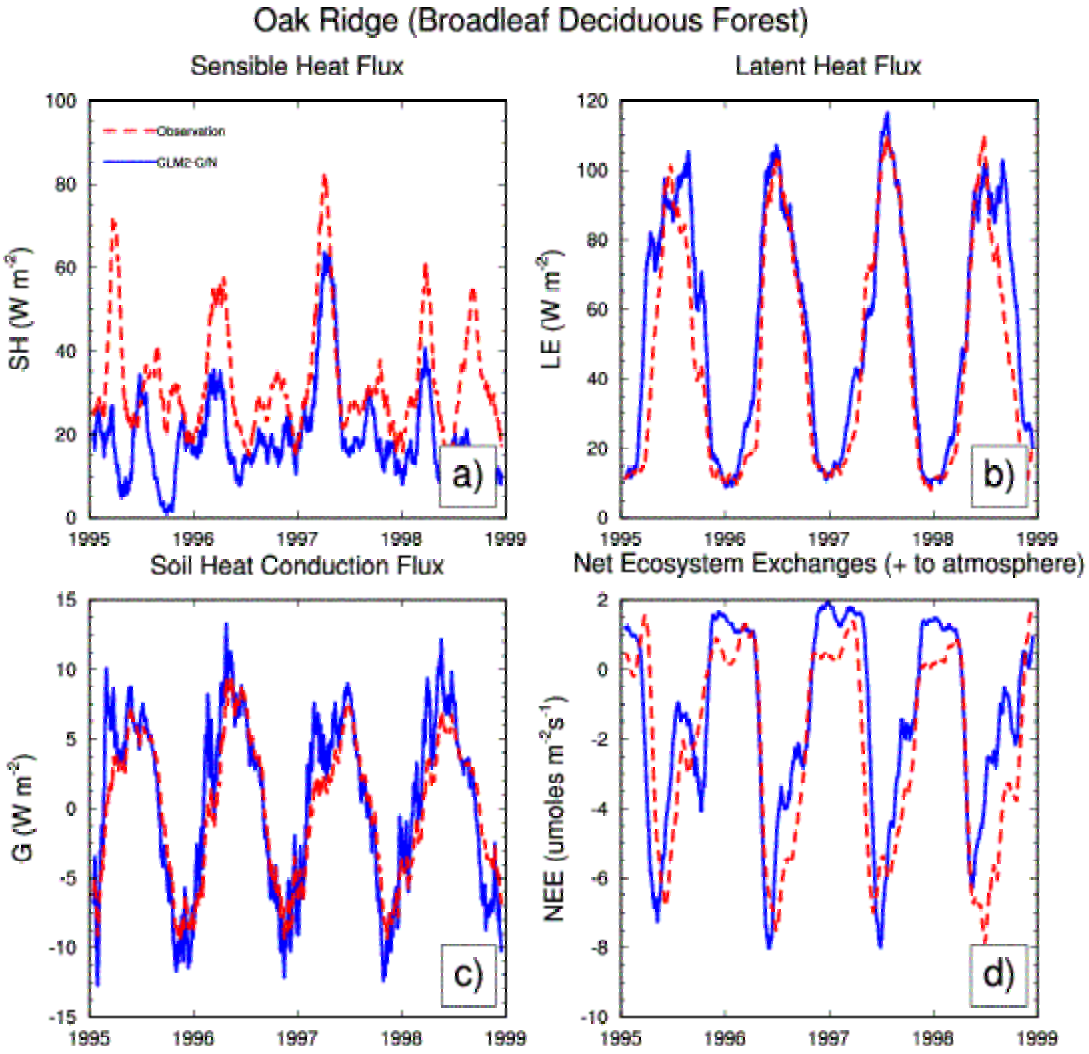

Figure 3.10. The same as figure 3.7 but the soil moisture regulation factor P is assumed ≥ 0.3.

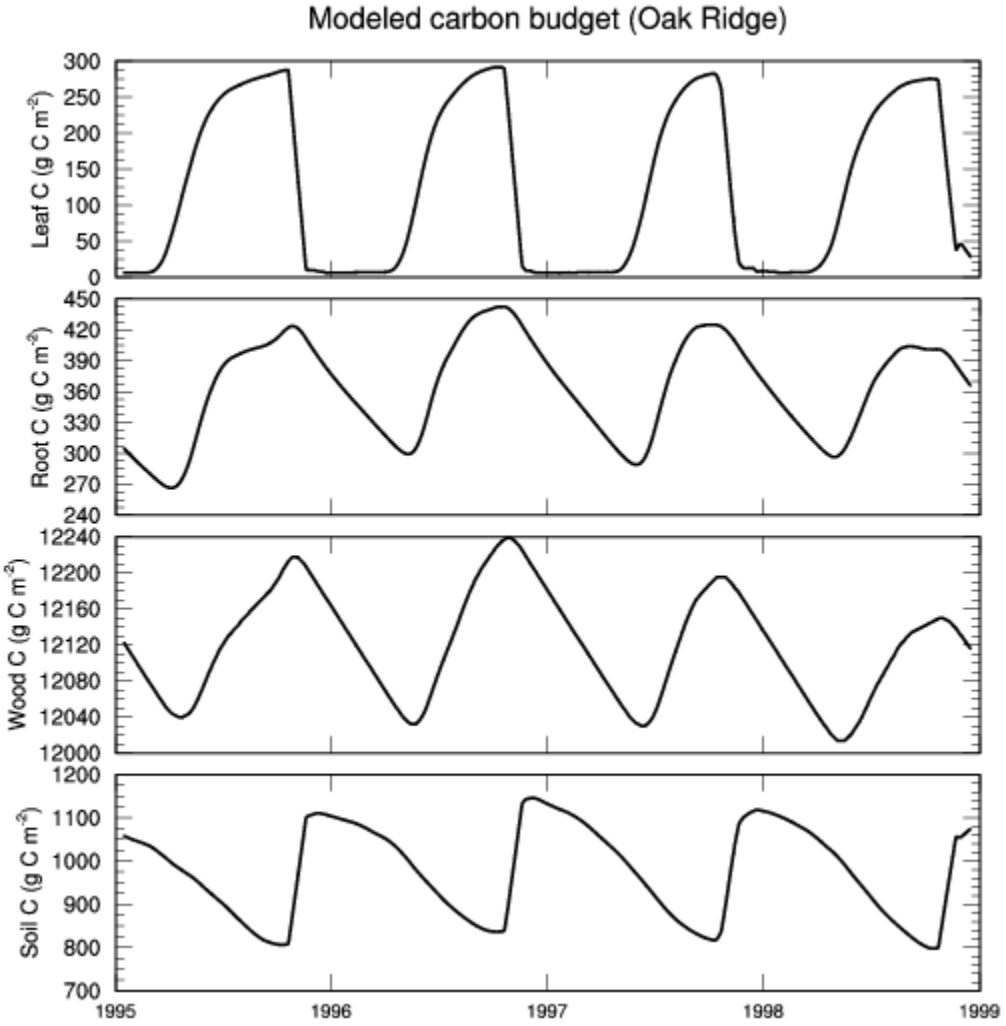

Figure 3.11. CLM-C/N modeled seasonal development of ecosystem carbon cycle at Oak Ridge. Four carbon pools are presented (from top to bottom panel): leaf, root, wood and soil carbon.

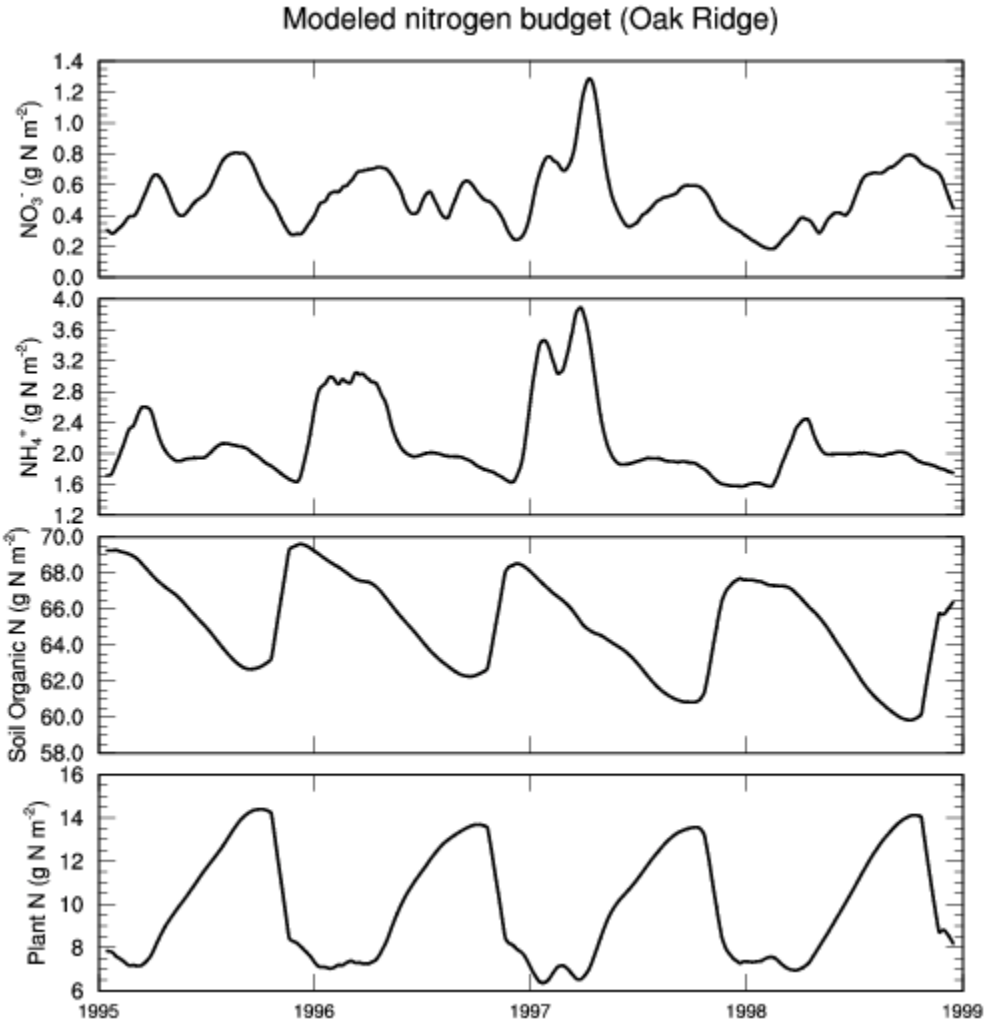

Figure 3.12. CLM-C/N modeled seasonal development of ecosystem nitrogen cycle at Oak Ridge. Four nitrogen pools are presented (from top to bottom panel): soil nitrate ion, soil ammonium ion, soil organic nitrogen and plant nitrogen.

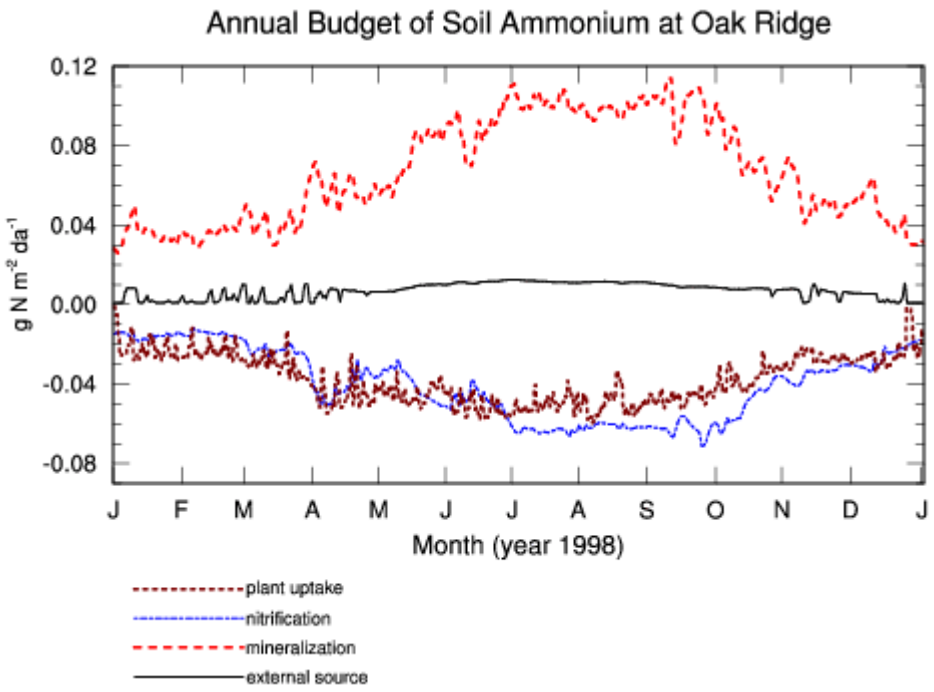

Figure 3.13. CLM-C/N modeled annual budget of soil ammonium at Oak Ridge.

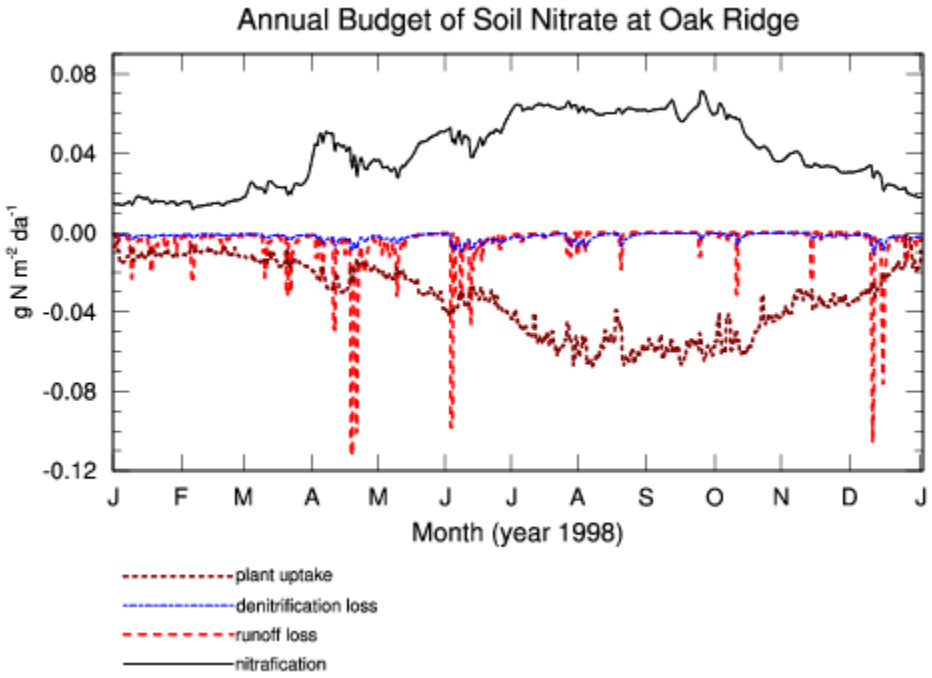

Figure 3.14. CLM-C/N modeled annual budget of soil nitrate at Oak Ridge.

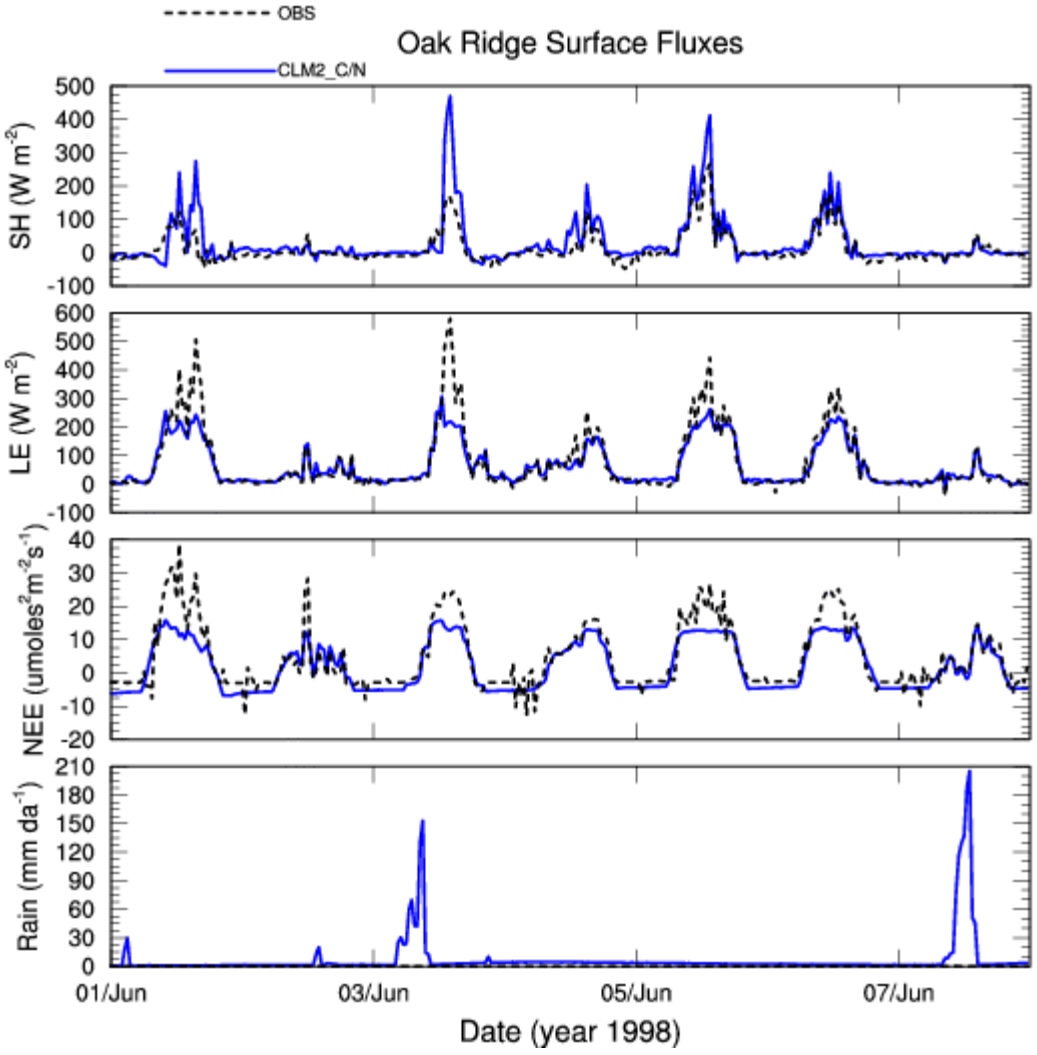

Figure 3.15. Comparison of observed (dashed line) and CLM-C/N modeled (solid line) surface heat and carbon fluxes from 1 June -7 June,1998 at Oak Ridge. The bottom panel shows the precipitation during the comparison period.

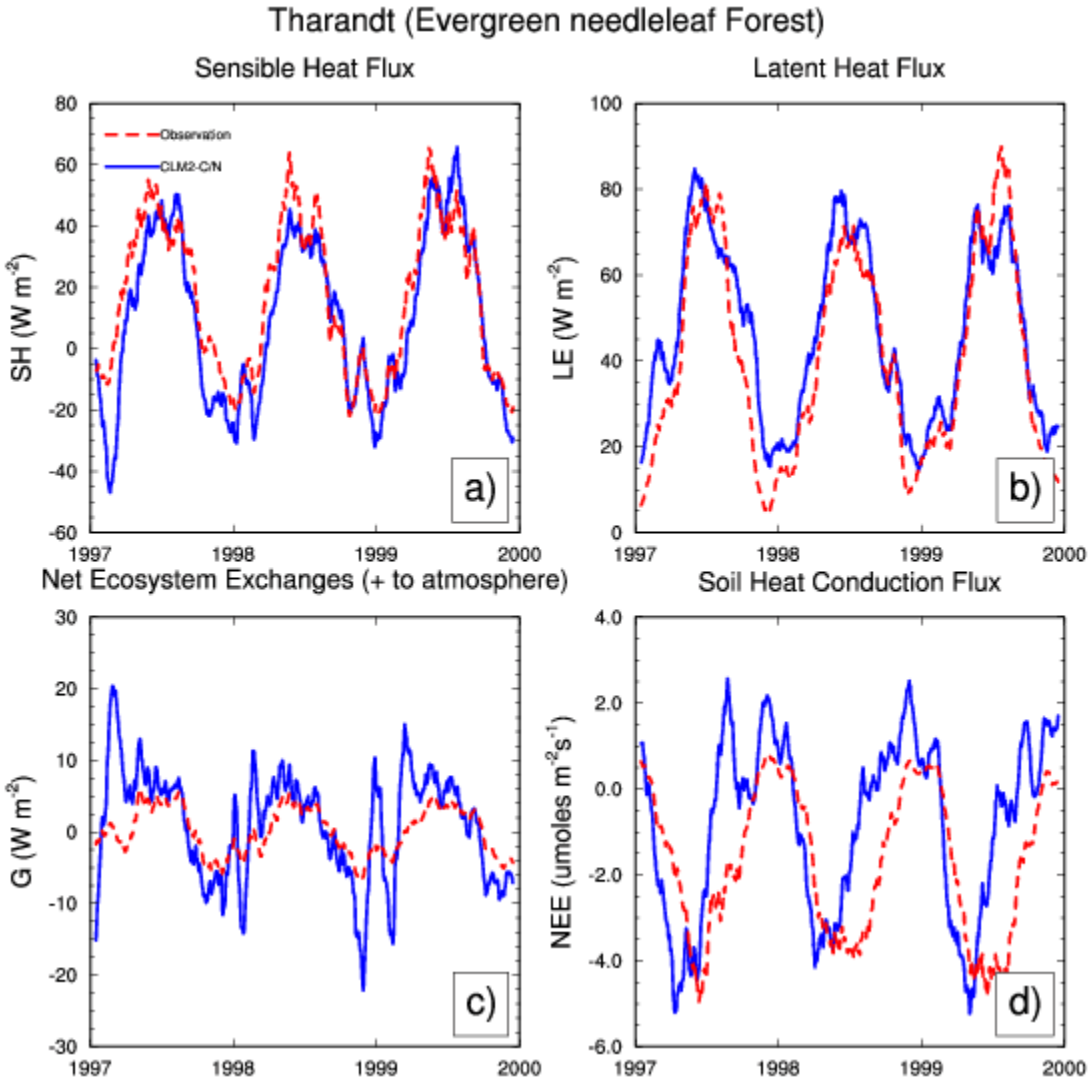

Figure 3.16. The same as figure 3.10 but at Tharandt and from January, 1997 to December, 1999 for 3 years.

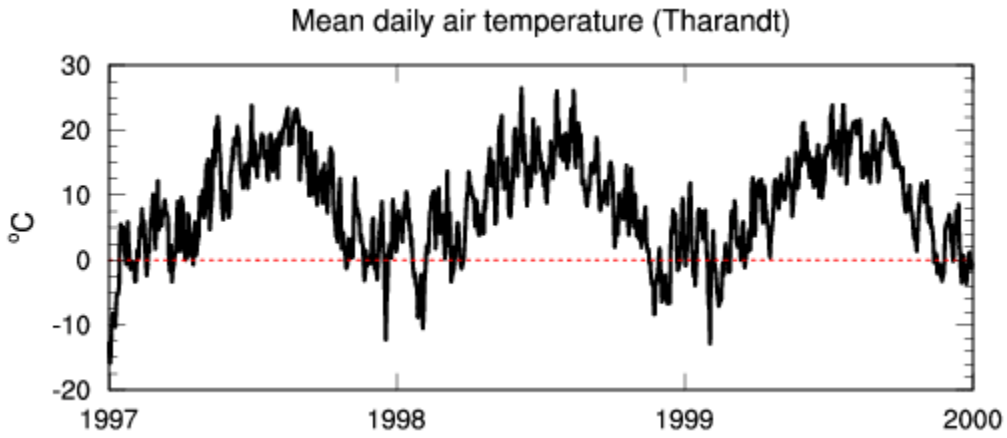

Figure 3.17. The daily mean air temperature at Tharandt for the 3-yr simulating period.

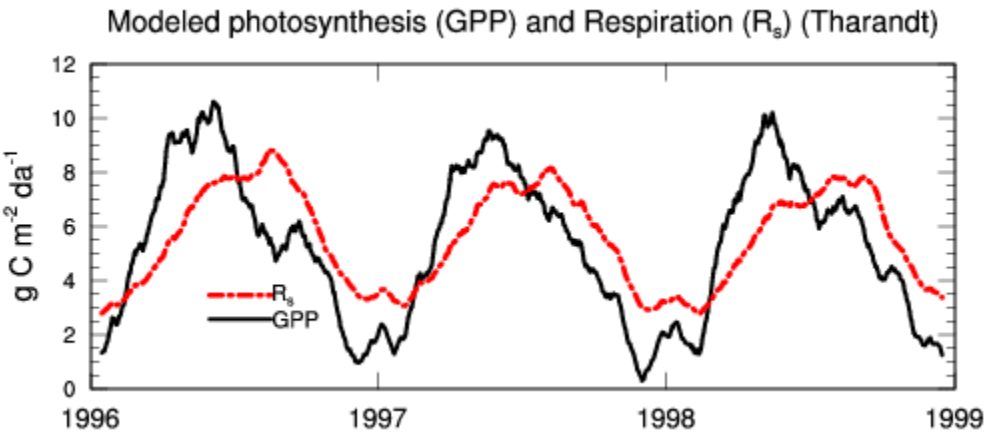

Figure 3.18. CLM-C/N modeled seasonal cycle of the photosynthesis GPP (solid line) and ecosystem respiration R_s (dashed line) at Tharandt for the 3-yr period.

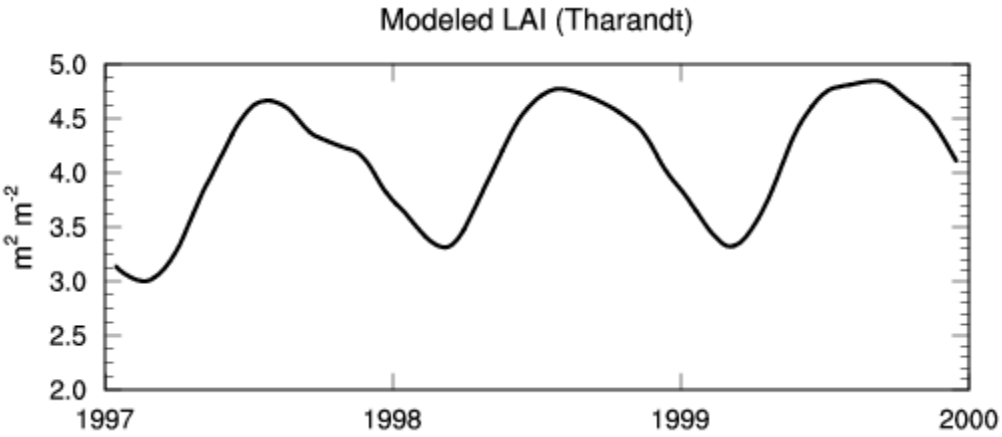

Figure 3.19. CLM-C/N modeled leaf area index LAI at Tharandt for the 3-yr period.

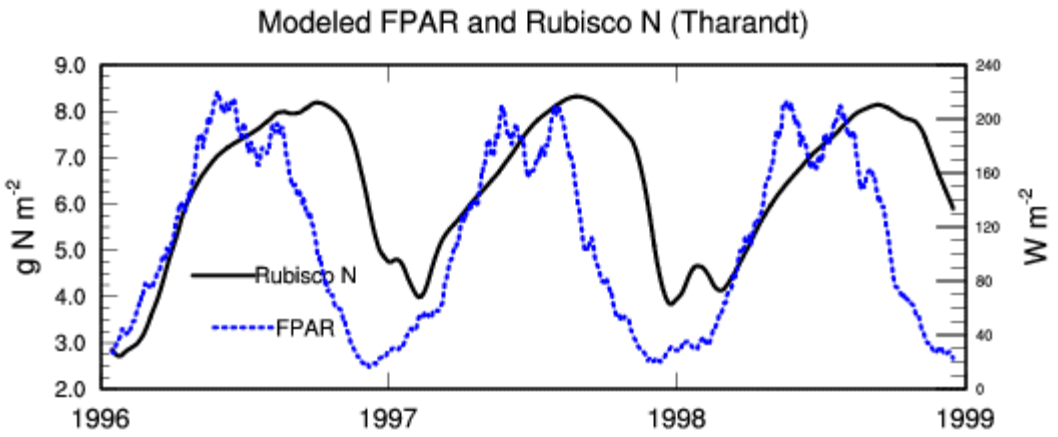

Figure 3.20. The modeled relationship between the absorption of PAR (dashed line) and the content of canopy Rubisco nitrogen (solid line) at Tharandt for the 3-yr period.

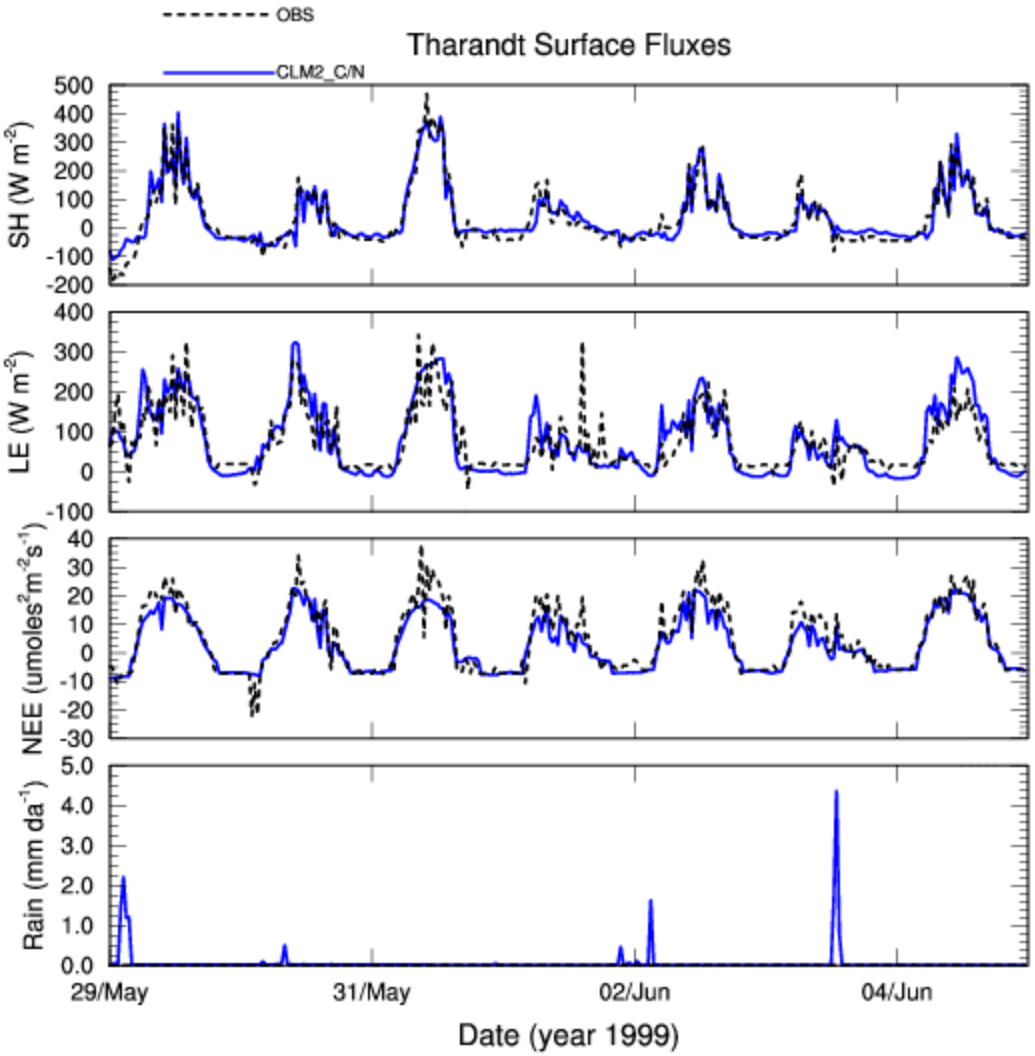

Figure 3.21. The same as figure 3.15 but for Tharandt and from 29 May to 4 June, 1999.

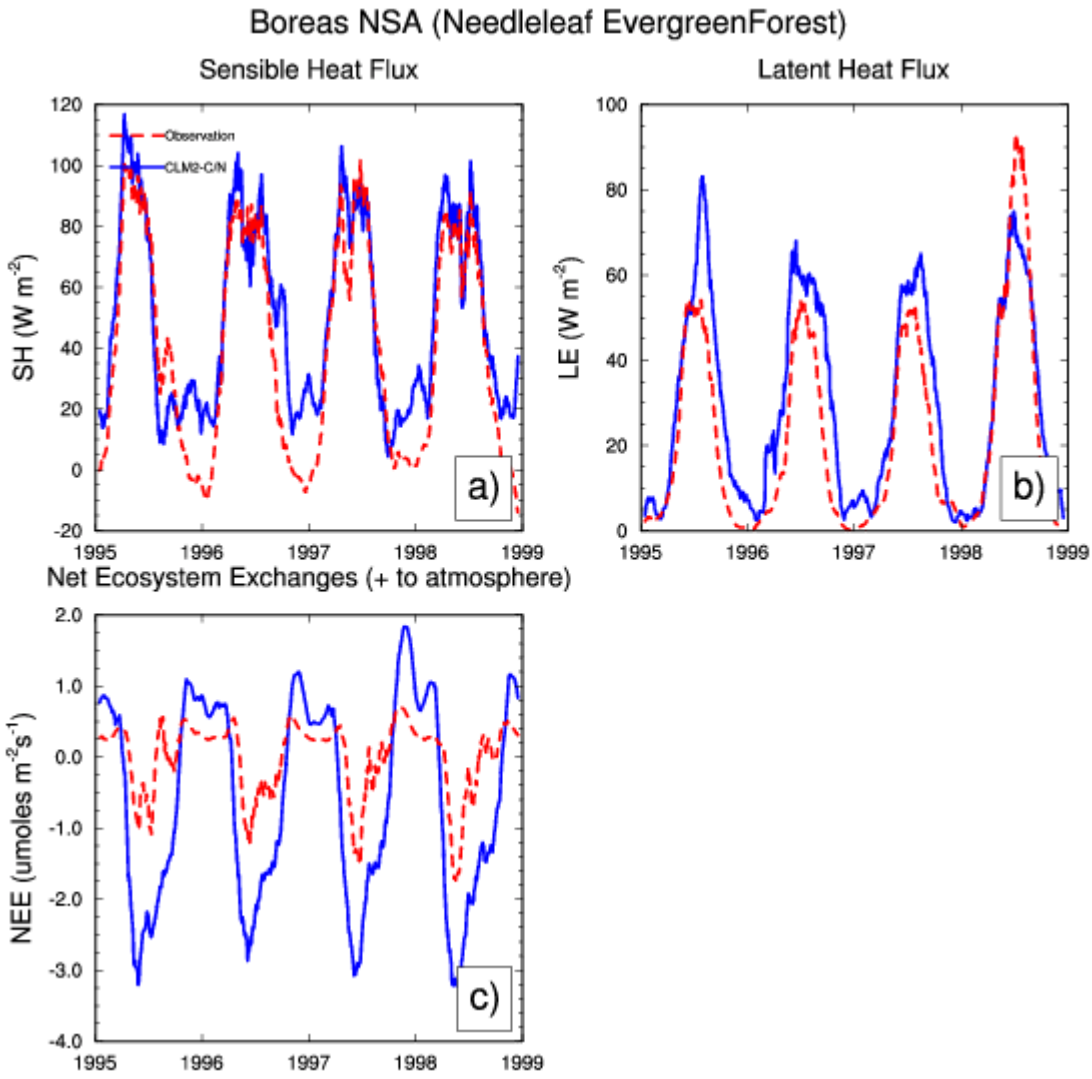

Figure 3.22. The same as figure 3.10 but for Boreas NSA and without comparison of soil heat conduction flux.

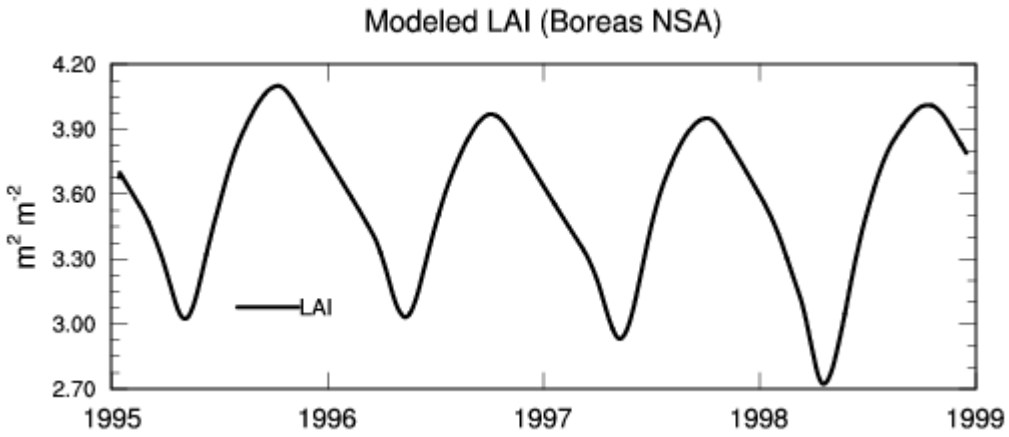

Figure 3.23. CLM-C/N Modeled seasonal evolution of LAI at Boreas NSA from 1995 to 1998.

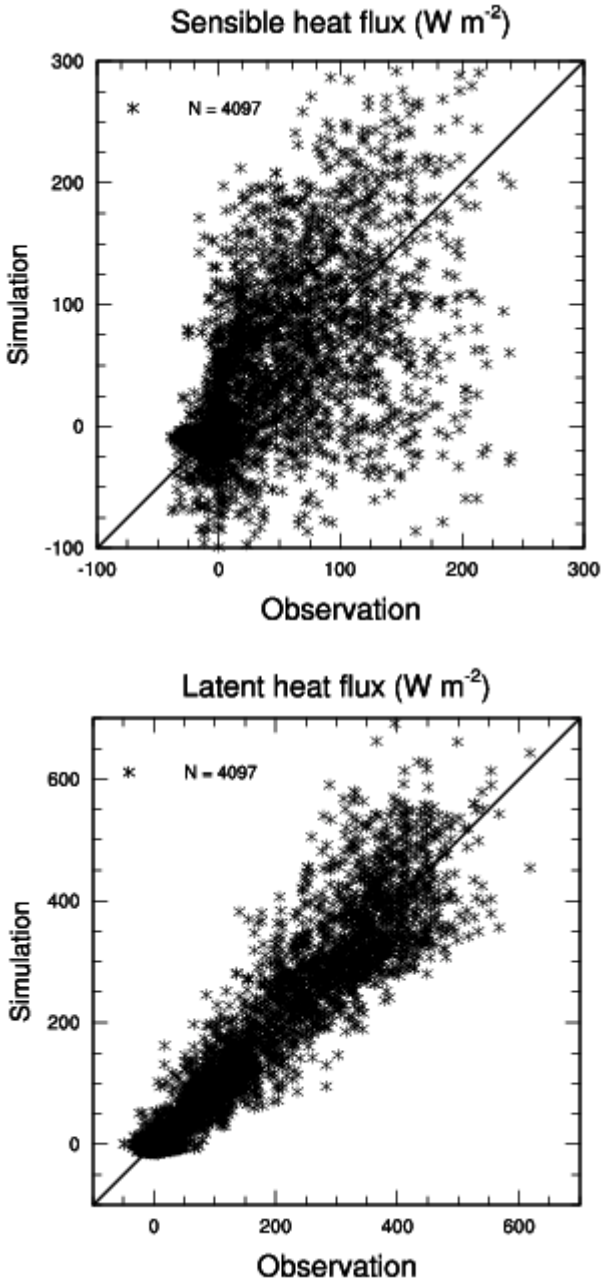

Figure 3.24 Comparison of observed and modeled surface sensible heat flux (upper panel) and latent heat flux (lower panel) at Reserva Jaru for 2 periods in 1992 and 1993: August 8 to October 4, 1992 and April 4 to July 26, 1993.

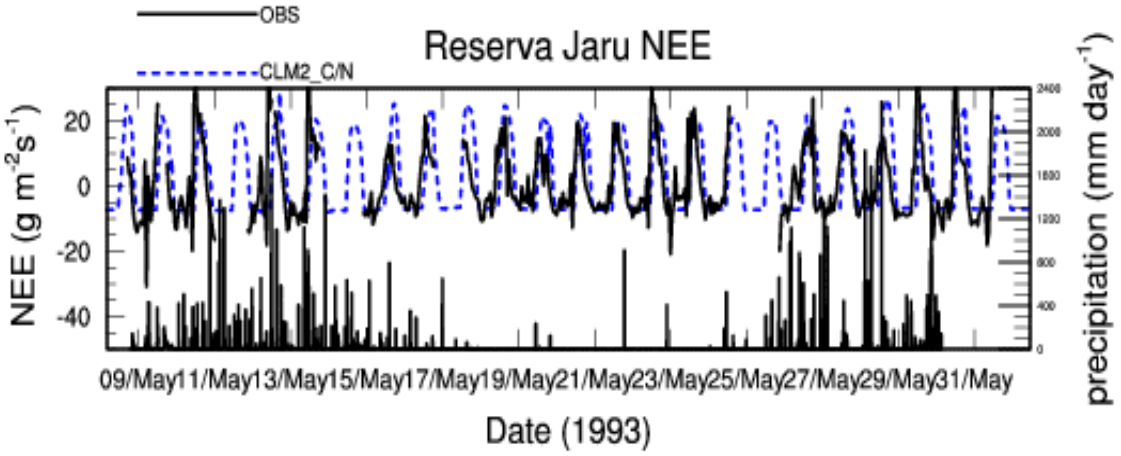

Figure 3.25. Comparison of observed (solid line) and modeled (dashed line) NEE from May 9 to May 31, 1993 at Reserva Jaru. The lower part of the panel shows the precipitation during this period.

Table 3.5. CLM-C/N predicted annual carbon budget (MOD) at each site and available observed values (OBS) from FLUXNET and Kruijt [2003][†].

	GPP		NPP		R_{hetero}		R_{auto}		NEE	
	MOD	OBS	MOD	OBS	MOD	OBS	MOD	OBS	MOD	OBS
Oak Ridge										
1995	2637		1414	1200	678		1223		736	610
1996	2558		1338		711	750	1220		627	597
1997	2668		1380		762		1288		618	618
1998	2576		1268		836		1308		432	592
Tharandt										
1997	2292		1050		509		1242		541	548
1998	2253		1010		565		1243		445	614
1999	2289	1790	1032		580		1257		452	690
Boreas NSA										
1995	785		405		257		380		148	-20
1996	726	825	357		264	560	369	280	93	7
1997	713	821	348		278		365		70	-11
1998	866	868	447		264		419		183	35
Reserva Jaru[†]										
1992	3435	3249	1344		696		2091		648	580
1993	3435		1339		700		2096		639	

3.4 Results from inclusion in CCSM

We perform climate model simulations using the National Center for Atmospheric Research (NCAR) Community Climate System Model, version 2 (CCSM2) [Blackmon et al., 2001] at about 2.8˚ resolution using observed sea surface temperature from January 1986 to December 1994 for 9 years. Initial conditions for the carbon/nitrogen pools and other land and atmospheric attributes were obtained by running the coupled model with repeated SST forcing until equilibrium is reached. Results from CCSM2 coupled to the CLM2 with the same SST forcing and initial condition are used for comparison. For simplicity, simulation of CCSM coupled with CLM-C/N and CLM2 will be referred to as CLM-C/N and CLM2 respectively. The predefined global distribution of the primary plant function type and its fraction in each grid are shown in figure 3.26.

The performance of the coupled CLM2 and Community Climate models have been discussed in several papers [Bonan et al., 2002; Zeng et al., 2002]. Here, we emphasize changes introduced by the enhanced consideration of ecosystem to assess how the interactions between physical and ecosystem are captured by the CLM-C/N. The CLM-C/N differs from the CLM2 in affecting the climatology through two biological factors: LAI and photosynthetic capacity (V_{max}). Both are prescribed in the CLM2 but predicted in the CLM-C/N.

Figure 3.27 shows the global distribution of the LAI modeled by CLM-C/N and the difference between the modeled LAI and that prescribed in CLM2 for northern winter (DJF) and summer (JJA) respectively. Monthly values of the simulation are averages from 1986 to 1991. The prescribed monthly LAI was derived from 1-km Advanced Very

High Resolution Radiometer (AVHRR) data for April 1992 to March 1993 [Bonan et al., 2002]. The simulated LAI (2a and 2b) has largest values in the tropics throughout the year with above 7 in Amazonia and central Africa. Areas in the mid and high latitude in northern hemisphere have strong seasonality with LAIs close to zero for all areas except the boreal forests zone between 50˚ -60˚N. The simulated LAI largely reflects the land cover and the climate regime. The differences between the simulated LAI and prescribed LAI for both seasons (2c and 2d) are most prominent in the tropics. Their simulated LAIs are larger than those prescribed by at least 3 in both seasons. The observations suffer from values of LAI over 4 not detectable because of too little contribution by more leaves to the observed reflectance. They also appear to be low because of cloud contamination. Compared to the prescribed LAI, the CLM-C/N has lower LAI over crop lands in their growing season including eastern United State, central Europe and southern south America and slightly higher LAIs over Eastern Asia and northern high latitude areas (>50˚N). These difference fields are similar to those found in comparing the derived LAIs from a new satellite observation, the MODIS, with the AVHRR-derived LAI [Tian et al., 2004a] except that the simulated LAIs over tropical regions are substantially larger than both satellite product. MODIS observations saturate at an LAI of 6. The simulated LAIs in tropics are within the range of field measurements, e.g. 6-16 for tropic rainforests with 8 as the most frequent values [Schulze, 1982].

Figure 3.28 and 3.29 compare the simulated surface temperature and precipitation from both runs for winter and summer respectively. The precipitation (4a and 4b) difference is insignificant over all regions, while the surface temperature (3a and 3b) is decreased by the CLM-C/N by several degrees over southern Africa and the Brazil

savanna and increased by the same over central Europe northern summer (JJA). These changes in the surface temperature are primarily contributed by the changes in leaf area from CLM2 to CLM-C/N because similar differences were observed when comparing the surface temperature simulated by the CLM2-CCSM using MODIS LAI and that using the standard AVHRR LAI [Tian et al., 2004b].

Figure 3.30 shows the areally-weighted latitudinal distribution of the estimated carbon cycle annual means. The highest carbon assimilation rates occur near the equator (10˚S to 10˚N), followed by a smaller peak between 35˚ and 45˚S; and a yet smaller peak between 50˚ and 60˚N. The simulated plant respiration shows a similar distribution pattern except that the northern high latitude peak is not as obvious as that in the carbon assimilation. The NPP as the difference between the assimilated carbon and plant respiration is strongest in the tropic and the mid latitude in the southern hemisphere. The NPP in northern high latitude regions is slightly higher than that in the northern mid latitude regions. The respiration and the NPP are comparable for regions beyond the tropics, while the most of the carbon assimilated in the tropics is released back to the atmosphere as respiration. The latitudinal pattern of simulated annual NPP reflects the relative distribution and productivity of biomass. The NPP generally increases from dry and cold biomes to warm, moist biomes. The result is comparable with the latitudinal distribution of the mean annual NPP from 16 ecosystem models [Hibbard and Sahagian], e.g. 1000 g C/m^2 for the tropics, 400 for the northern high latitude and 600 for the southern mid-latitude regions.

To get more insight into how the CLM-C/N models the ecosystem responses and effect on climate, we selected 4 regions for further discussion. Amazon (10˚S-0 and 50-

75˚W represents tropical evergreen forests. Northern Europe (60-70˚N and 20-70˚E) represents boreal forests. Western United States (30-50˚N and 110-120˚W) represents temperate grassland and southern south America (25-60˚S and 50-80˚W) represents temperate mixed wood and crop land. Monthly mean from 1988 to1993 of the simulation are presented.

The modeled LAIs (figure 3.31) over the four comparison regions all show prominent seasonal and interannual variability. Among them, the Amazon has the largest LAI magnitude with small seasonal variability corresponding to its vegetation cover type. Northern Europe has strong seasonality with peak values in a year above 4 and winter values about 1. The LAIs over the two temperate grass and woodlands are smaller compared to that over forests during the growing season. The small LAIs over western US are related to its summer dryness. The interannual variation of modeled LAIs corresponds well with that of precipitation (figure 3.32). For instance, the decrease of precipitation in 1991-1992 El Nino over Amazon results in lower LAI in 1992 there than other years.

Figure 3.33 shows the seasonal development of modeled carbon assimilation (GPP) and ecosystem respiration by the CLM-C/N for the four selected regions over the comparison period. Their annual carbon assimilations are largely balanced by annual carbon releases. For the Amazon, the carbon assimilation is larger than the respiration during the wet season, i.e. October to March, but smaller during dry season, at which time the GPP is limited by the soil dryness while the respiration is not limited because of the high temperature. Both carbon assimilation and respiration over northern Europe show strong seasonal variations compared to that of Amazon, which agrees well with

field observation that boreal forests have larger seasonal amplitudes of GPP and respiration [Falge et al., 2002]. The seasonal GPP and respiration over the western US and northern Europe are slightly out-of-phase with the respiration peak lagging carbon assimilation peak by about a month. Such a pattern does not appear in the Amazon and southern South America. The modeled ecosystem respiration does not take into account the carbon release from slow soil carbon pools. The annual budget of the modeled GPP over all the four regions is slightly larger that that of modeled respiration because of permanent storage in such a slow carbon pool.

The rate of carbon assimilation is controlled by multiple factors and thus it is difficult to relate it to the photosynthetic capacity which is proportional to the content of Rubisco N in the CLM-C/N. Plants invest assimilated N to Rubisco based on the availability of nitrogen and the optimization to environmental situation in particular the irradiance, so as to avoid overload. Thus, its seasonality should follow that of solar radiation when not limited by soil supply. Figure 3.34 presents the seasonal development of both solar radiation and Rubisco N together for the four selected regions. Both attributes are represented as fractions of their annual maximum. It shows that the Rubisco N acclimates to environment radiation quickly during the growing season over all regions except Amazon where the Rubisco N decreases during wet season. This decrease of Rubisco N results from the large structural cost of N in the period, indicating that the Rubisco N becomes limited during the wet season. It is also associated with large nitrate ion loss through runoff during the wet season.

Figure 3.35 shows the seasonal cycle of ammonium and nitrate soil ions over the four regions being compared. The soil mineral nitrogen is relatively stable from year to

year over Amazon, Northern Europe and western US and less so over southern South America due to assumed fertilization for croplands. The simulated nitrate ion concentration is mostly lower than the ammonium for the four regions associated with large runoff loss and quick uptake by plants. Their peaks correspond well with the dry period of a year. Northern Europe shows the largest absolute value and seasonal amplitude of soil ammonium ion concentration of the regions. This is associated with its relatively low and large seasonal-amplitude of temperature because both mineralization and nitrification processes are strong temperature dependent.

Figure 3.36 and 3.37 show the modeled canopy transpiration and Rubisco nitrogen content for the 4 regions. The transpiration and Rubisco N are closely correlated very well in particular in Northern Europe and southern South America. The control of nitrogen on photosynthesis is clearly illustrated by their similar seasonal cycle and year-to-year variation. For the Amazon, a large Rubisco N content is maintained throughout the year corresponding to its high photosynthetic activity. However, the soil moisture limitation is much stronger than the nitrogen limitation on photosynthesis, so that the Rubisco nitrogen appears to overload during the dry period. Similar pattern appear in the simulated transpiration and Rubisco N over western US.

Figure 3.38 shows the seasonal cycle of the simulated leaf and root biomass. Their annual patterns are adequately captured by the CLM-C/N, compared to the observed live fine root mass for different biomes (Jackson et al., 1997), i.e. 0.17 kg C/m^2 for tropic rainforest, 0.11 for boreal forest, 0.14 for woodland and shrubland and 0.42 for temperature grassland. The root mass over western US is substantially underestimated and that over Northern Europe overestimated. The result is consistent with the

simulations presented in Dickinson et al. [2002]. They have interpreted the discrepancies between modeled and observed root mass as due primarily to the root turnover parameterization.

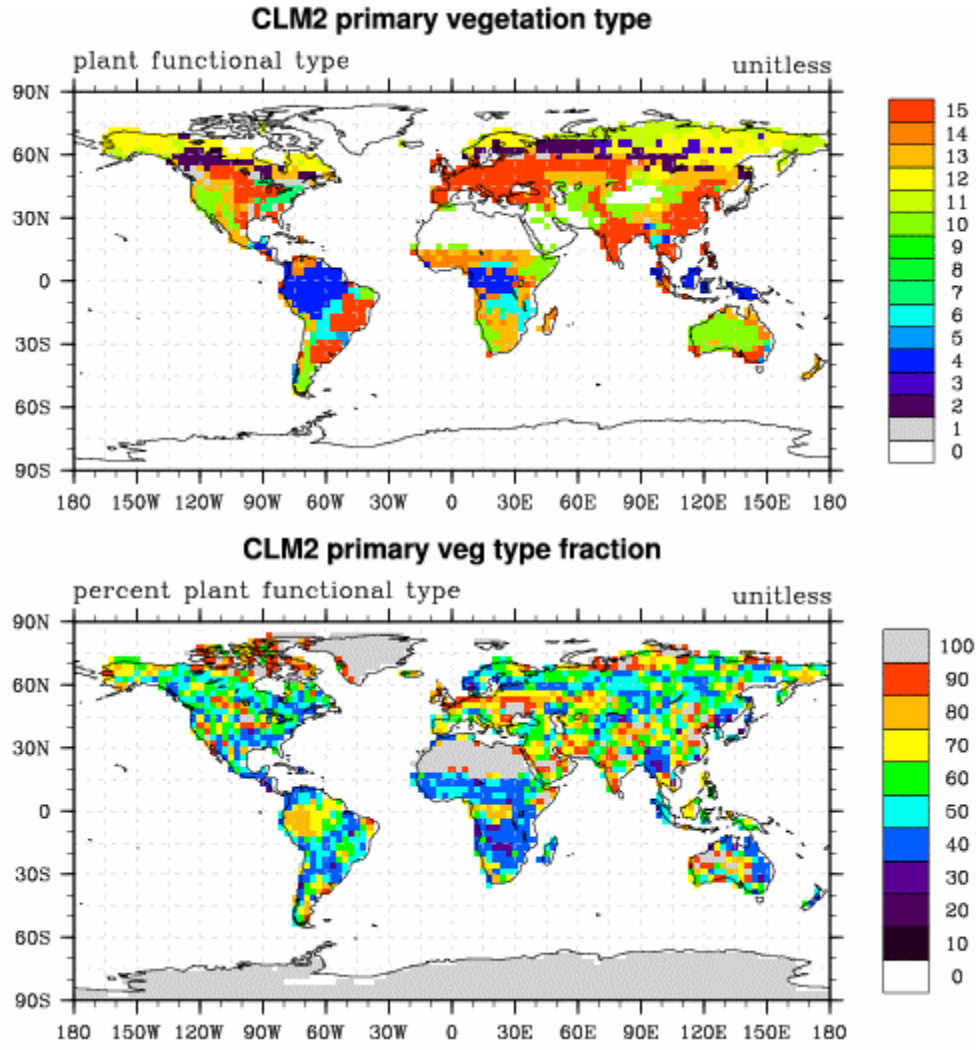

Figure 3.26. The global distribution of the CLM2 prescribed primary plant function type and its associated fraction for each grid.

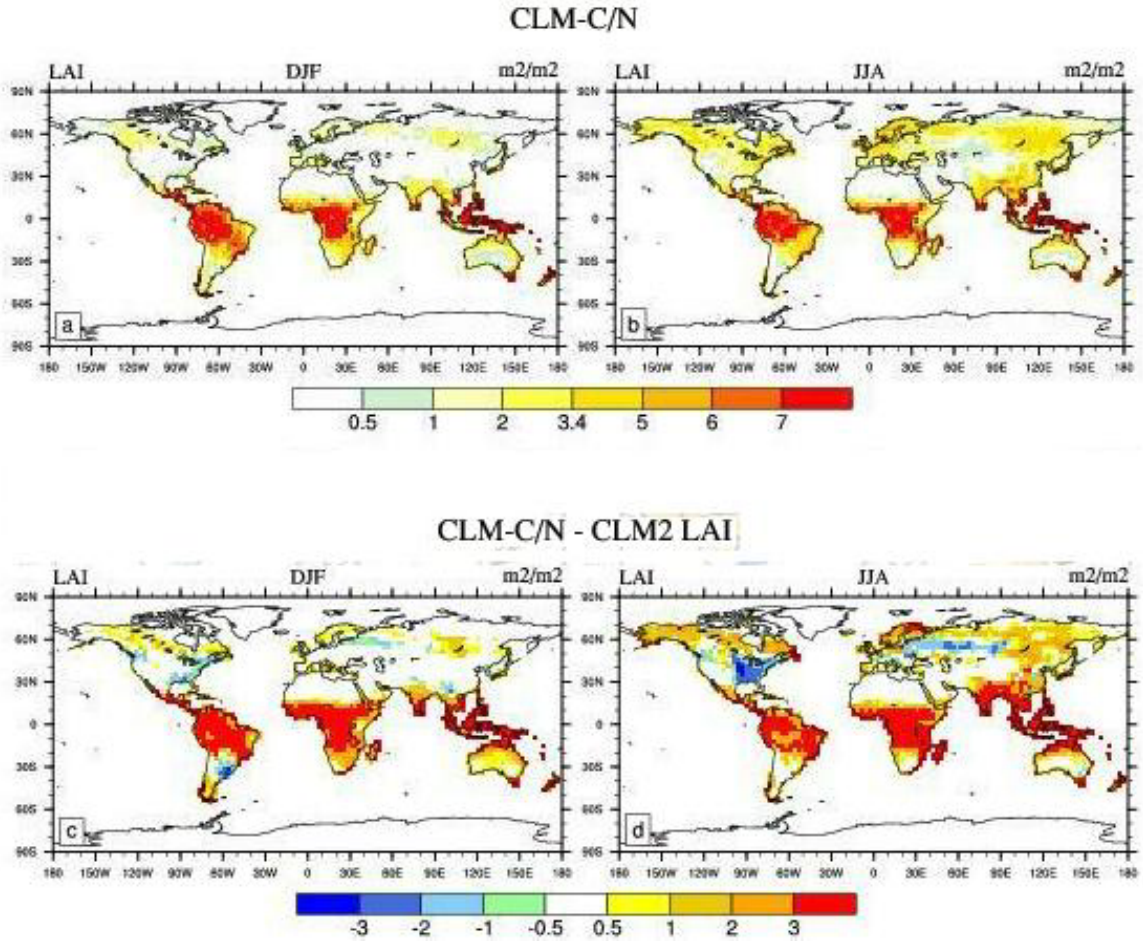

Figure 3.27. The modeled LAIs for northern winter (a) and summer (b) and the difference between them and the CLM2-prescribed LAIs (c and d).

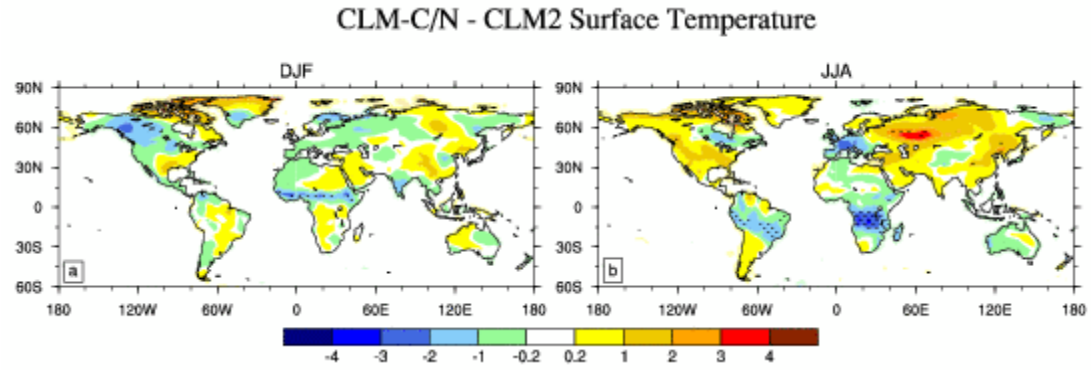

Figure 3.28. The difference between the simulated surface (2m height) temperature by the CLM-C/N-CAM and that by the CLM2-CAM for winter (a) and summer (b) respectively. Dotted areas indicate that the difference is significant based on a t-test ($p < 0.05$).

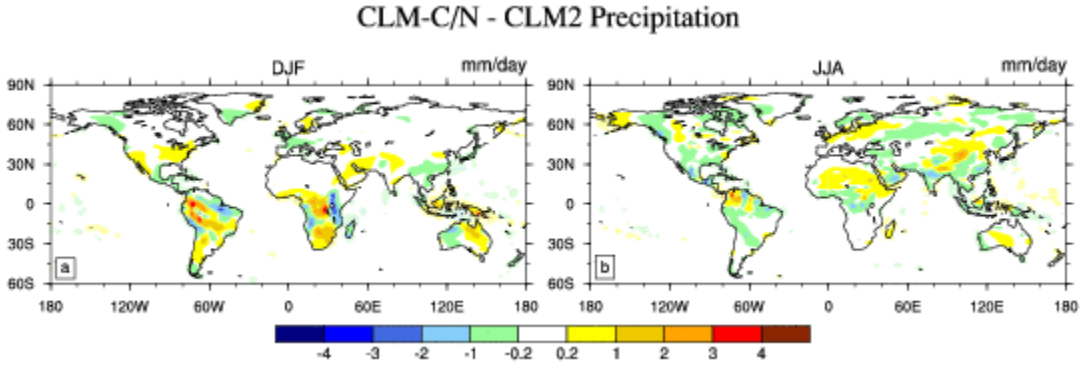

Figure 3.29. The difference between the simulated precipitation from CLM-C/N-CAM and that from CLM2-CAM for winter (a) and summer (b) respectively. Dotted areas indicate that the difference is significant based on a t-test ($p < 0.05$).

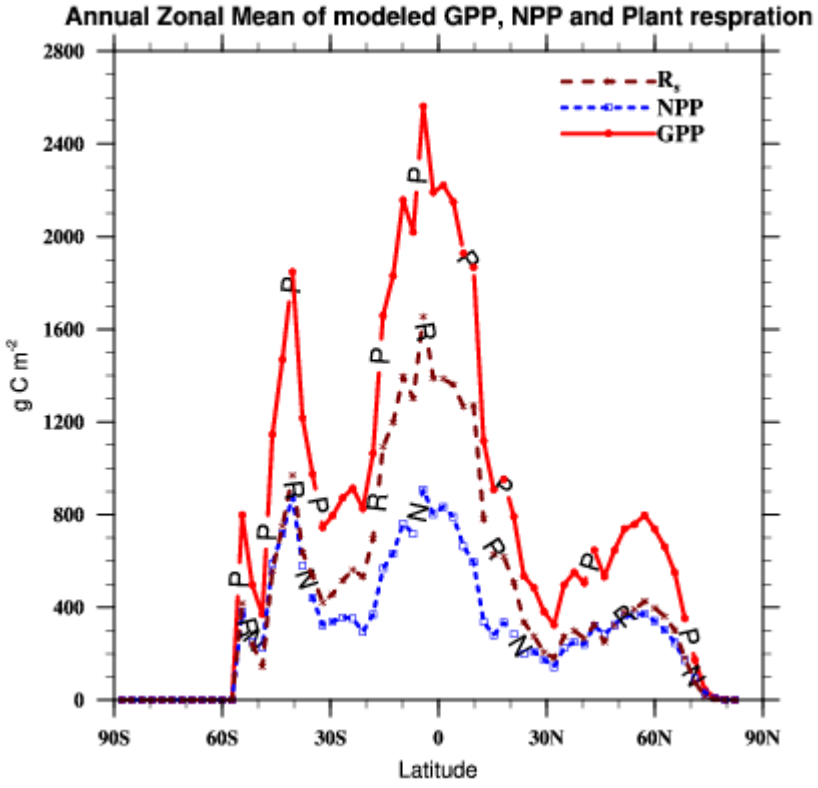

Figure 3.30. CLM-C/N annual zonal mean of photosynthesis (P), autotrophic respiration (R) and net primary productivity (N).

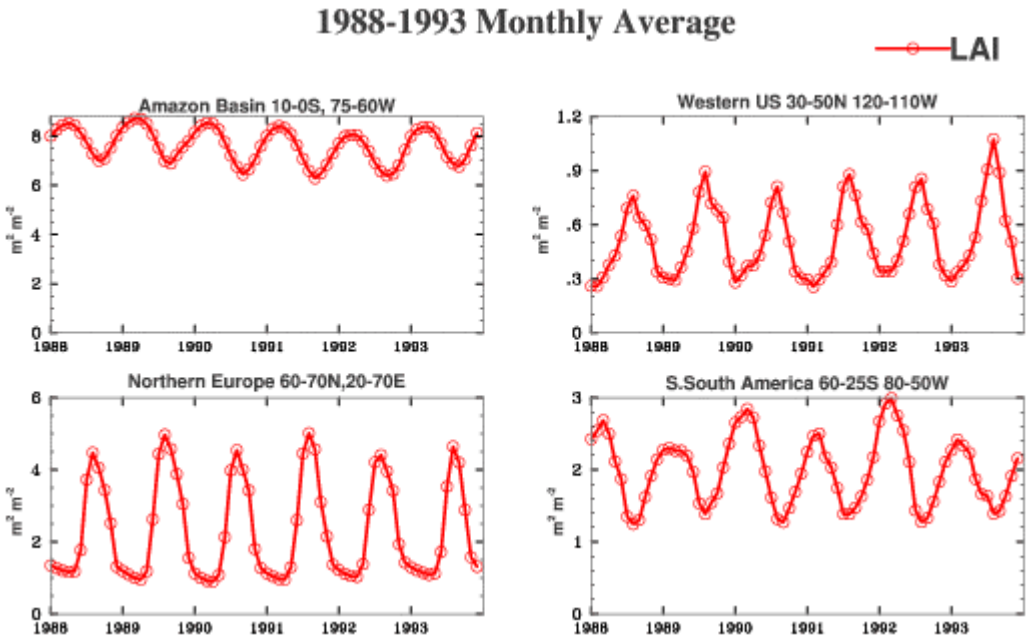

Figure 3.31. CLM2-C/N modeled LAI from 1988 to 1993 for 4 regions. The primary PFTs are tropic evergreen forest over Amazon Basin; boreal forest over northern Europe; grasslands over western US and mixed wood and croplands over southern South America.

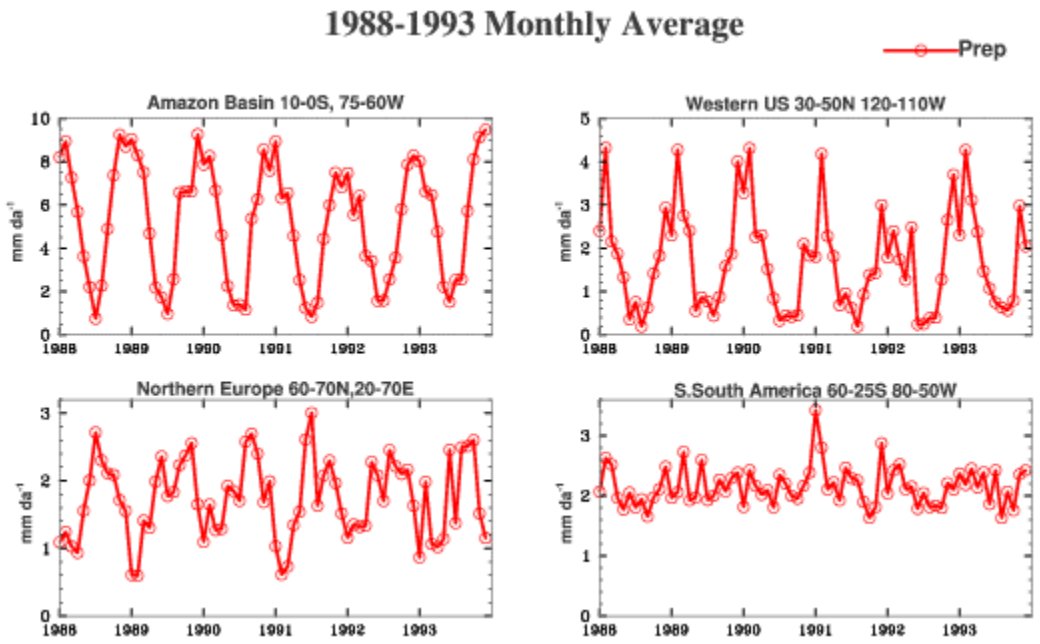

Figure 3.32. The same as 3.31 but the modeled precipitation.

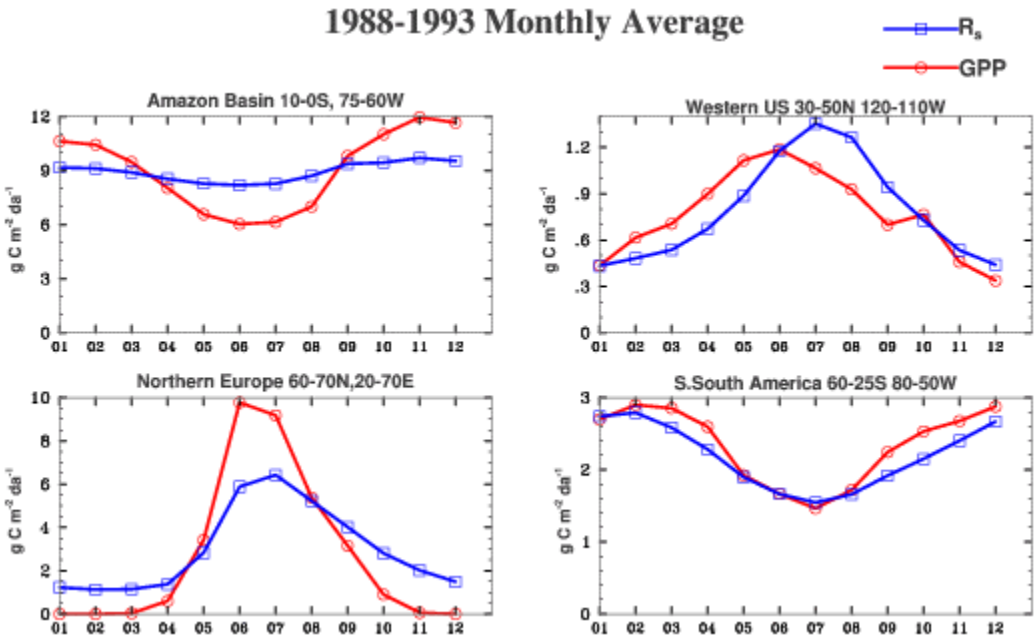

Figure 3.33. Seasonal cycle of the CLM-C/N modeled photosynthesis (GPP) and ecosystem respiration.

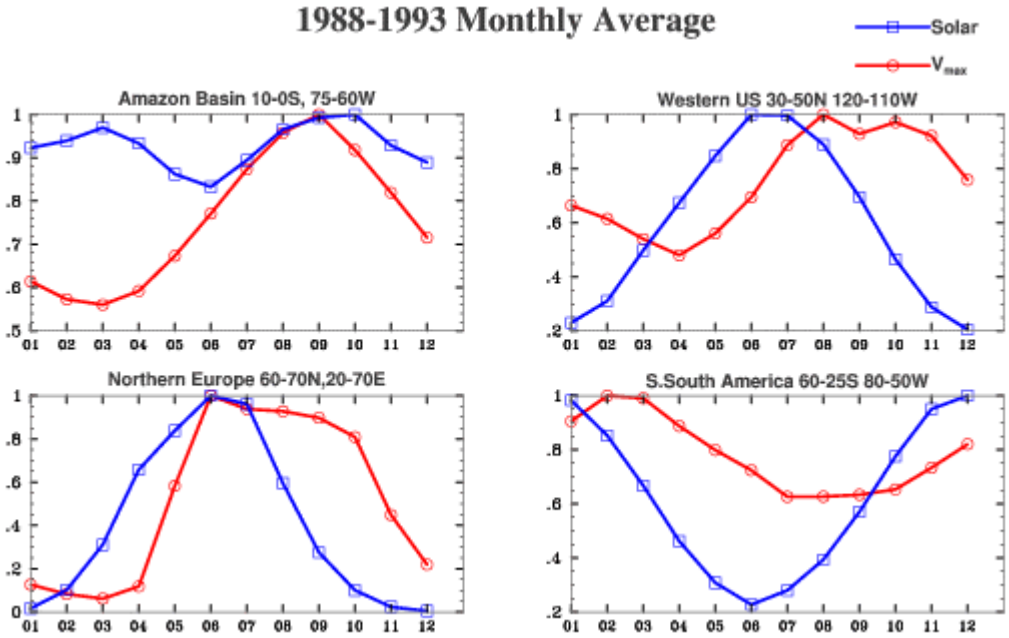

Figure 3.34. Seasonal evolution of CLM-C/N modeled incident solar radiation and canopy photosynthetic capacity.

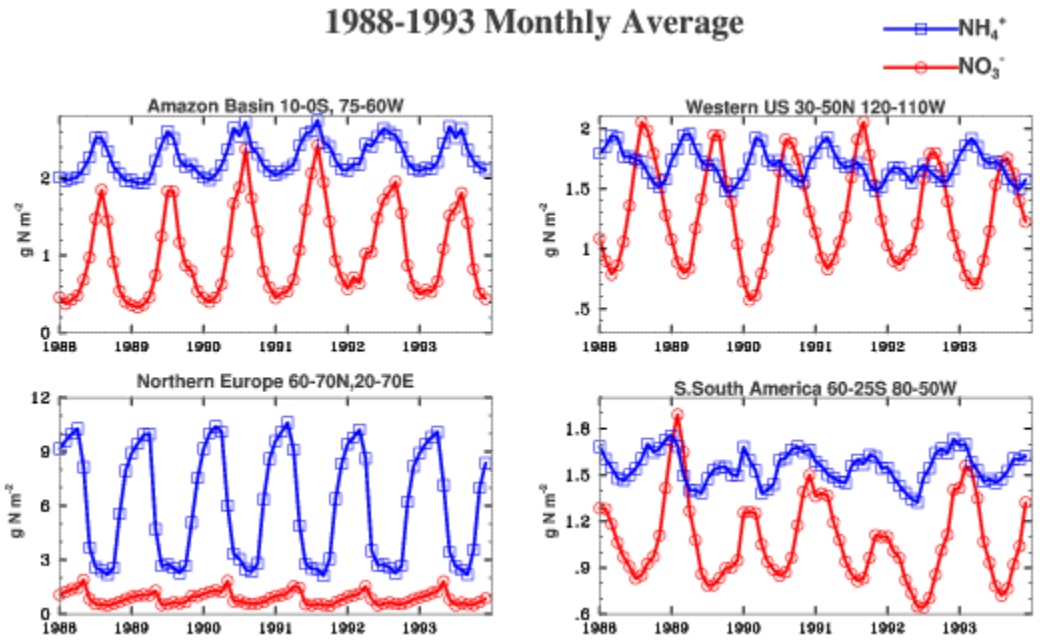

Figure 3.35. CLM-C/N modeled soil nitrate ion (NO_3^-) and ammonium ion (NH_4^+) concentrations.

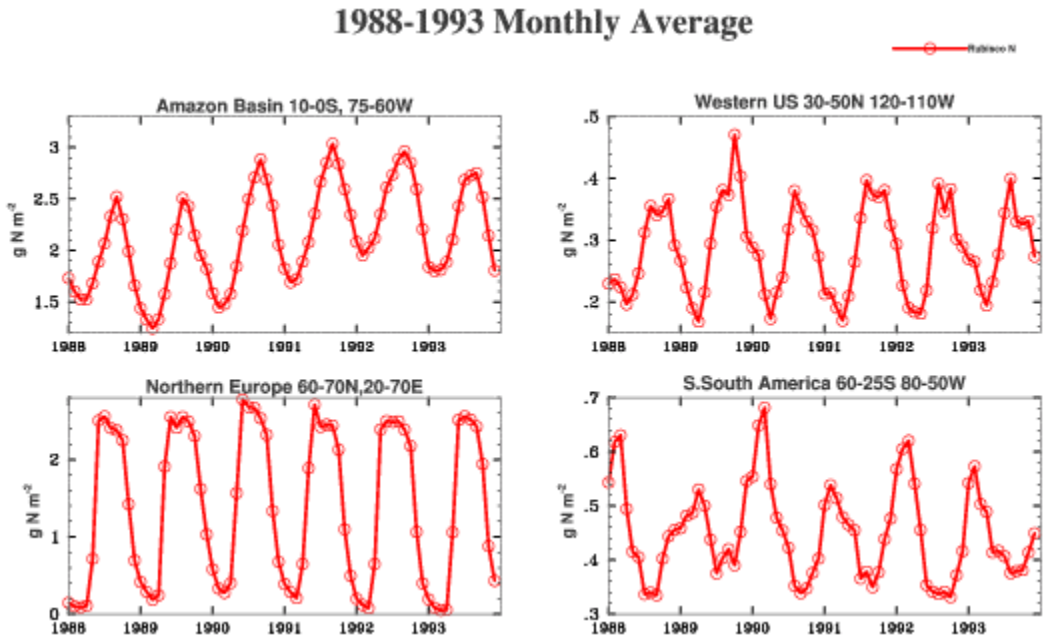

Figure 3.36. CLM-C/N modeled canopy Rubisco nitrogen.

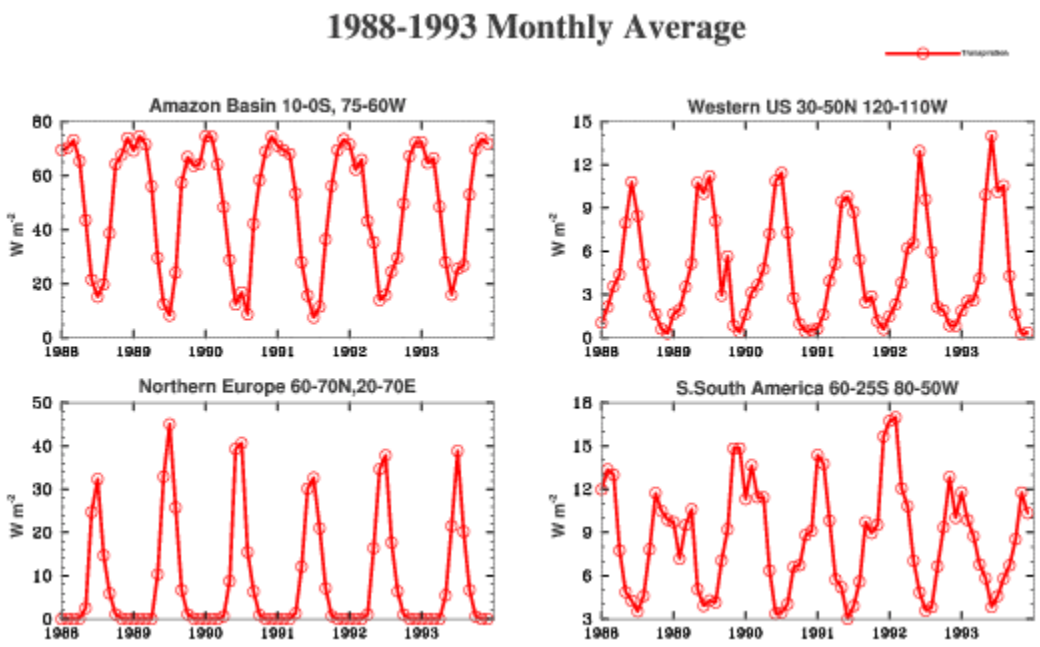

Figure 3.37. CLM-C/N modeled latent heat flux through canopy transpiration.

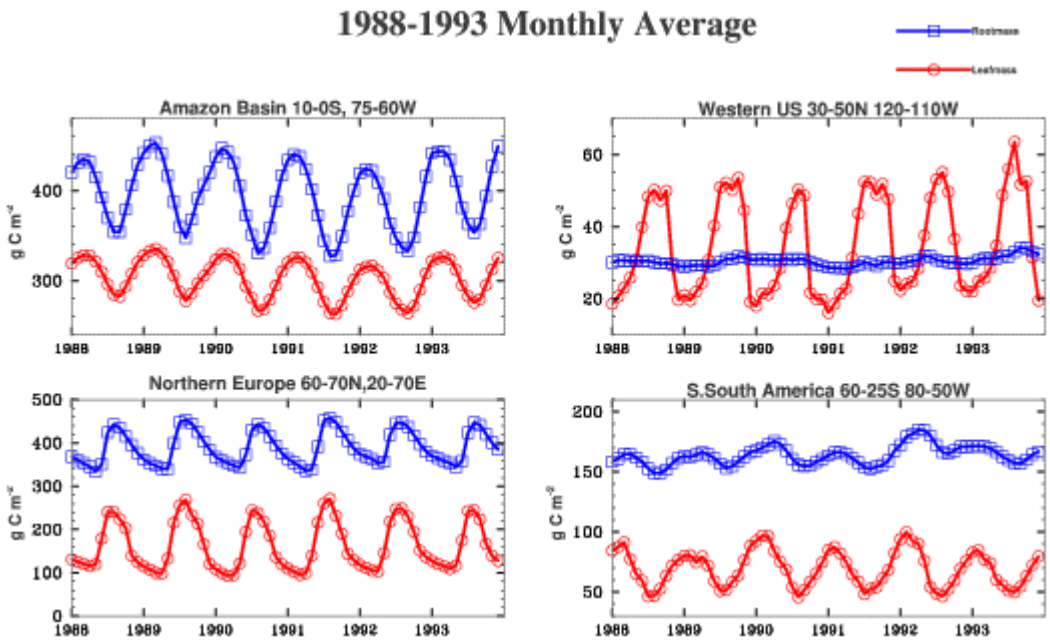

Figure 3.38. CLM-D/N modeled leaf biomass and root biomass over the four regions from 1988 to 1993.

CHAPTER 4

Conclusion Remarks

4.1 Research review and primary results

Land surface processes depend largely on soil and vegetation properties. The determinations of their magnitude and dynamics in land surface models (LSM) are important for accurate predictions of the heat, water, momentum and mass exchanges between land surface and the atmosphere. This thesis is one of many studies that aim to improve the parameterizations of soil and vegetation in LSMs. Our emphases are on two specific themes: 1) assessing and representing the effects of soil macropores on the soil hydraulic properties in LSMs for more accurate simulations of soil moisture and surface hydrology; and 2) integrating existing advances in understanding and modeling the land-surface biophysical and eco-physiological processes into the latest climate model framework for modeling climate and carbon cycle, taking into account the interactive role of land vegetation and ecosystems.

Although the significance of the effects of soil macropores on soil-water hydraulic properties have been widely recognized, most LSMs still use conventional texture-based hydraulic schemes that neglect these effects. Water-flow in the soil has high degree of dependency on its hydraulic properties; thus, we hypothesized that the neglect of macropores may results in serious errors in the simulated soil moisture and through it in the simulated surface hydrology. Our goals for the first theme were to

identify these effects and to represent them in LSMs in practical way.

To assess the macropore effects, we compared the simulated soil moisture and surface evapotranspiration (ET) of the standard Community Land Model (CLM), which uses a hydraulic scheme without macropore consideration, with those of the CLM with a modified hydraulic scheme that accounts for some effects of soil macropores. The results of this comparison showed that the inclusion of macropores affects the simulation of soil moisture and surface hydrology substantially. Their influence can be incorporated into land models by adding a second function to the pore-size distribution. With inclusion of the soil macropore effect on soil hydraulic conductivities, the estimation of the soil moisture for well-structured soils is much more accurate by allowing more water percolate down into soil column instead of being lost as surface runoff during the wet season. The increased water storage during wet season supplies the dry season evapotranspiration with an extended period and less limitation.

A more practical hydraulic scheme with macropore considerations was proposed as the existing schemes usually require too many input parameters and thus are not applicable for large-scale simulations. The proposed scheme was based on the physical attributes of the water in soil capillary pores in that it fills pores systematically from the smaller to the larger ones and the statistics of several global soil databases. The developed scheme has been tested against collected measurements of hydraulic conductivities from various soils. The new scheme has better prediction in the near-saturation range than the conventional one does. Another finding is that additional measurement points of hydraulic properties can further improve the prediction accuracy in the whole moisture range.

The implementation of the new hydraulic scheme in LSMs requires the macroporosity at each location as model input. We found that there is a close correlation between the macroporosity and the root abundance of a soil through statistical analysis of global data sets. Because root abundance can be generally inferred from the vegetation types, the geographic distribution of soil macropores can be derived from that of vegetation types when measurement is unavailable. Thus, the soil properties are related to the vegetation properties. We also found that an arbitrary assumption of vertical-decay of saturated hydraulic conductivity can be adequately substituted by the physically meaningful definition of vertical-decay of macroporosity. Such a macropore distribution is consistent with the observed relationship between roots and macropores as well as the observed vertical distributions of roots and soil organic carbon content, which is also a good indicator of soil macropores.

Global offline simulation of the CLM implemented with the developed hydraulic scheme forced by atmospheric data was performed. The preliminary results indicate that the proposed scheme captures the basic effects of macropores on the soil water and its transport. Some of these effects are allowing faster downward percolation of water, decreasing runoff generation and increasing water storage in deep soil layers and thus dry-period transpiration. The proposed hydraulic scheme can be the initiation of more extensive consideration of soil macropores in LSMs.

The second theme addresses the development of an integrated land/ecosystem model by extending the biophysically based CLM with explicit descriptions of the ecosystem carbon/nitrogen biochemical cycling processes. This development endeavors to meet the increasing need to understand the interactions between the climate and land

ecosystems. The integrated model (CLM-C/N) takes into account the interactions between the ecosystem and climate over the time-scales from several hours to several years through modeling the vegetation cover and leaf photosynthetic capacity dynamically as parts of the coupled carbon and nitrogen cycles. It has a much broader application potentials when implemented in climate system models than the CLM does as it models not only the fluxes of water, energy and momentum but also the biochemical exchanges of carbon and nitrogen between the atmosphere and land ecosystems.

The CLM-C/N retains the biophysical parameterizations as formulated in the CLM and physiological and ecological parameterizations as in Dickinson et al. [1998,2002] except that of cold and drought stresses on the carbon cycle, which has been modified in this study to be more consistent with field observations. The results from tests of the CLM-C/N at 4 forest sites with different environments showed that the model captures the seasonal and interannual dynamics of LAI and the nitrogen control on carbon assimilation adequately across different environment. It also reasonably reproduces seasonal and diurnal evolutions of the surface heat and carbon fluxes together for most sites. The simulated carbon and nitrogen cycles showed pronounced seasonal cycle with the size of each defined pool within its expected range. The CLM-C/N also models the dynamic feature of leaf Rubisco nitrogen and shows that it tends to adjust to the environmental irradiance well.

The simulated nitrogen cycle indicates that the annual plant nitrogen supply is primarily attributed to the recycling of ecosystem nitrogen instead of external sources. However, the nitrogen loss through runoff can be substantial and dominate the soil mineral nitrogen concentration momentarily. This is plausible, considering the timescale

applied to the model, i.e., several hours to several years. The simulated carbon cycle suggests that the carbon assimilation depends not only on the intensity of irradiance but also the diffuse/direct solar fraction. Several data sets showed that the model underestimated carbon assimilation around noon because of overestimation of direct solar fraction.

The tests also identified several areas of improvement for the CLM-C/N. In particular, the soil moisture limitation on carbon assimilation is exaggerated, at least over forested regions. Possible causes include improper parameterization of the soil stress term, underestimated root depth, lack of consideration of the ability of roots to uplift soil water, inaccuracy of soil moisture simulation, etc. A temporary fix was imposed to the CLM-C/N as to constrain the soil moisture influence on carbon assimilation for forests with a lower limit. Extensive evaluation of the model is necessary to find a permanent solution. Another area is the simulation of plant and soil respirations. The data sets suggested that the soil respiration from slow soil pool accounts for a significant portion of the ecosystem carbon release to the atmosphere over boreal areas but less over temperate and tropical areas. Thus, it is critical to take into account the carbon release contribution by slow soil carbon when estimating the net ecosystem exchange between the land and the atmosphere, especially over high-latitude regions. Another area that may cause simulation errors, is the formulation of the temperature dependence of respiration terms.

Global simulation of the CLM-C/N, coupled to a climate model, the Community Climate System Model (CCSM), was performed to assess the simulated global pattern. It was forced by prescribed interannually varying sea-surface temperatures. The results are somewhat consistent with the tests at single sites. In general, the simulated global

distribution of LAI is reasonable across various ecosystems. For instance in the Amazon, the simulated LAI is better in both magnitude and seasonal cycle than that obtained from the AVHRR satellite data. Global distribution of modeled NPP is in good agreement with that of other models.

Some other conclusions of the global simulation include 1) that the CLM-C/N simulates the temperature dependence of respirations over temperate regions less accurately than those over other regions; 2) the soil mineral nitrogen concentrations are associated largely with temperature and precipitation as well as the uptake rate of plants. Tropical forest regions with large annual precipitation have low soil mineral nitrogen concentrations with relatively higher values in the dry season and lower values in the wet season. Boreal regions have the largest annual amplitude of soil mineral nitrogen concentration corresponded to their large seasonal variation of temperature; and 3) the root turnover parameterization of the model remains uncertain and causes underestimation of root biomass for grasses in temperate regions.

4.2 Future research

Many aspects of this thesis work can be further extended and explored in the future. A few major ones are listed in the following.

1) The proposed macropore scheme can be further improved with increased soil measurements globally. The prediction of soil hydraulic properties largely depends on the soil data utilized. It has been found that it is preferable to use field measurements for natural soils. The derived scheme from one region is more reliable when used for soils in the same region than soils in rather other regions

[Tomasella, 1999], and increased measurement points can improve prediction accuracy. Thus, the global-scale soil measurement can contribute substantially to the development of the hydraulic estimation in LSMs.

2) The macropore investigation in this study only considers pores within the capillary range. In nature, large pores such as animal burrow, root channels and large cracks are usually out of such range and often are continuous over significant distances and allow flow to bypass parts of soil matrix [Beven, 1991]. Their effect on the surface hydrology especially on the runoff generation in watershed scale can be substantial. Thus, it is highly desirable to consider these macropores and their effect on soil water-flow in LSMs.
3) Runoff scheme in LSMs contains a number of tuned parameters. With introduction of the soil macropores in LSMs, some of these parameters need to be re-evaluated and given physical meanings. More insight will be gained and derive reasonable and meaningful parameters will be derived if LSMs with the proposed macropore scheme are tested against river discharge data at watershed scale.
4) The CLM-C/N can be further improved using observations of more attributes and more sites, in particular those with non-forest vegetation types. The soil water dependence of carbon assimilation is a serious issue, as it influences not only the carbon cycle but also the surface ET fluxes. It is promising to integrate the two studies in this thesis together in the same model as the proposed new hydraulic scheme aimed to improve the soil moisture simulation.
5) The CLM-C/N simulates the carbon and nitrogen cycles when ecosystems reach equilibrium. It is plausible when to simulate climate-ecosystem interactions in

short spans. Long-term interactions need to consider the anthropogenic alterations on global biogeochemical carbon and nitrogen cycles such as land cover change by deforestation and the increasing atmospheric nitrogen source by atmospheric deposition, and the slow ecosystem adjustment to environment such as varying temperature dependence of plant and soil respirations and increasing carbon assimilation with increasing atmospheric CO_2 concentration.

References

Aber, J.D. and C.A. Federer (1992): A generalized, lumped-parameter model of photosynthesis, evapotranspiration and net primary production in temperate and boreal forest ecosystems. *Oecologia*, 92, 463–474.

Aber, J.D., S.V. Ollinger, and C.T. Driscoll (1997): Modeling nitrogen saturation in forest ecosystems in response to land use and atmospheric deposition. *Ecological Modeling*, 101, 61–78.

Aber, J.D., S.V. Ollinger, C.A. Federer, P.B. Reich, et al.(1995): Predicting the effects of climate change on water yield and forest production in the northeastern United States. *Climate Research*, 5, 207–222.

Aber, J.D., P.B. Reich, and M.L. Goulden (1996): Extrapolating leaf CO_2 exchange to the canopy: a generalized model of forest photosynthesis compared with measurements by eddy correlation. *Oecologia*, 106, 257–265.

Anten, N.P.R. and T. Hirose (2001): Limitations on photosynthesis of competing individuals in stands and the consequences for canopy structure. *Oecologia*, 129, 186–196.

Arya, L.M. and J.F. Paris (1981): A Physico-empirical Model to Predict the Soil Moisture Characteristics from Particle-Size Distribution and Bulk Density Data. *Soil Science Society of America Journal*, 45, 1023–1030.

Arya, L.M., F.J. Leij, P.J. Shouse and M.T. van Genuchten (1999): Relationship between the Hydraulic Conductivity Function and the Particle-Size Distribution. *Soil Science Society of America Journal*, 63, 1063–1070.

Asner, G.P., A.R. Townsend, W.J. Riley, et al. (2001): Physical and biogeochemical controls over terrestrial ecosystem responses to nitrogen deposition *Biogeochemistry*, 54, 1–39.

Baldocchi, D.D. and K.B. Wilson (2001): Modeling CO_2 and water vapor exchange of a temperature broadleaved forest across hourly to decadal time scales. *Ecological Modeling*, 142, 155–184.

Batjes, N.H. (1996): Total carbon and nitrogen in the soils of the world. European Journal of Soil Science, 47, 151-163.

Batjes, N.H. (2002): ISRIC-WISE global data set of derived soil properties on a 0.5 by 0.5 degree grid (Version 2.0), *Report 2002/03, ISRIC, Wageningen*.

Benson, C.H. and D.E. Daniel (1990): Influence of clods on hydraulic conductivity of compacted clay. *Journal of Geotechnical Engineering*, 116(8), 1231–1248.

Beven, K.J and M.J. Kirkby (1979): A physically-based variable contributing area model of basin hydrology. *Hydrological Sciences Journal*, 24(1), 43-69.

Beven, K.J. and P. Germann (1982): Macropores and water flow in soils. *Water Resources Research*, 18, 1311–1325.

Beven, K.J. (1991): Modeling Preferential Flow: An Uncertain Future? *In Proc. Nat. Symp. Preferential flow. Chicago*, 1-11.

Blackmon, M.B., B. Boville, F. Bryan, R.E. Dickinson, et al. (2001): The Community Climate System Model. BAMS, 82(11), 2357-2376.

Bonan, G.B. (1995): Land-atmosphere CO_2 exchange simulated by a land surface process model coupled to an atmospheric general circulation model. *Journal of Geophysical Research*, 100, 2817–2831.

Bonan, G.B.(1996): The NCAR land surface model (LSM version 1.0) coupled to the NCAR Community Climate Model. *NCAR Technical Note NCAR/TN-429+STR. NCAR, Boulder, Colorado.*

Bonan, G.B., K.W. Oleson, M. Vertenstein, S. Levis, et al. (2002): The Land Surface Climatology of the Community Land Model Coupled to the NCAR Community Climate Model. *Journal of Climate*, 15(22), 3123–3149.

Bouma, J. (1989): Using soil survey data for quantitative land evaluation. Adv. Soil Sci., 9, 177-213.

Bounoua, L., G.J. Collatz, P.J. Sellers, D.A. Randall, et al. (1999): Interactions between vegetation and climate: radiative and physiological effects of doubled atmospheric CO_2. *Journal of Climate*, 12, 309–323.

Boville, B.A. and P.R. Gent (1998): The NCAR Climate System Model (version one). *Journal of Climate*, 11, 1115–1129.

Brejda, J.J., M.J. Mausbach, J.J. Goebel, D.L. Allan, et al. (2001): Estimating surface soil organic carbon content at a regional scale using the national resource inventory. *Soil Science Society of America Journal*, 65, 842–849.

Brooks, R.H. and A.T. Corey (1964): Hydraulic properties of porous media. *Hydrology paper No. 3*. Colorado State University, Fort Collins.

Buermann, W., J. Dong, X. Zeng, R.B. Myneni and R.E. Dickinson (2001): Evaluation of the utility of satellite-based vegetation leaf area index data for climate simulations. *J.*

Climate, 14, 3536-3550.

Campbell, G.S. (1974): A simple method for determining unsaturated conductivity from moisture retention data. *Soil Science*, 117, 311–314.

Campling, P., A. Gobin, K. Beven, and J. Feyen (2002): Rainfall-runoff modeling of a humid tropical catchment: the TOPMODEL approach. *Hydrological Processes*, 16, 231–253.

Canadell, J.G., H.A. Mooney, D.D. Baldocchi, J.A. Berry, et al.(2000): Carbon metabolism of the terrestrial biosphere: a multitechnique approach for improved understanding. *Ecosystems*, 3, 115–130.

Carson, D.J., and A.B. Sangster (1981): The influence of land-surface albedo and soil moisture on general circulation model simulations. *Numerical Experimentation Programme Report No. 2*, 5.14-5.21.

ChapinIII, F.S. (1991): Integrated Responses of Plants to Stress. *Bio Science*, 41(1), 29–35.

Charney, J.G., W.J. Quirk, S.H. Chow, and J. Kornfield (1977): A comparative study of the effects of albedo change on drought in semi-arid regions. *Journal of the Atmospheric Sciences*, 34, 1366-1385.

Charney, J., P. Stone, and W. Quirk (1975): Drought in the Sahara: a biogeophysical feedback mechanism. *Science*, 187, 434-435.

Chen, C., D.M. Thomas, R.E. Green, and R.J. Wagenet (1993): Two-Domain Estimation of Hydraulic Properties in Macropore Soils. *Soil Science Society of America Journal*, 57, 680–686.

Chen, C. and W.A. Payne (2001): Measured and modeled unsaturated hydraulic conductivity of a Walla silt loam. *Soil Science Society of America Journal*, 65, 1385–1391.

Chen, T. H. et al. (1997): Cabauw experimental results from Project for intercomparison of land surface parameterization schemes (PILPS). *J. Climate*, 10, 1194-1215.

Chen, Y., and M. Schnitzer (1976): Viscosity measurements on soil humic substances. *Soil Sci. Soc. Am. J.,* 40, 866–872.

Clapp, R.B. and G.M. Hornberger (1978): Empirical equations for some soil hydraulic properties. *Water Resources Research*, 14, 601–604.

Collatz, G.J., J.A. Berry, G.D. Farquhar, and J. Pierce (1990): The relationship between Rubisco reaction mechanism and models of photosynthesis. *Plant, Cell and Environment*, 13, 219–225.

Collatz, G.J., J.T. Ball, C. Grivet, and J.A. Berry (1991): Physiological and environmental regulation of stomatal conductance, photosynthesis and transpiration: a model that includes a laminar boundary layer. *Agricultural and Forest Meteorology*, 54, 107–136.

Coppola, A. (2000): Unimodal and bimodal descriptions of hydraulic properties for aggregated soils. *Soil Science Society of America Journal*, 64, 1252–1262.

Cornelis, W.M., J. Ronsyn, M.VanMeirvenne, and R. Hartmann (2001): Evaluation of Pedotransfer Functions for Predicting the Soil Moisture Retention Curve. *Soil Science Society of America Journal*, 65, 638–648.

Cosby, B.J., G.M. Hornberger, R.B. Clapp, and T.R. Ginn (1984): A statistical exploration of the relationships of soil moisture characteristics to the physical properties of soils. *Water Resources Research*, 20(6), 682–690.

Cox, P., C. Huntingford, and R. Harding (1998): A canopy conductance and photosynthesis model for use in a GCM land surface scheme. *Journal of Hydrology*, 212-213, 79-94.

Curtis, P.S., P.J. Hanson, P. Bolstad, C. Barford, el al. (2002): Biometric and eddy-covariance based estimates of ecosystem carbon storage in five eastern North American deciduous forests. *Agricultural and Forest Meteorology*, 113, 3-19.

Dai, Y., X. Zeng, R.E. Dickinson, I. Baker, et al. (2003): *Bulletin of the American Meteorological Society*, DOI: 10.1175/BAMS-84-8-1013, 1013–1023.

DeAngelis, D. L., R. H. Gardner, and H. H. Shugart (1997): NPP Multi-Biome: Global IBP Woodlands Data, 1955-1975. Dataset. Available on-line [http://www.daac.ornl.gov] from *Oak Ridge National Laboratory Distributed Active Archive Center*, Oak Ridge, Tennessee, U.S.A.

Delire, C., J.A. Foley, and S. Thompson (2003): Evaluating the carbon cycle of a coupled atmosphere-biosphere model. *Global Biogeochemical Cycles*, 17(1), 1012, doi:10.1029/2002GB001870,

Delire, C. and J.A. Foley (1999): Evaluating the performance of a Land Surface/Ecosystem model with biophysical measurements from contrasting environments. *Journal of Geophysical Research*, 104, 16895–16909.

Denning, A.S., G.J. Collatz, C. Zhang, D.A. Randall, et al. (1996): Simulations of terrestrial carbon metabolism and atmospheric CO_2 in a general circulation model. Part I: Surface Carbon Fluxes. *Tellus*, 48B, 521–542.

DePury, D.G. and G.D. Farquhar (1997): Simple scaling of photosynthesis from leaves to

canopies without the errors of big-leaf models. *Plant, Cell and Environment*, 20, 537–557.

Dickinson, R.E. (1983): Land surface processes and climate-surface albedos and energy balance. *Advances in Geophysics*, 25, 305-353.

Dickinson, R.E., A. Henderson-Sellers, P.J. Kennedy, and M.F. Wilson (1986): Biosphere -atmosphere transfer scheme (BATS) for the NCAR community climate model. *NCAR Technical Note NCAR/TN275+STR*. NCAR, Boulder, Colorado, USA.

Dickinson, R.E., and A. Henderson-Sellers (1988): Modeling tropical deforestation: A study of GCM land-surface parameterizations. *Q.J.R. Meteorol. Soc*., 114, 439-462.

Dickinson, R.E., A. Henderson-Sellers, and P.J. Kennedy (1993): Biosphere-Atmosphere Transfer Scheme (BATS) for the NCAR Community Climate Model *tech. rep*., NCAR, Boulder, CO.

Dickinson, R.E. (1995): Land processes in climate models. *International Satellite Land Surface Climatology Project special issue of Remote Sensing of Environment*, 51, 27-38.

Dickinson, R.E., M. Shaikh. R. Bryant, and L. Graumlich (1998): Interactive canopies for a climate model. *Journal of Climate*, 11, 2828–2836.

Dickinson, R.E. (2001): Linking ground hydrology to ecosystem s and carbon cycle in a climate model Present and Future of Modeling Global Environmental Change. *Toward Integrated Modeling* by TERRAPUB, 137-144.

Dickinson, R.E., J.A. Berry, G.B. Bonan, G.J. Collatz, et al. (2002): Nitrogen controls on climate model evapotranspiration. *Journal of Climate*, 15, 278–295.

Durner, W. (1994): Hydraulic conductivity estimation for soils with heterogeneous pore structure. *Water Resources Research*, 30, 211–223.

Ek, M. and R. H. Cuenca (1994): Variation in soil parameters: Implications for modeling surface fluxes and atmospheric boundary-layer development. *Bound.-Layer Meteorol.,* 70, 369-383.

Elsenbeer, H., K. Cassel, and J. Castro (1992): Spatial Analysis of Soil Hydraulic Conductivity in a Tropical Rain Forest Catchment. *Water Resources Research*, 28(12), 3201–3214.

Elsenbeer, H., B.E. Newton, T. Dunne, and M.D. Jorge (1999): Soil hydraulic conductivities of latosols under pasture, forest and teak in Rondonia, Brazil. *Hydrological Processes*, 13, 1417–1422.

Engel, V.C., M. Stieglitz, M. Williams, and K.L. Griffin (2002): Forest canopy hydraulic

properties and catchment water balance: observations and modeling. *Ecological Modeling*, 154, 263–288.

Entekhabi, D. and P. S. Eagleson (1989): Land surface hydrology parameterization for atmospheric General Circulation models including subgrid scale spatial variability, *Journal of Climate*, 2(8), 816-831.

Evans, J.R. and S. von Caemmerer (1996): Carbon dioxide diffusion inside leaves. *Plant Physiology*, 110, 339–346.

Falge, E., D. Baldocchi, R.J. Olson, P. Anthoni, M. Aubinet, et al. (2001): Gap filling strategies for longterm energy flux datasets. *Agricultural Forest and Meteorology*, 107, 71–77.

Falge, E., D. Baldocchi, J. Tenhunen, M. Aubinet, et al. (2002): Seasonality of ecosystem respiration and gross primary production as derived from FLUXNET measurements. *Agricultural and Forest Meteorology*, 113(1-4): 53-74.

Farquhar, G.D., S. von Caemmerer, and J.A. Berry (1980): A biochemical model of photosynthetic CO_2 assimilation in leaves of C3 species. *Planta* 149:78-90.

Fayer, M.J. and C.S. Simmons (1995): Modified soil water retention functions for all matric suctions. *Water Resources Research*, 31(5), 1233–1238.

Field, C.B., and H.A. Mooney (1986): The photosynthesis-nitrogen relationship in wild plants: In: Givnish, T.J. (ed.) *On the economy of plant form and function*, 25–55. Cambridge University Press, Cambridge, UK.

Field, C.B., J.T. Randerson, and C.M. Malmstrom (1995): Global net primary production: combining ecology and remote-sensing. *Remote Sensing of Environment*, 51, 74–88.

Foley, J., J. Kutzbach, M. Coe, and S. Levis (1994): Feedbacks between climate and boreal forests during the Holocene epoch. *Nature*, 371, 52-54.

Foley, J.A., I.C. Prentice, N. Ramunkutty, S. Levis, et al. (1996): An integrated biosphere model of land surface processes, terrestrial carbon balance and vegetation dynamics, *Global Biogeochemical Cycles*, 10, 603-628.

Friend, A.D. (1995): PGEN: an integrated model of leaf photosynthesis, transpiration and conductance. *Ecological Modelling*, 77, 233–255.

Galloway, J.N., W.H. Schlesinger, H. Levy, A. Michaels, et al. (1995): Nitrogen fixation: Anthropogenic enhancement-environmental response. *Global Biogeochemical Cycles*, 9(2), 235–253.

Gardner, W.R. (1960): Dynamic aspects of water availability to plants *Soil Science*, 89,

63–73.

Gardner, W.R., D. Hiller, and Y. Benyamini (1970): Post irrigation movement of soil water: I. Redistribution. *Water Resources Research*, 6, 851–861.

Gardner, W.R., D. Hiller, and Y. Benyamini (1970): Post irrigation movement of soil water: II. Simultaneous redistribution and evaporation. *Water Resources Research*, 6, 1148–1153.

Gash, J.H.C., C.A. Nobre, J.M. Roberts and R.L. Victoria (1996): An overview of ABRACOS. *Amazonian Deforestation and Climate*. John Wiley & Sons.

Germann, P. and K. Beven (1981): Water flow in soil macropores: I. An experimental approach. *Journal of Soil Sci.*, 32, 1–13.

Germann,P. and K. Beven (1981): Water flow in soil macropores: II. A combined flow model. *Journal of Soil Sci.*, 32, 15–29.

Germann, P.F. and L. DiPietro, (1996): When is porous-media flow preferential? A hydro- mechanical perspective. *Geoderma*, 74, 1–21.

Global Soil Data Task (2000): Global Soil Data Products CD-ROM (IGBP-DIS). CD-ROM. International Geosphere-Biosphere Programme, Data and Information System, Potsdam, Germany. Available from Oak Ridge National Laboratory Distributed Active Archive Center, Oak Ridge, Tennessee, U.S.A. [http://www.daac.ornl.gov].

Goulden, M.L., J.W. Munger, S.M. Fan, B.C. Daube, et al. (1996): Measurement of carbon storage by long-term eddy correlation: Methods and a critical assessment of accuracy. *Global Change Biology*, 2, 169-182.

Grace, J., J. Lloyd, J. McIntyre, A.C. Miranda, et al. (1996): Carbon dioxide flux over Amazonian rain forest in Rondonia. *In: Amazonian Deforestation and Climate*. John Wiley & Sons.

Gupta, S.C., W.E. Larson (1979): Estimating soil water retention characteristics from particle size distribution, organic matter content and bulk density. *Water Resource Research*,15(6),1633-1635.

Hanson P.J., D.E. Todd, M.A. Huston, J.D. Joslin, et al. (1998): Description and field performance of the Walker Branch Throughfall Displacement Experiment: 1993-1996. *ORNL/TM-13586*, Oak Ridge National Laboratory, Oak Ridge, Tennessee.

Haverkamp, R. and J.Y. Parlange (1986): Predicting the water-retention curve from particle-size distribution: 1. Sandy soils without organic matter. *Soil Science*. 142(6), 325–339.

Hendrix, P.F., R.W. Parmelee, D.A. Crossley, Jr., D.C. Coleman, et al. (1986): Detritus food webs in conventional and no-tillage agroecosystems. *BioScience*, 36, 374-380.

Herrera, R. and C.F. Jordan (1981): Nitrogen cycle in a tropical Amazonian rain forest: the Caatinga of low mineral nutrient status. *In: F. E. Clark & T. Rosswell (eds.) Terrestrial Nitrogen Cycles Ecological Bulletin (Stockholm)*, 33, 493–505.

Hillel, D. (1998): Environmental soil physics. *Academic Press*.

Hodnett, M.G., L.P. daSilva, H.R. daRocha, and R.C. Senna (1995): Seasonal soil water storage changes beneath central Amazonian rainforest and pasture. *Journal of Hydrology*, 170, 233–254.

Hodnett, M.G., M.D. Oyama, et al. (1996): Comparisons of long-term soil water storage behaviour under pasture and forest in three areas of Amazonia. In:Amazonian Deforestation and Climate. *John Wiley & Sons.*

Hollis, J.M., R.J.A. Jones, and R.C. Palmer (1977): The effects of organic matter and particle size on the water retention properties of some soils in the west Midlands of England. *Geoderma*, 17, 225–238.

Hwang,S.I., K.P. Lee, D.S. Lee, and S.E. Powers (2002): Models for Estimating Soil Particle-Size Distributions. *Soil Science Society of America Journal*, 66, 1143–1150.

IPCC (2001): Climate change 2001: the scientific basis. *Intergovernmental Panel on Climate Change*, http://www.grida.no/climate/ipcc_tar/wg1/index.htm.

Jackson, R.B., H.A. Mooney and E.D. Schulze (1997): A global budget for fine root biomass, surface area, and nutrient contents. *Proceedings of the National Academy of Sciences, USA*, 94, 7362-7366.

Jobbágy, E.G., R.B. Jackson (2000): The vertical distribution of soil organic carbon and its relation to climate and vegetation. *Ecological Applications,* 10, 423-436.

Jordan, C.F., W. Caskey, G. Escalante, R. Herrera, et al. (1982): The nitrogen cycle in a 'Terra Firme' rainforest on oxisol in the Amazon Territory of Venezuela. *Plant and Soil*, 67, 325–332.

Kaiser, J.(1998): New network aims to take the world's CO_2 pulse. *Science*, 281, 506–507.

Kalnay, E., M. Kanamitsu, R. Kistler, W. Collins, et al. (1996): The NCEP/NCAR 40-year reanalysis project. *Bullet. Amer. Meteorol. Soc.*, 77, 437-471.

Keague, M.C., J.A. Wang et al. (1982): Estimating saturated hydraulic conductivity from soil morphology. *Soil Science Society of America Journal*, 46, 1239–1244.

Kirkby, M.J. (1997): TOPMODEL: a personal view. *Hydrological Processes*, 11, 1087–1097.

Kistler, R., E. Kalnay, W. Collins, S. Saha, et al. (2001): The NCEP-NCAR 50-Year Reanalysis: Monthly Means CD-ROM and Documentation. *BAMS,* 82**,** 247-268.

Kleidon, A. and M. Heimann (2000): Assessing the role of deep rooted vegetation in the climate system with model simulations: mechanism, comparison to observations and implications fro Amazonian deforestation. *Climate Dynamics*, 16, 183–199.

Klooster, S.A. (1993): Terrestrial ecosystem production: a process model-based on global satellite and surface data. *Global Biogeochemical Cycles*, 7, 811–841.

Klute, A. (1986): Water retention: laboratory methods. In: Methods of soil analysis, Part 1, physical and mineralogical methods. (Ed: A. Klute). *Agr. Monogr. ASA and SSSA Madison WI*, 635-662.

Klute, A. and C. Dirksen (1986): Hydraulic conductivity and diffusivity: laboratory methods. In: methods of soil analysis, Part1, physical and mineralogical methods. (Ed: A. Klute) *Agr. Monogr. 9.ASA and SSSA, Madison WI*, 687-734.

Knorr, W. (2000): Annual and interannual CO_2 exchanges of the terrestrial biosphere: process-based simulations and uncertainties. *Global Ecology and Biogeography*, 9, 225-252.

Kosugi, K., K. Mori, and H. Yasuda (2001): An inverse modeling approach for the characterization of unsaturated water flow in an organic forest floor. *Journal of Hydrology*, 246, 96–108.

Koster, R.D., and M.J. Suarez (1994): The Components of a SVAT Scheme and Their Effects on a GCMs Hydrological Cycle. *Adv. Water Resources*, 17, 61-78.

Koster, R.D. and P.C. Milly (1997): The interplay between transpiration and runoff formulations in land surface schemes used with atmospheric models. *J. Climate,* 10, 1578-1591.

Koster, R. D., M.J. Suarez, A. Ducharne, M. Stieglitz and P. Kumar (2000): Catchment-Based Approach to Modeling Land Surface Processes in a GCM - Part I: Model Structure, *JGR-Atmos,* 105(D20), 24809-24822.

Kruijt, B. (2003): Soil respiration measurements and modeling at short and long timescales**.** *Conference within the ESF-programme "The role of soils in the terrestrial carbon balance" Salzau Castle*.

Kull, O. and P.G. Jarvis (1995): The role of nitrogen in a simple scheme to scale up

photosynthesis from leaf to canopy. *Plant, Cell and Environment*, 18, 1174– 1182.

Larcher, W. (1995): Physiological Plant Ecology, third edition. *Springer*.

Leij, F.J., W.J. Alves, M. van Genuchten, and J.R. Williams (1996): The UNSODA unsaturated soil hydraulic database, version 1.0, *EPA report EPA/600/R-96/095, EPA National Risk Management Laboratory, G-72, Cincinnati, OH*. Available at: http://www.ussl.ars.usda.gov/MODELS/unsoda.htm.

Leij, F.J., W.B. Russell, and S.M. Lesch (1997): Closed-Form Expressions for Water Retention and Conductivity Data. *Ground Water*, 35(5), 848–853.

Leuning, R., F.M. Kelliher, D.G.G. dePury and E.D. Schulze (1995): Leaf nitrogen, photosynthesis, conductance and transpiration: scaling from leaves to canopies. *Plant, Cell and Environment*, 18, 1183–1200.

Liang, X., D.P. Lettenmaier, E.F. Wood, and S.J. Burges (1994): A simple hydrologically based model of land surface water and energy fluxes for general circulation models. *J. Geophys. Res*., 99(D7), 14415-14428.

Liang, X. and Z. Xie (2003): Important factors in land-atmosphere interactions: surface runoff generations and interactions between surface and groundwater. *Global and Planetary Change*, 38, 101–114.

Lilly, A. (2000): The relationship between field-saturated hydraulic conductivity and soil structure: development of class pedotransfer functions. *Soil Use and Management*, 16, 56–60.

Lin, H.S., K.J. McInnes, L.P. Wilding, and C.T. Hallmark (1999): Effects of soil morphology on hydraulic properties: I. Quantification of soil morphology. *Soil Science Society of America Journal*, 63, 948–954.

Lin, H.S., K.J. McInnes, L.P. Wilding, and C.T. Hallmark (1999): Effects of soil morphology on hydraulic properties: II. Hydraulic pedotransfer functions. *Soil Science Society of America Journal*, 63, 955–961.

Liu, Q., and R.E. Dickinson (2003): Use of a two-mode soil pore size distribution to estimate soil water transport in a land surface model. *Geophys. Res. Lett.,* 30(6),1331, doi:10.1029/2002GL016562.

Mackay, D.S. and L.E. Band (1997): Forest ecosystem processes at the watershed scale: Dynamic coupling of distributed hydrology and canopy growth. *Hydrological Processes*, 11, 1197–1217.

Maidment, D. (1993): Handbook of hydrology. *McGraw-Hill Professional*.

Matson, P.A., W.H. McDowell, A.R. Townsend, and P.M. Vitousek (1999): The globalization of N deposition: ecosystem consequences in tropical environments. *Biogeochemistry*, 46, 67–83.

McGuire, A.D., J.M. Melillo, L.A. Joyce, D.W. Kicklighter, et al. (1992): Interactions between carbon and nitrogen dynamics in estimating net primary productivity for potential vegetation in North America. *Global Biogeochemical Cycles*, 6, 101–124.

Mecke, M., C.J. Westman, and H. Hvesniemi (2000): Prediction of near-saturated hydraulic conductivity in three podzolic boreal forest soils. *Soil Science Society of America Journal*, 64, 458–492.

Mecke,M., C.J. Westman, and H. Ilvesniemi (2002): Water retention capacity in coarse podzol profiles predicted from measured soil properties. *Soil Science Society of America Journal*, 66, 1–11.

Milly,P.C.D. and A.B. Shmakin (2002): Global modeling of land water and energy balances. Part I: the Land Dynamics (LaD) Model. *Journal of Hydrometeorology*, 3, 283–299.

Milly,P.C.D. and A.B. Shmakin (2002): Global modeling of land water and energy balances. Part II: land-characteristics contributions to spatial variability. *Journal of Hydrometeorology*, 3, 301–310.

Milly,P.C.D. and A.B. Shmakin (2002): Global modeling of land water and energy balances. Part III: interannual variability. *Journal of Hydrometeorology*, 3, 311–321.

Mohanty, B.P. (1999): Scaling hydraulic properties of a macroporous soil. *Water Resources Research*, 35(6), 1927–1932.

Mohanty, B.P. (2000): Saturated hydraulic conductivity and soil water retention properties across a soil-slope transition. *Water Resources Research*, 36(11), 3311–3324.

Mualem, Y. (1976): A new model for predicting the hydraulic conductivity of unsaturated porous media. *Water Resources Research*, 12(3), 513–522.

Nimmo, J.R.(1977): Modeling structural influences on soil water retention. *Soil Science Society of America Journal*, 61, 712–719.

Niu,G.Y. and Z.L. Yang (2003): The versatile integrator of surface atmospheric processes. Part 2: evaluation of three topography-based runoff schemes. *Global and Planetary Change*, 38, 191–208.

Oyedele, D.J., P. Schjønning, E. Sibbesen, and K. Debosz (1999): Aggregation and organic matter functions of three Nigerian soils as affected by soil disturbance and incorporation of plant material. *Soil & Tillage Research*, 50, 105–114.

Pachepsky,Y.A. and W.J. Rawls (1999): Accuracy and Reliability of Pedotransfer Functions as Affected by Grouping Soils. *Soil Science Society of America Journal*, 63, 1748–1757.

Pachepsky, Y., W.J. Rawls and D. Gimenez (2001): Comparison of soil water retention at field and laboratory scales. *Soil Science Society of America Journal*, 65, 460–462.

Parton, W.J., A.R. Mosier, D.S. Ojima, D.W. Valentine, et al. (1996): Generalized model for N2 and N2O production from nitrification and denitrification. *Global Biogeochemical Cycles*, 10(3), 401–412.

Paustian, K., J. Six, E.T. Elliott, and H.W. Hunt (2000): Management options for reducing CO_2 emissions from agricultural soils. *Biogeochemistry*, 48, 147-163.

Pitman, A.J., Z.L. Yang, J.G. Cogley, and A. Henderson-Sellers (1991): Description of the Bare Essentials of Surface Transfer for the Bureau of Meteorology Research Centre AGCM. BMRC Research Report No. 32, *Bureau of Meteorology Research Centre, Melbourne, Australia*.

Pitman, A.J., A. Henderson-Sellers, F. Abramopoulos, R. Avissar, et al. (1993): Results from the off-line Control Simulation Phase of the Project for Intercomparison of Land surface Parameterization Schemes (PILPS), GEWEX technical note, *IGPO Publication Series*, 7, 47.

Poorter, H. and J.R. Evans (1998): Photosynthetic nitrogen-use efficiency of species that differ inherently in specific leaf area. *Oecologia*, 116, 26–37.

Poulsen, T.G., P. Moldrup, B.V. Iversen and O.H. Jacobsen (2002): Three region Campbell Model for Unsaturated Hydraulic Conductivity in Unidistribute Soils. *Soil Science Society of America Journal*, 66, 744–752.

Rawls, W.J., D.L. Brakensiek, and K.E. Saxton (1982): Estimation of Soil Water Properties. *Transactions of the American Society of Agricultural Engineers*, 25, 1316–1320.

Rawls, W.J.and D.L. Brakensiek, (1989): Estimation of soil water retention and hydraulic properties. In: Mmore-Seytoux, H.J. (Ed.), Unsaturated Flow in Hydrologic Modeling Theory and Practice. *Kluwer Academic Publishing*.

Rawls, W.J., Y.A. Pachepsky, J.C. Ritchie, T.M. Sobecki, et al. (2003): Effect of soil organic carbon on soil water retention. *Geoderma*, 116, 61–76.

Ross, P.J. and K.R.J. Semttem (1993): Describing soil hydraulic properties with sums of simple functions. *Soil Science Society of America Journal*, 57, 26–29.

Running, S.W. and Gower, S.T. (1991): FOREST-BGC, a general model of forest ecosystem processes for regional applications. II. Dynamic carbon allocation and nitrogen budgets. *Tree Physiology*, 9, 147–160.

Sato, N., P.J. Sellers, D.A. Randall, E.K. Schneider, et al. (1989): Effects of implementing the simple biosphere model in a general circulation model. *J. Atmos. Sci*., 46, 2757–2782.
Saxton, K.E., W.J. Rawls, J.S. Romberger, and R.I. Papendick (1986): Estimating Generalized Soil-water Characteristics from Texture. *Soil Science Society of America Journal*, 50, 1031–1036.

Scanlon, T.M., J.P. Raffensperger, G.M. Hornberger, and R.B. Clapp (2000): Shallow subsurface storm flow in a forested headwater catchment: Observations and modeling using a modified TOPMODEL. *Water Resources Research*, 36(9), 2575–2586.

Schaap, M.G. and F.J. Leij (2000): Improved Prediction of Unsaturated Hydraulic Conductivity with the Mualem-van Genuchten Model. *Soil Science Society of America Journal*, 64, 843–851.

Schenk, H.J., R.B. Jackson (2002): Rooting depths, lateral root spreads, and belowground/ aboveground allometries of plants in water limited ecosystems. *Journal of Ecology*, 90, 480-494.

Schulze E.D. (1982): plant life forms and their carbon, water and nutrient relations. In: Lange OL, Nobel PS, Osmond CB, Ziegler H (eds) *Encyclopedia of plant physiology 12 B. Springer, Berlin Heidelberg New York*, pp 615-676.

Sellers, P.J. (1986): Simple biosphere model (SiB) for use within general circulation models. *Journal of Atmospheric Science*, 43, 505-531.

Sellers, P.J., D.A. Randall, G.J. Collatz, J.A. Berry, et al. (1996): A revised land surface parameterization (SiB2) for atmospheric GCMs. Part I: Model Formulation. *Journal of Climate*, 9, 676–705.

Sellers, P.J., R.E. Dickinson, D.A. Randall, A.K. Betts, et al. (1997): Modeling the exchanges of energy, water, and carbon between continents and the atmosphere. *Science*, 275, 502-509.

Shao, Y. and A. Henderson-Sellers (1996): Modeling soil moisture : a project for intercomparison of land surface parameterization schemes Phase 2(b). *JGR*, 101, 7227-7250.

Shaver, G.R., J. Canadell, F.S. Chapin, J. Gurevitch, et al. (2000): Global Warming and Terrestrial Ecosystems: A Conceptual Framework for Analysis. *BioScience*, 50(10), 871–882.

Shaw, J.N., L.T. West, D.E. Radcliffe, and D.D. Bosch (2000): Preferential flow and

pedotransfer functions for transport properties in Sandy Kandiudults. *Soil Science Society of America Journal*, 64, 670–678.

Shirazi,M.A., L. Boersma, and C.B. Johnson (2001): Particle-Size Distributions: Comparing Texture Systems, Adding Rock, and Predicting Soil Properties. *Soil Science Society of America Journal*, 65, 300–310.

Six, J., K. Paustian, E.T. Elliott, and C. Combrink (2000): Soil structure and soil organic matter: I. Distribution of aggregate size classes and aggregate associated carbon. *Soil Sci. Soc. Am. J.*, 64, 681-689.

Skaggs, T.H., L.M. Arya, P.J. Shouse, and B.P. Mohanty: Estimating Particle-Size Distribution from Limited Soil Texture Data. *Soil Science Society of America Journal*, 65, 1038–1044.

Steele, S.J., S.T. Gower, J.G. Vogel, and J.M. Norman (1997): Root mass, net primary production, and turnover in aspen, jack pine, and black spruce forests in Saskatchewan and Manitoba, Canada. *Tree Physiol*., 17, 577–587.

Stieglitz, M., D. Rind, J. Famiglietti, C. Rosenzweig (1997): An Efficient Approach to Modeling the Topographic Control of Surface Hydrology for Regional and Global Climate Modeling. *J. of Climate*, 10(1), 118-137.

Tempel**,** P., N.H. Batjes, and V.W.P. van Engelen (1996): IGBP-DIS data set for pedotransfer function development. *Work. Pap. 96/06 , ISRIC, Wageningen*.

Terashima, I., S.I. Miyazawa, and Y.T. Hanba (2001): Why are sun leaves thicker than shade leaves? Consideration based on Analyses of CO_2 Diffusion in the Leaf. *Journal of Plant Research*, 14, 93–105.

Tian, Y., R.E. Dickinson, L. Zhou, X. Zeng, et al. (2004): Comparison of seasonal and spatial variations of LAI/FPAR from MODIS and Common Land Model, *J. Geophys. Res.,* 109 (D1), D01103, 10.1029/2003JD003777.

Tian, Y., R.E. Dickinson, L. Zhou, and M. Shaikh (2004).: Impact of new land boundary condition from MODIS data on the climatology of land surface variables. *J. Geophys. Res.*, submitted.

Tietje, O. and M. Tapkenhinrichs (1993): Evaluation of Pedo-Transfer Functions. *Soil Science Society of America Journal*, 57, 1088–1095.

Timlin,D.J., L.R. Ahuja, Y. Pachepsky, R.D. Williams, et al. (1999): Use of Brooks-Corey Parameters to Improve Estimates of Saturated Conductivity from Effective Porosity. *Soil Science Society of America Journal*, 63, 1086–1092.

Tomasella, J., Y. Pachepsky, S. Crestana, and W.J. Rawls (2003): Comparison of Two

Techniques to Develop Pedotransfer Functions for Water Retention. *Soil Science Society of America Journal*, 67, 1085–1092.

Tomasella, J. and M.G. Hodnett (1998): Estimating soil water retention characteristics from limited data in Brazilian Amazonia. *Soil Science*, 163(3), 190–202.

Tomasella, J., M.G. Hodnett, and L. Rossato (2000): Pedotransfer Functions for the Estimation of Soil Water Retention in Brazilian Soils. *Soil Science Society of America Journal*, 64, 327–338.

van Genuchten, M.T. (1980): A closed-form equation for predicting the hydraulic conductivity of unsaturated soils. *Soil Science Society of America Journal*, 44, 892–898.

Vereecken, H., J. Feyen, J. Maes, and P. Darius (1989): Estimating the soil moisture retention characteristic from texture, bulk density and carbon content. *Soil Science*, 148, 389–403.

Verseghy, D.L. (1991): CLASS - A Canadian land surface scheme for GCMs. I. Soil Model. *Intl. J. Climatology*, 11, 111-133.

Vertessy, R.A. and H. Elsenbeer (1999): Distributed modeling of storm flow generation in an Amazonian rain forest catchment: Effects of model parameterization. *Water Resources Research*, 35(7), 2173–2187.

Vitousek, P.M. and R. Howarth (1991): Nitrogen limitation on land and in the sea: how can it occur? *Biogeochemistry*, 13, 87–115.

Wagner, B., V.R. Tarnawski, V. Hennings, et al. (2001): Evaluation of pedotransfer functions for unsaturated soil hydraulic conductivity using an independent data set. *Gerderma*, 102, 275–297.

Wang, G.L., E.A.B. Eltahir (2000): Biosphere-atmosphere interactions over West Africa. Part 1: Development and validation of a coupled dynamic model. *Quarterly Journal of the Royal Meteorological Society*, 126(565), 1239-1260.

Wang, G.L., E.A.B. Eltahir (2000): Biosphere-atmosphere interactions over West Africa. Part 2: Multiple climate equilibria. *Quarterly Journal of the Royal Meteorological Society*, 126(565), 1261-1280.

Wang, Y.P. and R, Leuning (1998): A two-leaf model for canopy conductance, photosynthesis and partitioning of available energy. I. Model description. *Agricultural and Forest Meteorology*, 91, 89-111.

Warrach, K., M. Stieglitz, H. Mengelkamp, and E. Raschke (2002): Advantages of a Topographically Controlled Runoff Simulation in a Soil-Vegetation-Atmosphere

Transfer Model. *Journal of Hydrometeorology*, 3, 131–148.

Warren, C.R. and M.A. Adams (2001): Distribution of N, Rubisco and photosynthesis in Pinus pinaster and acclimation to light. *Plant, Cell and Environment*, 24, 597–609.

Watson, K.W. and R.J. Luxmore (1986): Estimating macroporosity in a forest watershed by use of tension infiltrometer. *Soil Science Society of America Journal*, 50, 578–582.

White, M.A., P.E. Thornton, S.W. Running, and R.R. Nemani (2000): Parameterization and sensitivity analysis of the BIOME-BGC terrestrial ecosystem process model: net primary production controls. *Earth Interactions*, 4(3), 1-85.

Williams, R., L. Ahuja, and J. Naney (1992): Comparison of methods to estimate soil water characteristics fro soil texture, bulk density and limited data. *Soil Science*, 153, 172–184.

Wilson, K.B. and D.D. Baldocchi (2000): Seasonal and interannual variability of energy fluxes over a broadleaved temperate deciduous forest in North America. *Agricultural and Forest Meteorology*, 100, 1-18.

Woodrow, I.E., J.T. Ball, and J.A. Berry (1990): Control of photosynthetic carbon dioxide fixation by the boundary layer, stomata and ribulose 1,5-biphosphate carboxylase/ oxygenase. *Plant, Cell and Environment*, 13, 339–347.

Wösten, J.H.M., A. Lilly, A. Nemes, and C. LeBas (1999): Development and use of database of hydraulic properties of European soils. *Geoderma*, 90, 169–185.

Xue, Y., P. J. Sellers, J.L. Kinter III, and J. Shukla (1991): A simplified biosphere model for global climate studies. *J. Climate*, 4, 345-364.

Xue, Y. and J. Shukla (1993): The influence of land surface properties on Sahel climate. Part I: Desertification. *J. Climate*, 6, 2232-2245.

Xue Y., F.J. Zeng, C.A. Schossler (1996): SSiB and its sensitivity to soil properties-A case study using HAPEX-Mobilhy data. *Global and Planetary Change*, 13, 183-194.

Yang, Z.L. and G.Y. Niu (2003): The versatile integrator of surface and atmosphere processes. Part 1. Model description. *Global and Planetary Change*, 38, 175– 189.

Young, I.M., E. Blanchart, C. Chenu, et al. (1998): The interaction of soil biota and soil structure under global change. *Global Change Biology*, 4, 703– 712.

Young, I.M., J.W. Crawford, and C. Rappoldt (2001): New methods and models for characterizing structural heterogeneity of soil. *Soil & Tillage Research*, 61, 33–45.

Young, I.M. and K. Ritz (2000): Tillage, habitat space and function of soil microbes. *Soil*

& Tillage Research, 53, 201–213.

Zavattaro, L. and C. Grignani (2001): Deriving Hydrological Parameters for Modeling Water Flow under Field Conditions. *Soil Science Society of America Journal*, 65, 655–667.

Zhang, H., A. Henderson-Sellers, and K. McGuffie (1996): Impacts of tropical deforestation I: process analysis of local climate change. *J. Climate*, 9, 1497-1517.

Zhang, R. and M.T. van Genuchten (1994): New models for unsaturated soil hydraulic properties. *Soil Science*, 158(2), 77–85.

Zeng, X., M. Shaikh, Y. Dai, R.E. Dickinson, and R. Myneni (2002): Coupling of the Common Land Model to the NCAR Community Climate Model. *J. Climate*, 14, 1832-1854.

Zeng, X., Y. Dai, R.E. Dickinson, and M. Shaikh (1998): The role of root distribution for climate simulation over land. *Geophysical Research Letter*, 25(24), 4533–4536.

Zeng, X., R.E. Dickinson, M. Barlage, Y. Dai, G. Wang and K. Oleson (2004): Treatment of under-canopy turbulence in land models. *Journal of Climate*. Submitted

Zhu, J. and B.P. Mohanty (2002): Spatial Averaging of van Genuchten Hydraulic Parameters for Steady-State Flow in Heterogeneous Soils: A Numerical Study. *Vadose Zone Journal*, 1, 261–272.

Vita

Qing Liu was born on March 23, 1973 in Sichuan, P.R. China. In 1992, she attended Yunnan University, Kunming, P.R. China, where she graduated with her B.S. degree in Atmospheric Dynamics in 1996. After her graduation, she went to Institute of Atmospheric Physics, Chinese Academe of Sciences, Beijing, China and received her M.S. degree there in Atmospheric Physics in 1999. She joined the School of Earth and Atmospheric Sciences, the Georgia Institute of Technology from January 2000. In May 2004, she received her Ph.D. after more than four years as a research assistant for Porf. Robert E. Dickinson.